Site-Switchable Dynamic Nuclear Polarization NMR Measurement on Dynamics of Liposome-Environment Water

（リポソーム近傍の水のダイナミクスの位置可変型動的核分極 NMR による計測）

Gyeorye Lee

北海道大学　大学院総合化学院　総合化学専攻

物質化学コース　分子物質化学講座　液体化学研究室

2022

Site-Switchable Dynamic Nuclear Polarization NMR Measurement on Dynamics of Liposome-Environment Water

リポソーム近傍の水のダイナミクスの

位置可変型動的核分極 NMR による計測

Gyeorye Lee

Hokkaido University

北海道大学

2022

Site-Switchable Dynamic Nuclear Polarization NMR Measurement on Dynamics of Liposome-Environment Water

Contents

Chapter 1.

Chapter 1. Introduction

1.1. Measurement of molecular dynamics of water

The phenomena of life are based on a complex of chemical processes, wherein water plays a variety of important roles, as indicated by the fact that it makes up to 70% of human body. For instance, water is essential in maintaining the isothermal non-equilibrium state of the living system and serves as a medium for transporting nutrients and excreting wastes. Furthermore, it contributes to the construction of the living system by promoting hydrophobic interaction between organic molecules: biological membranes were formed due to the existence of water. On a more microscopic level, water of hydration also aids in the folding of proteins and genes, their molecular recognitions, and the chemical reactions involved in their functions. [1–4] Thus, water is indispensable to life at all levels, macroscopic to microscopic.[5–9]

To advance the molecular-level understanding of various biological phenomena, many scientists have studied the properties and rheology of water of hydration around biological complexes, such as proteins and membranes.[10, 11]Various methods such as vibrational (infrared) spectroscopy, neutron scattering, and nuclear magnetic resonance (NMR) were employed to quantify the dynamics of water of hydration. Vibrational spectroscopy detects not only the bond oscillation of the water of hydration but also the intermolecular hydrogen bond within the water molecules.[12, 13] Neutron scattering can provide information on fluctuations in the network of water molecules in the hydrated layer.[14–15] On the other hand, NMR relaxometry[6, 12, 16] is a method that can determine the molecular motion in the correlation time region of 10 ps to 10 ns. Relaxometry is currently applied in a common method for tracking water, known as magnetic resonance imaging (MRI) in

medical diagnosis.[17, 18] However, in the investigation of water dynamics in biological system at the microscopic level, it remains challenging to determine whether the measurements sense bulk water or hydrated water. Furthermore, the low sensitivity of NMR is a problem with NMR. Alternatively, dynamic nuclear polarization NMR (DNP NMR), which overcomes the sensitivity restrictions posed by general NMR for investigating water of hydration, has attracted attention in recent years. The DNP NMR is a nuclear spin polarization method via Overhasuer effect that utilizes the saturation and relaxation of electron spins.

In this study, the author aimed at understanding the dynamics of water incorporated into and surrounding lipid bilayers (Figure 1-1), especially the vesicular assembly which has a hollow spherical structure, using the DNP-NMR method. As representing by the cell membrane and thylakoid membrane, liposomal assembly plays an important role in the living system: it distinguishes the inside and the outside of a cell and an organelle, constructs the structure of the living system, and provides a medium for the transportation of materials and information. Inside the liposomal membrane, the phospholipids are aligned with their polar groups toward the surface and their aliphatic chain toward the center of the membrane. Classically, it was considered that the surface of the vesicle is surrounded by stern layer and the shear plane is around it: the plane is located 2 Å away from the surface of the vesicle. But this classical consideration was developed from the viewpoint that the vesicle was a rigid body. In addition, vesicular membrane was considered to be impervious to water because of its hydrophobic property. However, with advancements in the understanding of the vesicular membrane by considering the thermal motion of molecules, it has been suggested that the membrane is permeable to water.[19–21] Thus, from the dynamics perspective of molecules, the understanding of the properties

of liposomal vesicles, which play a fundamental role in vivo, has changed dramatically in these last few decades.

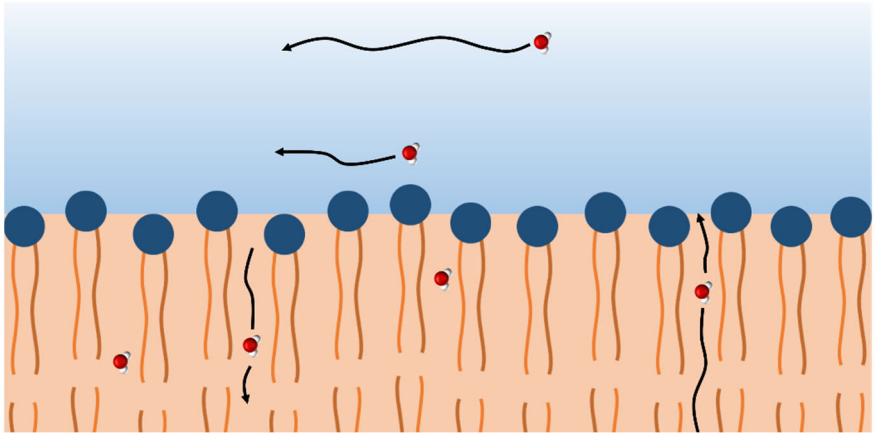

Figure 1-1: Dynamics of water molecules in the vicinity of phospholipids

1.2. General principle of DNP-NMR

NMR is a method of observing transitions between spin states of Zeeman splitting under a magnetic field. In the embryo stage of NMR, its interests were in the determination of the magnetic moments of nuclei, but since the discovery of various nuclear spin interactions for molecules and condensed matter, e.g. dipole interaction, quadrupole interaction, chemical shift, spin-spin coupling etc., NMR has been employed for the determination of molecular dynamics based on relaxation time measurements and spectrum shape analysis. High-resolution NMR spectra are commonly used to determine the structure of organic compounds. However, NMR has a fundamental limitation in that its signal strength is relatively wea: the small Zeeman energy, energy gap between the spin states, causes the small polarization in magnetization.

Typically, an NMR signal can be enhanced by increasing the magnetic field.[22] In addition, lowering the temperature to increase magnetization based on Boltzmann's distribution, increasing the concentration of the measurement sample, and reducing the

size of the radio frequency coil (rf-coil)[23] for NMR signal measurement, also contribute to an increase in the signal-to-noise ratio of NMR spectroscopy. Another method is to transfer the polarization of the spins with larger magnetic moment to the spins with smaller; it is known as Overhauser effect. DNP-NMR is a method that employs the Overhauser effect between an electron spin and a nuclear spin. Depending on the interaction between the one-electron and one-nuclear spin systems (in case the spin quantum number of the nuclear spin is 1/2), four different spin levels are formed by Zeeman splitting under a magnetic field (Figure 1-2).[24]

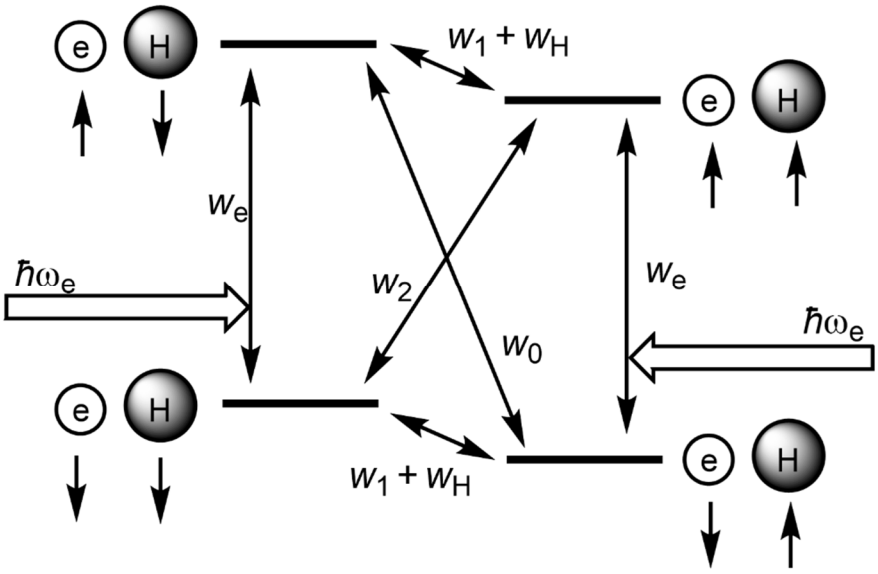

Figure 1-2: Two spin systems and relaxation paths in DNP-NMR

The large enhancement on signals by DNP-NMR is applied to the structural determination of proteins in small amounts. As this enhancement is a result of the distance-dependent dipole–dipole interactions between an electron spin and a nuclear spin, they need to be present close to each other. The region of influence of the Overhauser effect between either spin is less than 1.5 nm. In other words, the DNP-NMR selectively enhances only the NMR signals of proton nuclei near the electron spins, which makes it

possible to measure water molecules site-selectively.[25, 26] Next, the general principle of relaxometry is introduced. Water molecules entering the effective region of an electron spin are polarized, and then relaxed. Specifically, the enhancement in the NMR signal is proportional to the number of protons passing through the effective region of DNP within the relaxation period of the proton spin. This method thus allows the site-selective determination of the dynamics of water molecules within a microscopic environment using enhanced NMR signals (Figure 1-3).

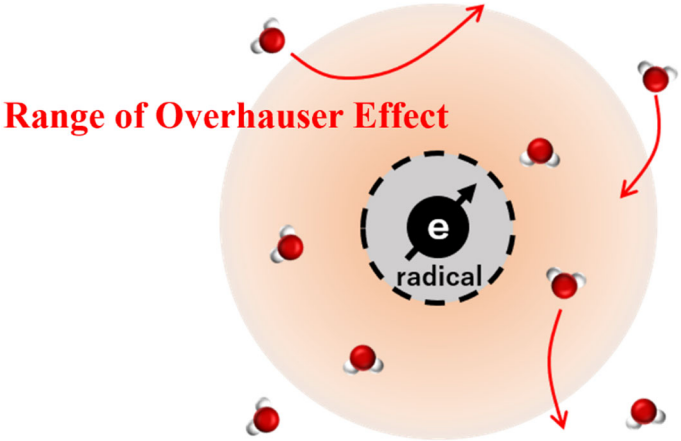

Figure 1-3: Schematic illustration of translational motion of water molecules around the Overhauser effective region

1.3. Background on Relaxometry by DNP-NMR

In this section, the author discusses the theory and protocol for the determination of translational dynamics of hydrated water molecules by the hydration dynamics Overhauser DNP (HD-ODNP) method. The protocol is mainly derived from the discussion established by Frank and Han.[25] The HD-ODNP method measures the dynamics of water passing within the Overhauser effect's range of a spin probe modified to a soft matter dispersed in water.

The enhancement E(p) in the NMR signal by the Overhauser effect is expressed as a function of the incident microwave power (p).

$$\mathrm{E}(p) = 1 - \xi\, \mathrm{f}\, \mathrm{s}(p) \left|\frac{\omega_\mathrm{e}}{\omega_\mathrm{H}}\right| \qquad (1)$$

ω_e and ω_H are the Larmor frequencies of the electron spin and proton spin, respectively. s(p) is the saturation factor of electron spin under microwave irradiation. Herein, the microwave causes the magnetization of the electron spin. The leakage factor, f, is a parameter that results in the loss of proton magnetization enhancement due to efficient paramagnetic relaxation by the existing electron spins. It can be determined experimentally using the following equation:

$$\mathrm{f} = \frac{T_{1,0} - T_1}{T_{1,0}} \qquad (2)$$

. T_1 and $T_{1,0}$ are the longitudinal relaxation times of protons in the sample in the presence and absence of the radical probe, respectively. The former is responsible for additional

paramagnetic relaxation.

In a two spin system with spin interaction (Figure 1-2), the coupling factor, ξ, which is the contribution for NMR enhancement through spin dynamics, can be shown by the spectral density function $J(\omega, \tau_c)$ as

$$\xi = \frac{6J(\omega_e - \omega_H,\tau_c) - J(\omega_e + \omega_H,\tau_c)}{6J(\omega_e - \omega_H,\tau_c) + 3J(\omega_H,\tau_c) + J(\omega_e + \omega_H,\tau_c)} \qquad (3)$$

. The correlation time, τ_c, is the time during which the nuclear spins exist in the same region as the Overhauser effect's region of influence for the electron spins. In this thesis, the force-free hard-sphere model was applied for $J(\omega, \tau_c)$:

$$J(\omega, \tau_c) = Real\left(\frac{1 + \frac{z}{4}}{1 + z + \frac{4}{9}z^2 + \frac{1}{9}z^3}\right) \qquad (4)$$

$$z = \sqrt{i\ \omega\ \tau_c} \qquad (5)$$

. By substituting the corresponding values to ωs (i.e., $2\pi \times 9.4$ GHz for the electron spin resonance and $2\pi \times 14.3$ MHz for the nuclear magnetic resonance) in this study, the relationship between τ_c and ξ under experimental conditions can be calculated as shown in Figure 1-4.

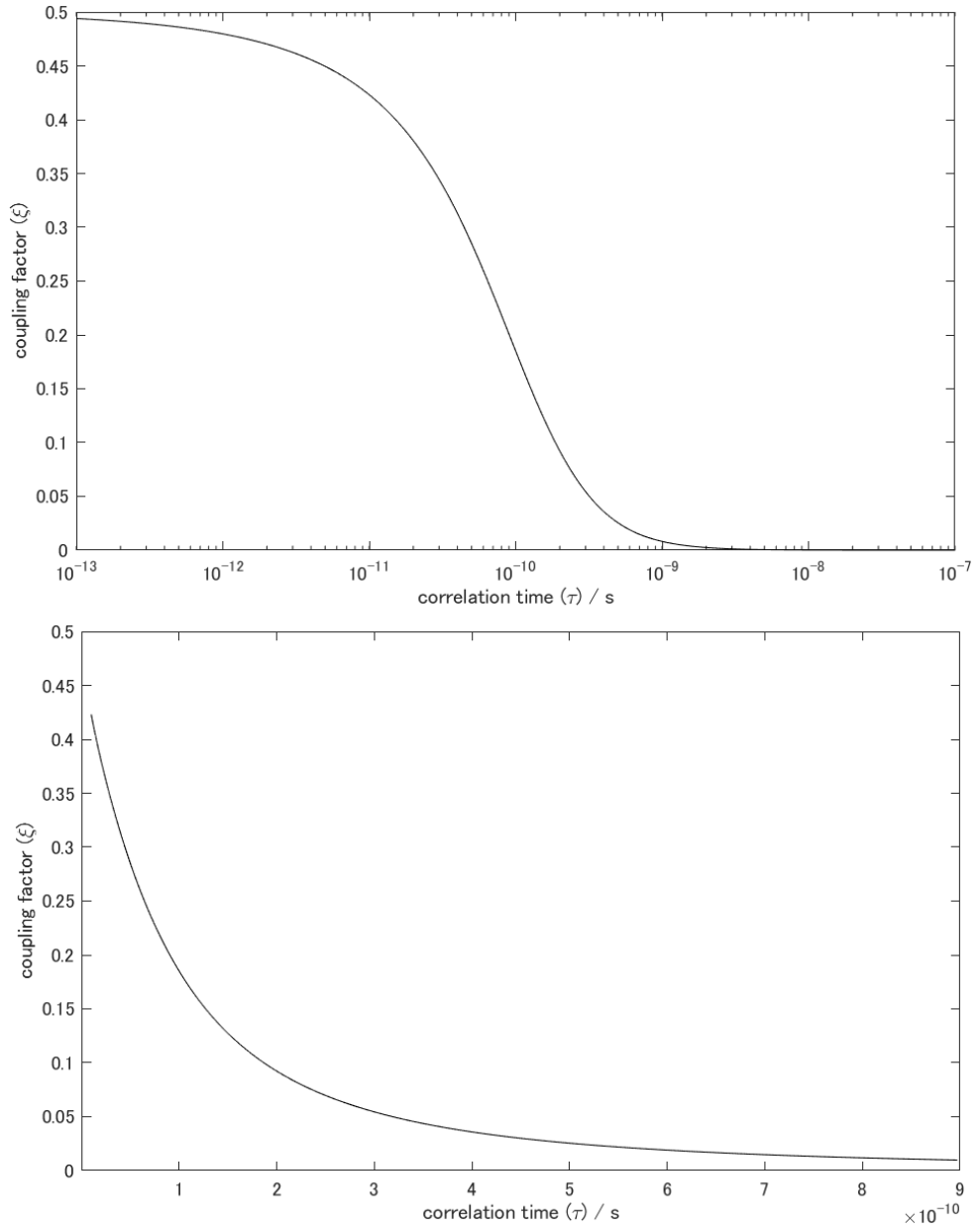

Figure 1-4: Relationship between coupling factor and correlation time

Han expressed the local dipolar cross-relaxation rate (k_σ) and the local dipolar self-relaxation rate (k_ρ) of proton magnetization as

$$k_\sigma C = (k_2 - k_0) \qquad (6)$$

$$k_\rho\, C = \left(k_0 \;+\; 2\, k_1^{\mathrm{H}} \;+\; k_2\right) \qquad (7)$$

, where C is the apparent concentration of the radical spin in the dispersed solution, and k_0, k_1^{H}, and k_2 are the relaxation rates for the processes indicated with the corresponding subscripts in Figure 1-2.

Using these equations, ξ is represented as

$$\xi \;=\; \frac{k_\sigma\, C}{k_\rho\, C} \;=\; \frac{k_\sigma}{k_\rho} \qquad (8)$$

, and f is represented as

$$\mathrm{f} \;=\; \frac{k_\rho\, C}{k_\rho\, C + T_{1,0}^{-1}} \qquad (9)$$

. As T_1^{-1} is the sum of $T_{1,0}^{-1}$ and the local dipolar self-relaxation rate ($k_\rho\, C$),

$$k_\rho\, C \;=\; \frac{1}{T_1} \;-\; \frac{1}{T_{1,0}} \qquad (10)$$

. Substituting Equations (8) and (9) into Equation (1) results in the following equation.

$$1 - E(p) = C\; T_1(p)\; k_\sigma\; \mathrm{s}(p)\; \left|\frac{\omega_e}{\omega_H}\right| \qquad (11)$$

When the polarization of the electron spin is saturated under strong microwave irradiation, the equation is expressed as

$$k_\sigma \, s_{(p_{sat})} = \frac{1 - E(p_{sat})}{C \, T_1(p_{sat})} \left|\frac{\omega_H}{\omega_e}\right| \qquad (12)$$

, where p_{sat} is the incident microwave power at saturated electron spin. As $T_{1,0}$, $T_1(p_{sat})$, and $E(p_{sat})$ have been determined experimentally, $k_\rho C$ and $k_\sigma C$ can be calculated using Equations (10) and (12), respectively. By substituting these values, f and ξ can be quantified using Equations (8) and (9), and then the correlation time (τ_c) of water to immobilize radicals can be determined by Equation (3), as shown in Figure 1-4.

It is known that the translational correlation time of two molecules can be expressed as a function of the diffusion coefficients of both molecules and the intermolecular distance between them:

$$\tau_c = d^2 / (D_e + D_H) \qquad (13)$$

, where D_e and D_H are the diffusion coefficients of the electron spin and nuclear spin, respectively. The distance between either spin is expressed as d. When the electron spin is immobilized in a slowly diffusive matter, D_e can be regarded as zero.

As elaborated in this section, the diffusion coefficient of the water close to electron spin is determined by measuring the values of $T_1(p)$, T_{10}, and $E(p)$ using HD-ODNP NMR.

1.4. Purpose and Overview

The rheology of water of hydration around spin-labeled DNAs,[27] proteins,[28–31] liposomes,[14, 26, 32–34], and artificial nanotubes is site-selectively measured using HD-ODNP.[35] For these measurements, a sample dispersion of customized spin label is prepared. A small amount of this dispersion is placed in a tube, which is set on a cavity resonator for measurement. This operation with sample exchange leads to experimental errors because of the resonance conditions and the degree of dielectric loss change. The effective concentration of the spin label in a heterogeneous system may depend on the preparation method. It was assumed that this constrains the measurement and analysis of the water of hydration dynamics using DNP-NMR.

Therefore, the author decided to design a novel method for the site-selective measurement and analysis of the dynamics of the water of hydration interacting with vesicular membranes while eliminating the need for sample exchange. By adding photolabile groups to spin labels, the relative position of the spin label in a heterogeneous system can be changed simply by exposure to light without requiring sample exchange. In other words, it will be possible to measure the rheology of water of hydration at different locations for the same vesicle (Figure 1-5-a).

The author designed the radical probe shown in Figure 1-5-b as a prototype spin label. It consists of a radical moiety that polarizes the nuclear spin distribution of water molecules by the Overhauser effect, a photolabile group that changes the position of the radical moiety relative to its anchored part, an anchor group that connects the probe to a vesicular membrane, and a linker group that characterizes the position of the radical moiety relative to its anchored part. The prototype radical probe was synthesized and its photoreactivity was investigated. Based on the results, two photolabile radical probes

were designed and synthesized. They were used in the DNP-NMR measurement of the dynamics of water of hydration in phospholipid vesicles.

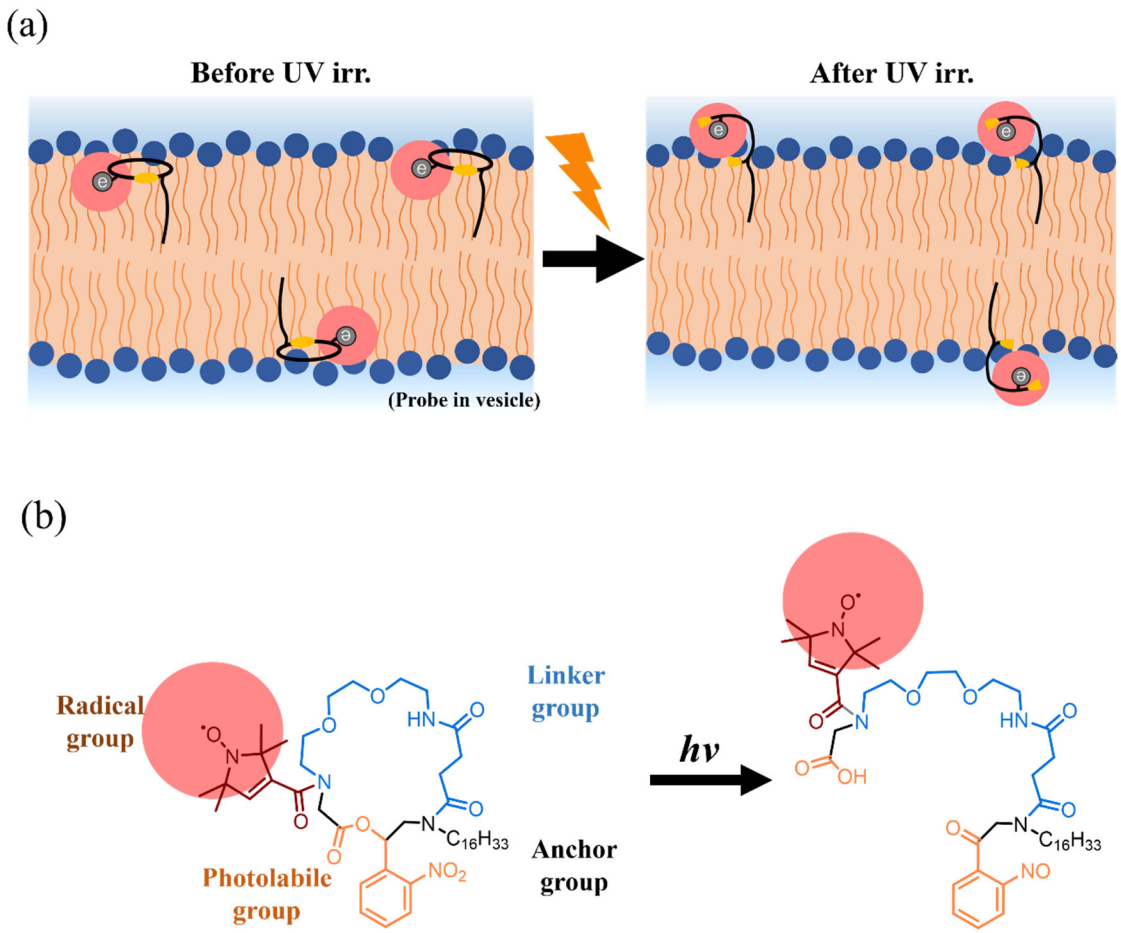

Figure 1-5: Design of a radical probe for site-specific measurements

Chapter 2.

Chapter 2. Experimental

2.1. General

All reagents for chemical synthesis were purchased from Fujifilm Wako Chemicals (Japan), Tokyo Chemical Industry (Japan), Kanto Chemical (Japan), and Merck (Germany) and Sigma-Aldrich (USA), and used without further purification. Water for the NMR relaxometry was used an Inductively Coupled Plasma (ICP) analysis grade ultrapure water purchased from Fujifilm Wako Chemicals. Deuterium solvents containing small amount of tetramethyl silane for solution NMR were purchased from ISOTECH (France). For identification of molecular structure, JEX270 and JNM-ECZ400S NMR spectrometers (JEOL, Japan), and a Chromaster 5610 mass detector (HITACHI, Japan) were used. Exactive and Exactive Plus (Thermo Scientific, USA) mass spectrometers were also used for *m/z* analysis by the operation of the technicians of Global Facility Center in Hokkaido University. For tracking of photolysis, a High Performance Liquid Chromatography (HPLC) system with a UV absorption detector (JASCO LC-2000 series, Japan) and a Cosmosil ARII column (Nacalai Tesque, Japan) connected to a mass detection unit (HITACHI Chromaster 5610, Japan) was employed.

2.2. Synthesis of radical probe **1**

2.2.1. Preparation of 2-hydroxy-2-(2-nitrophenyl)acetonitrile (**8**)

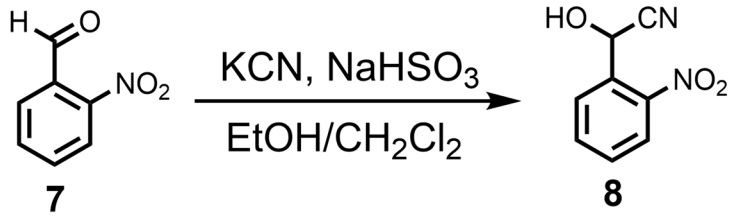

Figure 2-1: Nitrile formation for synthesis of 8

To a 10 mL solution of *o*-nitrobenzaldehyde (**7**, 500 mg, 3.31 mmol) in a 1:1 mixed solvent of CH_2Cl_2 and EtOH, $NaHCO_3$ (125 mg, 13.2 mmol) was added at 0 °C and stirred for 30 min. After dropwise addition of an aqueous KCN solution (961 mg, 9.5 mmol in 3 mL of water), the reaction solution was stirred at room temperature (r.t.) for 4 h. The organic layer was separated by three times extraction with CH_2Cl_2, was dried over Na_2SO_4. After evaporation of the solvent under reduced pressure and *in vacuo*, 518 mg (85% yield) of **8** was obtained as a colorless crystal.

^{1}H-NMR δ($CDCl_3$, 270 MHz): 8.20 (d, J = 8.1 Hz, 1H), 7.98 (d, J = 8.1 Hz, 1H), 7.81 (t, J = 8.1 Hz, 1H), 7.66 (t, J = 8.1 Hz, 1H), 6.19 (d, J = 8.1 Hz, 1H), 3.70 (d, J = 8.1 Hz, 1H).

2.2.2. Preparation of 2-hydroxy-2-(2-nitrophenyl)ethylamine (**9**)

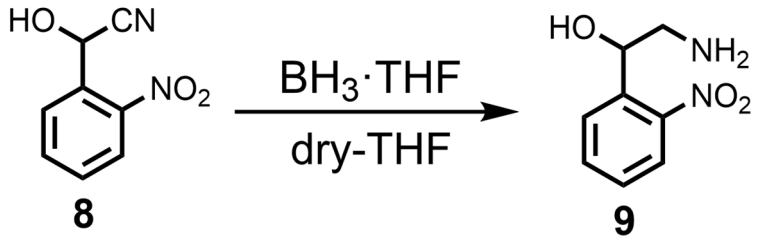

Figure 2-2: Reduction of 8 to form 9

A 1 M tetrahydrofran (THF) solution of BH_3·THF complex (1.00 mL, 1.00 mmol) was added to a THF (10 mL) solution of **8** (50.0 mg, 0.28 mmol). After refluxing for 1 h and further stirring at r.t. for 12 h, the reaction was quenched by the addition of methanol (MeOH, 0.50 mL). HCl gas, which was generated by the addition of H_2SO_4 to NaCl, was flown into the solution to form precipitates, which were separated by suction filter and was desiccated *in vacuo*. As a colorless powder, 46.9 mg of **9** (92% yield) was obtained.

^{1}H-NMR δ(CD_3OD, 270 MHz): 8.05 (d, J = 8.1 Hz, 1H), 8.00 (d, J = 8.1 Hz, 1H), 7.80 (t, J = 8.1 Hz, 1H), 7.58 (t, J = 8.1 Hz, 1H), 5.41 (dd, J = 2.7 Hz, 8.1 Hz, 1H), 3.41 (dd, J = 2.8 Hz, 12.7 Hz, 1H), 3.01 (dd, J = 12.8 Hz, 9.8 Hz, 1H).

2.2.3. Synthesis of *N*-(2-hydroxy-2-(2-nitrophenyl)ethyl)hexadecane-amide (**10**)

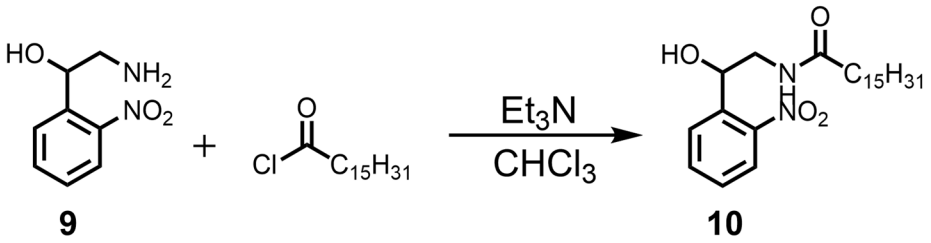

Figure 2-3: Formation of 10 from 9 and the corresponding acid chloride

A $CHCl_3$ (5 mL) solution of **9** (100 mg, 0.45 mmol) was treated with Et_3N (93.1 mg, 0.92 mmol), and then palmitoyl chloride (124 mg, 0.45 mmol) was added to the solution. After stirring for 3 h at 0 °C, 5.0 mL of 0.1 M HCl aq was added, and the organic layer was separated by four times extraction with CH_2Cl_2 from the solution, and was dried over Na_2SO_4. The solvent was removed under reduced pressure and *in vacuo* to give 191 mg (99% yield) of **10** as a colorless powder.

^{1}H-NMR δ($CDCl_3$, 270 MHz): 7.99 (d, J = 8.2 Hz, 1H), 7.95 (d, J = 7.8 Hz, 1H), 7.68 (t, J = 7.8 Hz, 1H), 7.45 (t, J = 8.2 Hz, 1H), 6.12 (t, J = 5.5 Hz, 1H), 5.37 (br, 1H), 3.68 (t, J = 6.0 Hz, 2H), 2.24 (t, J = 7.3 Hz, 2H), 1.63 (quin, J = 7.3 Hz, 2H), 1.22–1.41 (m, 26H), 0.88 (t, J = 7.9 Hz, 3H).

2.2.4. Preparation of *N*-(2-hydroxy-2-(2-nitrophenyl)ethyl)-*N*-hexadecylamine (**11**)

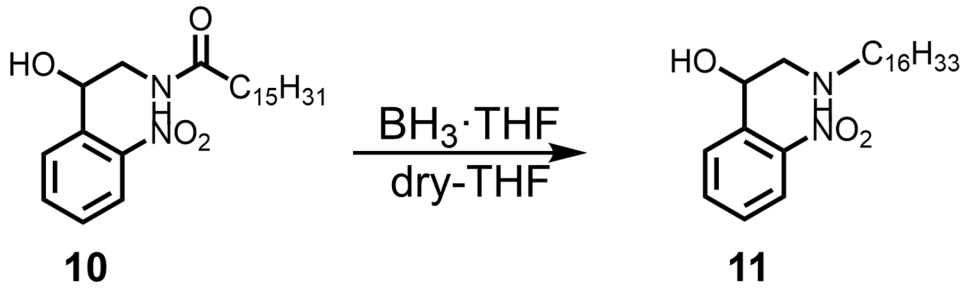

10 **11**

Figure 2-4: Reduction of 10 to form 11

To a THF (5 mL) solution of **10** (100 mg, 0.24 mmol), a 1 M THF solution of BH_3· THF (1.5 mL, 1.5 mmol) was added and stirred for 2 days at r.t.. The reaction solution was washed by saturated $NaHCO_3$ aq (10.0 mL), the separated organic layer via extraction using CH_2Cl_2 was dried over Na_2SO_4, and the solvent was evaporated under reduced pressure to give 84.5 mg of reaction crude. The compound **11** was obtained in 40% yield (38.4 mg) as pale yellow oil after silica gel column chromatography using 1:1 mixture of *n*-hexane (*n*Hex) and ethyl acetate (EtOAc) as the eluent.

^{1}H-NMR δ($CDCl_3$, 270 MHz):7.96 (d, J = 6.9 Hz, 1H), 7.91 (d, J = 6.9 Hz, 1H), 7.65 (t, J = 9.1 Hz, 1H), 7.44 (t, J = 9.1 Hz, 1H), 5.25 (dd, J = 3.6, 9.1 Hz, 1H), 3.19 (dd, J = 3.6, 12.4 Hz, 1H), 2.53–2.76 (m, 3H), 1.49 (quin, J = 6.9 Hz, 2H), 1.18–1.36 (m, 26H), 0.88 (t, J = 6.4 Hz, 3H).

2.2.5. Preparation of ethyl 13-(2-nitrophenylsulfonylamino)-8,11-dioxa-5-aza-tridecane-4-one-ate (**15**)

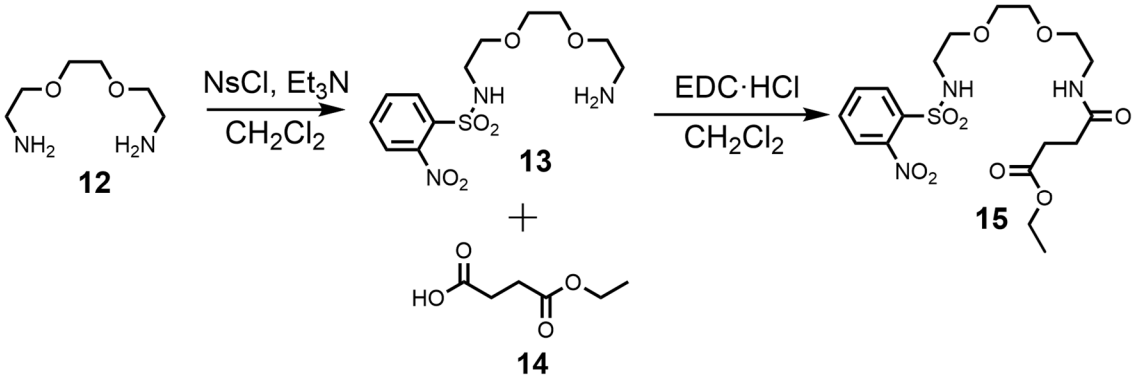

Figure 2-5: Nosyl (Ns) protection and amide condensation to form 15

To a 40 mL CH_2Cl_2 solution of **12** (1.00 g, 6.75 mmol) and Et_3N (1.40 mL, 13.5 mmol), 2-nitrobenzenesulfonyl chloride (NsCl) (1.65 g, 7.43 mmol) was added slowly at 0 °C, and the solution was vigorously stirred at 0 °C for 2 h and at r.t. for overnight. Subsequently, after the addition of monoethyl succinate (1.31 mL, 10.1 mmol) and EDC·HCl (1.99 g, 10.1 mmol) to the reaction solution at 0 °C, Et_3N (1.40 mL, 13.5 mmol) was added, and the solution was stirred at 0 °C for 2 h and at r.t. for overnight. After addition of 100 mL of 0.1 M HCl aq to the reaction solution, the organic layer was separated by four times extraction using 15 mL of CH_2Cl_2, and dried over Na_2SO_4. After the removal of the solvent under reduced pressure and *in vacuo*, 4.07 g of the reaction crude was obtained. By the separation using silica gel column chromatography with EtOAc eluent, 1.15 g (2.49 mmol, 37% yield) of **15** was obtained as pale yellow oil.

^{1}H-NMR δ($CDCl_3$, 400 MHz): 8.12–8.19 (m, 1H), 7.86–7.92 (m, 1H), 7.72–7.80 (m, 2H), 6.28 (brs, 1H), 6.11 (t, J = 8.4 Hz, 1H), 4.14 (quin, J = 7.2 Hz, 2H), 3.53–3.61 (m, 8H), 3.46 (td, J = 8.0, 8.8 Hz, 2H), 3.29 (td, J = 8.0, 8.8 Hz, 2H), 2.65 (t, J = 8.1 Hz, 2H), 2.51

(t, J = 8.1 Hz, 2H), 1.25 (t, J = 6.8 Hz, 3H).

^{13}C-NMR δ($CDCl_3$, 100 MHz): 173.0, 171.7, 147.9, 133.6, 132.8, 130.9, 125.4, 70.3, 70.0, 68.9, 60.5, 43.5, 39.2, 30.7, 29.5, 14.1.

MS(ESI) m/z 484.14 ($M+Na^+$), HRMS(ESI) m/z found 484.13544 ($M+Na^+$), $C_{18}H_{27}O_9N_3NaS$ ($M+Na^+$) requires 484.13602.

2.2.6. Preparation of 13-(2-nitrophenylsulfonylamino)-8,11-dioxa-5-aza-tridecane-4-one-ic acid (**16**) by hydrolysis of **15**

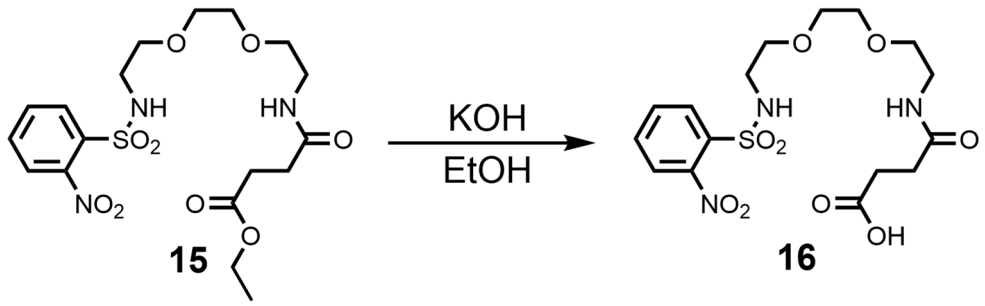

Figure 2-6: Hydrolysis of 15 to form 16

To a 50 mL ethanol in a round-bottom flask, potassium hydroxide (404 mg, 7.2 mmol) was dissolved, and then **15** (1.15 g, 2.49 mmol) was added. After stirring at r.t. for overnight, the solution was neutralized by the addition of 0.62 mL of conc HCl aq. The solution was concentrated under reduced pressure, and then 5.0 mL of THF was added to the solution. The precipitate was removed by suction filtration, and the filtrate was dried over Na_2SO_4. The solvent was removed under reduced pressure and *in vacuo* to give 977 mg (2.25 mmol, 90% yield) of **16** as pale yellow oil.

^{1}H-NMR δ(CD_3OD, 270 MHz): 8.13–8.06 (m, 1H), 7.84–7.74 (m, 3H), 3.54–3.49 (m, 8H), 3.36–3.30 (m, 2H), 3.20 (t, *J* = 5.4 Hz, 2H), 2.44 (s, 4H).

^{13}C-NMR δ($CDCl_3$, 100 MHz): 175.4, 173.3, 148.0, 133.8, 133.0, 131.2, 125.6, 70.5, 70.1, 69.9, 69.1, 43.5, 39.7, 30.8, 30.4,

MS(ESI) *m/z* 456.10 ($M+Na^+$), 432.11 ($M–H^+$); HRMS(ESI) *m/z* found 456.10377 ($M+Na^+$), $C_{16}H_{23}O_9N_3NaS$ ($M+Na^+$) requires 456.10472.

2.2.7. Preparation of *N*-(14-hexadecyl-16-hydroxy-16-(2-nitrophenyl)-3,6-dioxa-9,14-diaza-hexadecyl-10,13-dione)-2-nitrobenzenesulfonamide (**17**)

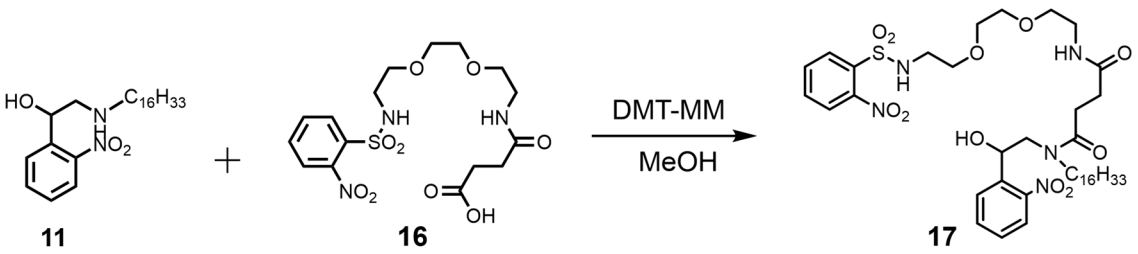

Figure 2-7: Amide condensation between 11 and 16

A MeOH solution of **16** (254 mg, 1.40 mmol) was added to a MeOH solution of **11** (629 mg, 1.45 mmol) and 4-(4,6-dimethoxy-1,3,5-triazin-2-yl)-4-methylmorpholinium chloride (DMT-MM) (440 mg, 1.60 mmol), and the reaction solution was stirred at r.t. for overnight. The solvent was evaporated under reduced pressure to give 1.46 g of reaction crude. The crude was developed on a silica gel column chromatography with a mixed eluent of EtOAc and MeOH in 10:1 volume ratio to obtain 478 mg (55% yield) of **17** as a colorless powder.

^{1}H-NMR δ($CDCl_3$, 400 MHz) 8.12 (m, 1H, Ns), 7.94–7.99 (m, 2H, NB), 7.84–7.91 (m, 1H, Ns), 7.72–7.78 (m, 2H, Ns), 7.69 (t, *J* = 7.6 Hz, 1H, NB), 7.44 (t, *J* = 8.2 Hz, NB), 6.50 (t, *J* = 4.0 Hz, 1H), 6.33 (t, *J* = 4.0 Hz, 1H), 5.87 (brs, 1H), 5.42 (d, *J* = 7.8 Hz, 1H), 3.99 (dd, *J* = 4.0, 16.0 Hz, 1H), 3.18–3.81 (m, 15H), 2.75 (t, *J* = 8.0 Hz, 2H), 2.55–2.65 (m, 2H), 1.47–1.67 (m, 2H), 1.15–1.43 (m, 26H), 0.88 (t, *J* = 7.0 Hz, 3H).

2.2.8. Preparation of *N*-((19-bromo-14-hexadecyl-16-(2-nitrophenyl)-3,6,17-trioxa-9,14-diaza-nonadecyl)-10,13,18-trione)-2-nitrobenzene-sulfonamide (**18**)

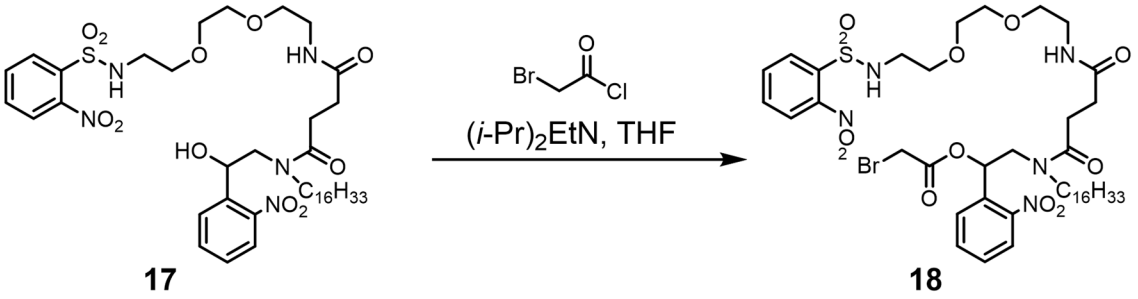

Figure 2-8: Esterification of 17 to form 18

To a solution of **17** (150 mg, 182 μmol) in a 15 mL of dry THF, bromoacetyl chloride (272 μL, 3.32 mmol), *N,N*-diisopropylethylamine (68.0 μL, 0.40 mmol) and 4-(dimethylamino)pyridine (DMAP, 5.00 mg) were added sequentially under nitrogen atmosphere, and the solution was stirred at 35 °C for 2 h. After addition of CH_2Cl_2, the reaction solution was washed with sat $NaHCO_3$ aq and water, and was dried over with Na_2SO_4. After evaporation of the solvent, the 240 mg of reaction crude was obtained, which was developed on a silica gel column chromatography using EtOAc as the eluent to give 98.7 mg (58% yield) of **18** as pale yellow oil.

^{1}H-NMR δ($CDCl_3$, 400 MHz): 8.15 (dd, J = 6.2 Hz, 3.4 Hz, 1H), 8.00 (d, J = 7.8 Hz, 1H), 7.71–7.82 (m, 2H), 7.65–7.70 (m, 1H), 7.46–7.57 (m, 1H), 6.52 (dd, J = 8.9 Hz, 3.4 Hz, 1H), 6.23–6.31 (m, 1H), 3.18–4.35 (m, 17H), , 2.55–2.80 (m, 4H), 1.46-1.70 (m, 2H), 1.17–1.43 (m, 26H), 0.88 (t, J = 7.0 Hz, 3H).

2.2.9. Preparation of 13-hexadecyl-11-(2-nitrophenyl)-7-(2-nitrophenyl-sulfonyl)-1,4,10-trioxa-7,13,18-triazacycloicosan-9,14,17-trione (**19**)

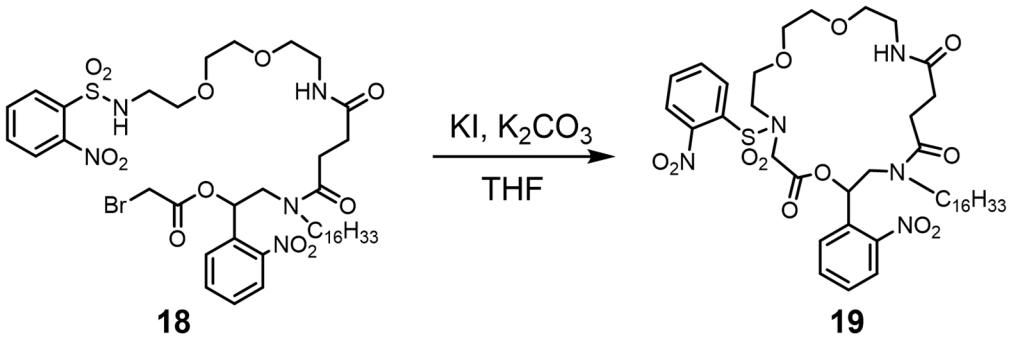

Figure 2-9: Cyclization reaction to form 19

In the presence of K_2CO_3 (28.0 mg, 200 μmol) and KI (17.4 mg, 150 μmol), **18** (150 mg, 182 μmol) in THF (120 mL) stirred at r.t. for 3 days. After the addition of CH_2Cl_2, the reaction solution was washed with water and dried over Na_2SO_4. Reaction crude (171 mg) was obtained after evaporation of the solvent, and was developed on a silica gel column chromatography with a mixed eluent of EtOAc and MeOH in 60:1 volume ratio to give 91.6 mg (67% yield) of **19** as pale yellow oil.

^{1}H-NMR δ($CDCl_3$, 400 MHz): 8.04 (d, J = 8 Hz, 1H), 8.00 (d, J = 7.2 Hz, 1H), 7.79–7.83 (d, 1H), 7.69–7.76 (m, 2H), 7.57–7.67 (m, 2H), 7.47–7.56 (m, 1H), 6.87 (t, J = 5.2 Hz, 3.4 Hz, 1H), 6.40–6.45 (m, 1H), 4.15–4.55 (m, 2H), 3.45–3.80 (m, 13H), 2.95–3.35 (m,

2H), 2.45–2.85 (m, 3H), 1.40–1.65 (m, 2H), 1.22–1.32 (m, 26H), 0.88 (t, *J* = 7.0 Hz, 3H). MS(ESI) *m*/*z* 884.80 ($M+Na^+$); HRMS(ESI) *m*/*z* found 884.40913 ($M+Na^+$) calc.

2.2.10. Preparation of 13-hexadecyl-11-(2-nitrophenyl)-1,4,10-trioxa-7,13,18-triazacycloicosan-9,14,17-trione (**20**) by deprotection of **19**.

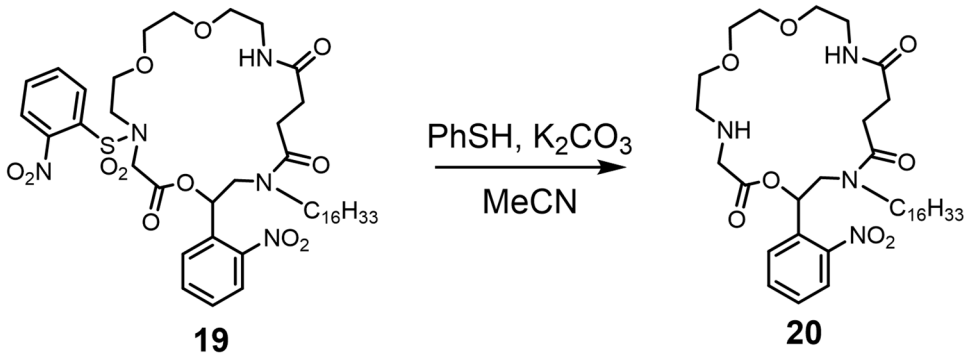

Figure 2-10: Deprotection of Ns group to form 20

The nosyl-protected compound **19** (72.8 mg, 85 μmol) was treated with PhSH (30.2 mg, 250 μmol) and K_2CO_3 (35.0 mg, 250 μmol) in MeCN (15.0 mL) for overnight at r.t.. After the addition of CH_2Cl_2, the reaction solution was washed with brine and was dried over Na_2SO_4. The solution was evaporated under reduced pressure to give reaction crude (225 mg). After the separation using a silica gel column chromatography with a mixed eluent of EtOAc and MeOH in 5:1 volume ratio, 53.5 mg (94% yield) of **20** was yielded as pale yellow oil.

^{1}H-NMR δ($CDCl_3$, 400 MHz): 8.04 (d, *J* = 8.2 Hz, 1H), 7.90 (d, *J* = 7.8 Hz, 1H), 7.71 (t, *J* = 7.8 Hz, 1H), 7.52 (t, *J* = 7.8 Hz, 1H), 6.86 (brs, 1H), 6.70 (d, *J* = 9.6 Hz, 1H), 4.51 (dd, *J* = 14.2 Hz, 10.1 Hz, 1H), 2.35–3.70 (m, 23H), 1.48–1.69 (m, 1H), 1.18–1.38 (m, 26H), 0.88 (t, *J* = 6.6 Hz, 3H).

HRMS(ESI) *m*/*z* found 677.44904 ($M+H^+$), $C_{36}H_{62}O_8N_4$ ($M+H^+$) requires 677.44839.

2.2.11. Preparation of 2,2,5,5-tetramethyl-3-(13-hexadecyl-11-(2-nitrophenyl)-1,4,10-trioxa-7,13,18-triazacycloicosan-9,14,17-trione-7-yl)carbonyldihydropyrrol-*N*-yloxyl radical (**1**)

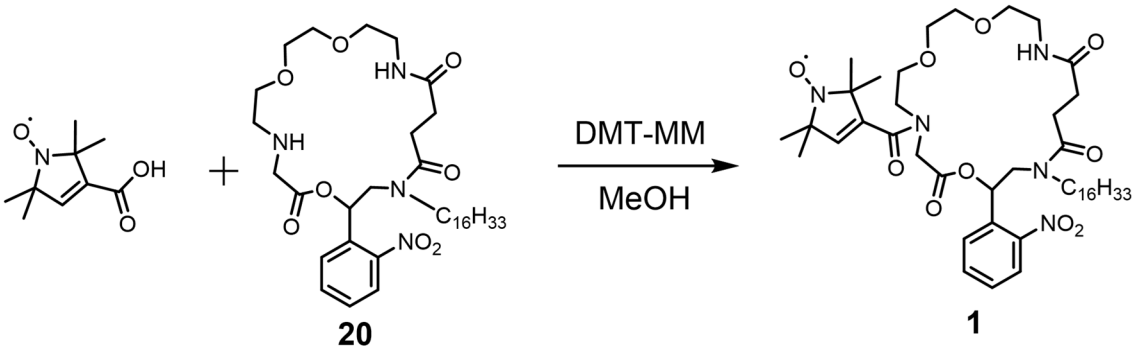

Figure 2-11: Synthesis of radical probe 1

To a 20 mL of MeOH solution of 2,2,5,5-tetramethyl-3-carboxy-3-pyrroline-1-oxyl radical (29.5 mg, 160 μmol) and **20** (53.5 mg, 79.1 μmol), DMT-MM (44.2 mg, 160 μmol) was added and the solution was stirred at r.t. for 3 days. After the addition of EtOAc, the reaction solution was washed with saturated $NaHCO_3$ aq and was dried over Na_2SO_4. The evaporation of the solvent gave 107.2 mg of reaction crude, which was developed on an octadecylsilyl silica gel column chromatography using a mixed solution of MeOH and water in 95:5 volume ratio as the eluent to give 8.70 mg (13% yield) of probe **1** as pale yellow oil.

MS(ESI) *m*/*z* 865.70 ($M+Na^+$), 843.70 ($M+H^+$); HRMS(ESI) *m*/*z* found 865.51685 ($M+Na^+$), $C_{45}H_{72}O_{10}N_5Na$ ($M+Na^+$) requires 865.51714.

2.3. Synthesis of radical probe **2**

2.3.1. Preparation of 2-(2-nitrophenyl)-1,3-dioxolane (**21**)

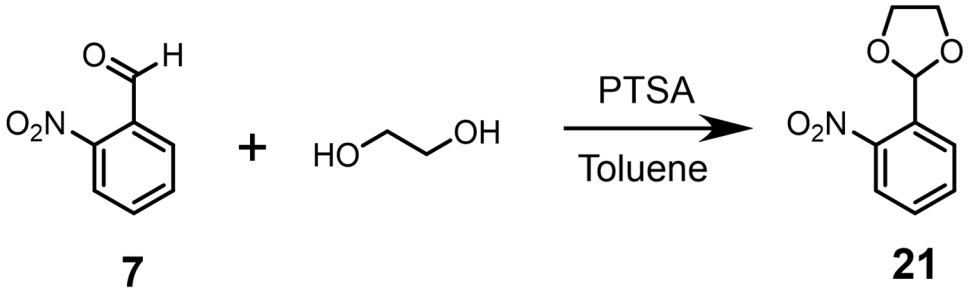

Figure 2-12: Oxolane formation from the corresponding benzaldehyde

To a toluene solution of **7** (3.00 g, 19.7 mmol), 6 mL of ethylene glycol and *p*-toluenesulfonic acid monohydrate (40.0 mg, 0.24 mmol) were added, and the reaction solution was refluxed for 18 h in a reactor fitted with a Dean-Stark apparatus. Then, the solution was washed by saturated $NaHCO_3$ aq and was dried over Na_2SO_4. After the evaporation of the solvent under reduced pressure, 3.82 g (99% yield) of **21** was obtained as pale yellow oil.

^{1}H-NMR δ($CDCl_3$, 400 MHz): 7.91 (d, J = 7.6 Hz, 1H), 7.81 (d, J = 7.6 Hz, 1H), 7.63 (t, J = 7.6 Hz, 1H), 7.51 (t, J = 7.6 Hz, 1H), 6.49 (s, 1H), 4.00–4.10 (m, 4H),

^{13}C-NMR δ($CDCl_3$, 100 MHz): 148.9, 133.3, 133.0, 129.8, 127.7, 124.5, 99.7, 65.4.

2.3.2. Preparation of 2-(2-hydroxyethoxy)-2-(2-nitrophenyl)acetonitrile (**22**)

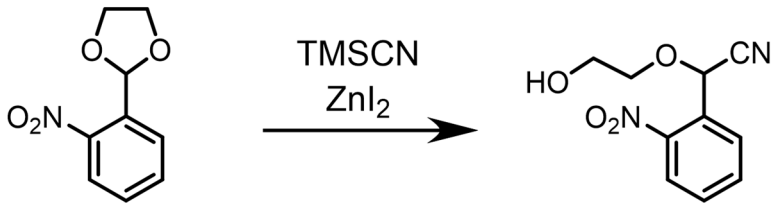

21 **22**

Figure 2-13: Synthesis of *o*-nitrobenzyl ether derivatives

Trimethylsilyl cyanide (TMSCN) (2.38 mL, 19.0 mmol) and ZnI_2 (150 mg) were added to **21** (3.52 g, 18.0 mmol) in a round-bottom flask. After 15 min stirring at r.t., 1 M HCl aq (15.0 mL) and CH_2Cl_2 (15.0 mL) were added, and the solution was vigorously stirred for 15 min. The organic layer was extracted three times with CH_2Cl_2, and was dried over Na_2SO_4. After the evaporation of the solvent under reduced pressure, 4.18 g of reaction crude was obtained and was developed on a silica gel column chromatography with the eluent of 3:1 mixture of *n*Hex and EtOAc to give 3.89 g (96% yield) of **22** as pale yellow oil.

^{1}H-NMR δ($CDCl_3$, 400 MHz): 8.14 (d, J = 7.6 Hz, 1H), 7.99 (d, J = 7.6 Hz, 1H), 7.78 (t, J = 7.6 Hz, 1H), 7.65 (t, J = 7.6 Hz, 1H), 6.06 (s, 1H), 4.00–4.07 (m, 1H), 3.85–3.90 (m, 2H), 3.78–3.84 (m, 1H), 1.96 (t, J = 6.0 Hz, 1H)

^{13}C-NMR δ($CDCl_3$, 100 MHz): 147.3, 134.4, 131.0, 129.1, 128.8, 125.6, 116.1, 72.8, 67.8, 61.5.

HRMS(ESI) *m/z* found 245.05372 ($M+Na^+$), $C_{10}H_{10}O_4N_2Na$ ($M+Na^+$) requires 245.05328.

2.3.3. Preparation of 2-(2-hydroxyethoxy)-2-(2-nitrophenyl)ethylamine (**25**)

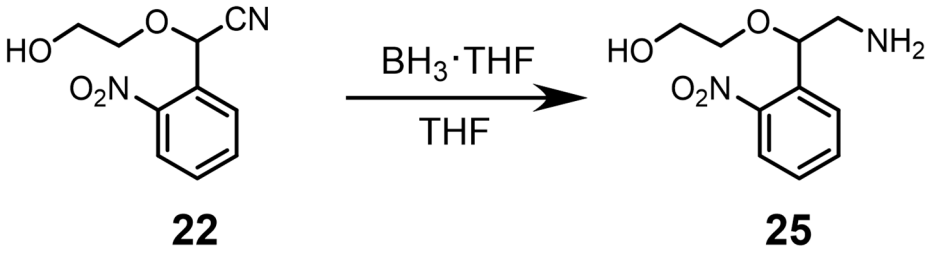

22 **25**

Figure 2-14: Reduction of 22 to form 25

A 1.0 M solution of BH_3·THF complex in THF (50 mL) was added into the solution of **22** (3.75 g, 16.9 mmol) in dry THF (15 mL). After refluxing for 1 h, the solution was cooled down to r.t. and was stirred for 2 h additionally. The alkaline solution by adding 1 M NaOH aq, the organic layer was extracted three times with EtOAc and was dried over Na_2SO_4. The crude afforded after evaporation of the solvent, was developed on a silica gel column chromatography using a mixed solvent of EtOAc, MeOH, and Et_3N in 80:20:1 volume ratio as the eluent to give 1.33 g (35% yield) of **25** as pale yellow oil.

^{1}H-NMR δ($CDCl_3$, 400 MHz): 8.00 (d, *J* = 8.4 Hz, 1H), 7.79 (d, *J* = 8.4Hz, 1H), 7.68 (t, *J* = 8.4 Hz, 1H), 7.46 (t, *J* = 8.4 Hz, 1H), 5.00 (dd, *J* = 2.4 Hz, 8.4 Hz 1H), 3.78 (t, *J* = 4.8 Hz, 2H), 3.60 (td, *J* = 4.8 Hz, 10.4 Hz 1H), 3.46 (td, *J* = 4.8 Hz, 10.4 Hz 1H), 3.15 (dd, *J* = 2.4 Hz, 12.8 Hz 1H), 2.86 (dd, *J* = 8.4 Hz, 12.8 Hz 1H), 2.24 (brs, 3H).

^{13}C-NMR δ($CDCl_3$, 100 MHz): 148.5, 136.4, 133.8, 128.6, 128.5, 124.8, 79.9, 71.7, 61.7, 48.5

HRMS(ESI) *m*/*z* found 227.10288 ($M+H^+$), $C_{16}H_{23}O_9N_3S$ ($M+H^+$) requires 227.10263.

2.3.4. Synthesis of 1-hexadecanal (**24**)

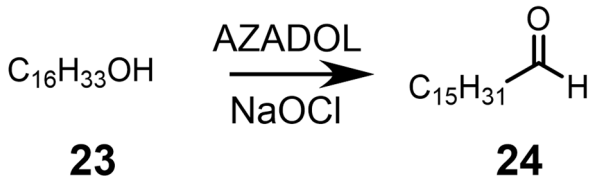

Figure 2-15: Oxidation of 23

In a 100 mL round-bottom flask, 1-hexadecanol **23** (3.00 g, 12.4 mmol) was dissolved in 30 mL of CH_2Cl_2. Then, the solution was cooled down to 0 ℃ after addition of 9 mL of $NaHCO_3$ aq and 3.00 mg (19.6 μmol) of AZADOL.

To the solution, a mixed solution of 5% NaOCl aq (23.7 mL) and sat $NaHCO_3$ aq (33 mL) was added dropwise, and the reaction solution was vigorously stirred at 0 °C for 40 min. After quenched by addition of 20% $Na_2S_2O_4$ (9 mL), the organic layer was extracted three times with ether and was dried over Na_2SO_4. After removal of the solvent under reduced pressure, 2.73 g (92% yield) of 1-hexadecanal **24** was obtained as a colorless powder.

^{1}H-NMR δ($CDCl_3$, 400 MHz): 9.77 (s, 1H), 2.43 (t, J = 7.5 Hz, 2H), 1.63 (quin, J = 7.4 Hz, 2H), 1.21–1.36 (m, 26H), 0.88 (t, J = 6.7 Hz, 3H).

2.3.5. Preparation of *N*-2-(2-hydroxyethoxy)-2-(2-nitrophenyl)ethyl-*N*-hexylamine (**26**)

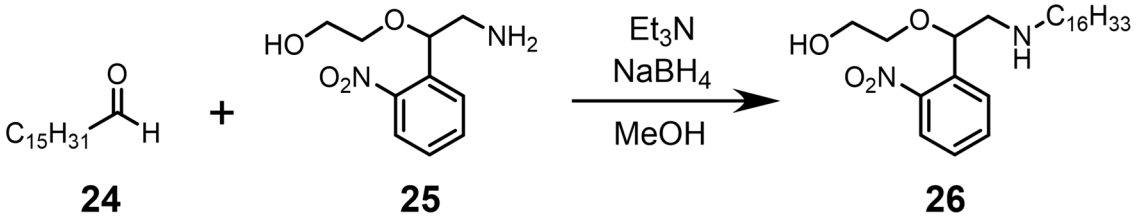

24 **25** **26**

Figure 2-16: Reductive amination of 25 with 24 to form 26

After 4 h stirring of a 30 mL CH_2Cl_2 solution of **24** (1.44 g, 6.00 mmol) and **25** (1.32 g, 5.85 mmol) at r.t., $NaBH_4$ (359 mg, 9.5 mmol) was added to the reaction solution, which was alkaline by the addition of 1 M NaOH aq after 30 min stirring at r.t.. The organic layer was extracted three time with CH_2Cl_2 and was dried over Na_2SO_4. The reaction crude was obtained after evaporation of the solvent, and developed on a silica gel column chromatography with a mixed solution of *n*Hex and EtOAc in 1:1 volume ratio to give 1.14 g (42% yield) of **26** as pale yellow oil.

^{1}H-NMR δ($CDCl_3$, 400 MHz): 8.00 (d, J = 8.4 Hz, 1H), 7.84 (d, J = 8.4 Hz, 1H), 7.67 (t, J = 8.4 Hz, 1H), 7.45 (t, J = 8.4 Hz, 1H), 5.16 (dd, J = 2.4 Hz, 8.4 Hz, 1H), 3.68–3.80 (m, 3H), 3.41–3.49 (m, 1H), 2.97 (dd, J = 2.4 Hz, 12.8 Hz, 1H), 2.61–2.83 (m, 3H), 1.53 (quin, J = 7.2 Hz, 2H), 1.20–1.35 (m, 26H), 0.88 (t, J = 6.8 Hz, 3H)

^{13}C-NMR δ($CDCl_3$, 100 MHz): 147.6, 137.1, 133.8, 128.5, 128.4, 124.6, 72.1, 61.8, 56.3, 49.6, 41.1, 31.9, 29.7, 27.3, 22.7, 14.1.

HRMS(ESI) *m*/*z* found 451.35295 ($M+H^+$), $C_{26}H_{47}O_4N_2$ ($M+H^+$) requires 451.35303.

2.3.6. Preparation of *N*-(19-hydroxy-14-hexadecyl-16-(2-nitrophenyl)-3,6,17-trioxa-9,14-diaza-nonadecyl-10,13-dione)-2-nitrobenzenesulfonamide (**27**)

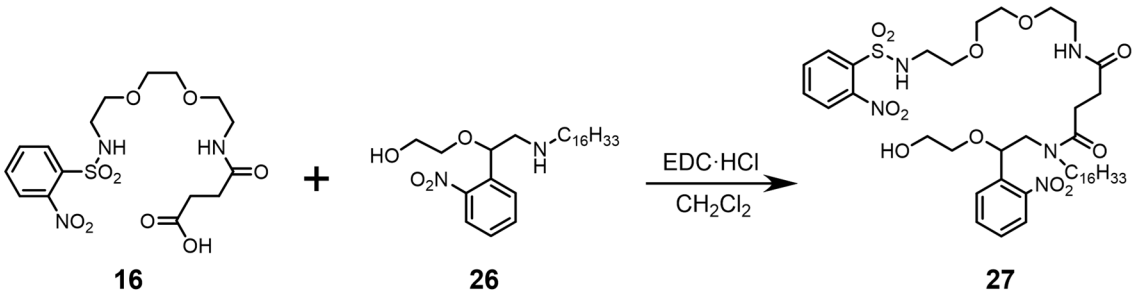

16 **26** **27**

Figure 2-17: Amide condensation between 16 and 26

To a solution of **16** (1.08 g, 2.50 mmol), EDC·HCl (575 mg, 3.00 mmol), and DMAP (15.0 mg) in CH_2Cl_2 (20 mL), **26** (0.98 g, 2.17 mmol) was added, and the solution was stirred at 0 °C for 4 h and then at r.t. overnight. After the addition of 0.1 M HCl aq (100 mL), the layers were separated, the aqueous layer was extracted with CH_2Cl_2, and the combined organic layers were washed with 10% NaCl aq and dried over Na_2SO_4. After removal of the solvent under reduced pressure, 2.81 g of crude product was obtained, which was developed on a silica gel chromatography using 600:50:1 (v/v/v) EtOAc/MeOH/Et_3N as the eluent to afford 1.36 g (72% yield) of **27** as a yellow oil of an isomeric mixture.

Major isomer:

^{1}H-NMR δ($CDCl_3$, 400 MHz): 8.12–8.15 (m, 1H), 8.03 (d, J = 8.2 Hz, 1H), 7.82–7.93 (m, 2H), 7.69–7.76 (m, 3H), 7.49 (d, J = 8.35 Hz, 1H), 6.55 (t, J = 5.5 Hz, 1H), 6.36–6.43 (br, 1H), 5.13 (t, J = 8.5 Hz, 1H), 3.62–3.76 (m, 3H), 3.14–3.60 (m, 19H), 2.35–2.78 (m, 2H), 1.42–1.64 (m, 2H), 1.2–1.35 (m, 26H), 0.87 (t, J = 6.8 Hz, 3H).

^{13}C-NMR δ ($CDCl_3$, 400 MHz): 173.8, 172.7, 148.6, 148.1, 135.7, 134.5, 134.0, 133.6, 132.8, 131.1, 129.0, 128.8, 125.5, 125.0, 76.6, 72.2, 70.5, 70.1, 69.2, 61.7, 53.0, 45.8, 43.7, 39.4, 32.0, 31.5, 29.8-28.9, 27.8, 27.2, 22.8, 14.2.

HRMS(ESI) *m*/*z* found 888.44061 ($M+Na^+$), $C_{42}H_{67}O_{12}N_5NaS$ ($M+Na^+$) requires 888.43991.

2.3.7. *N*-(14-(2-(2-methylsulfonyloxyethoxy)-2-(2-nitrophenyl)ethyl)-3,6-dioxa-9,14-diaza-triacontyl-10,13-dione)-2-nitrobenzenesulfonamide (**28**)

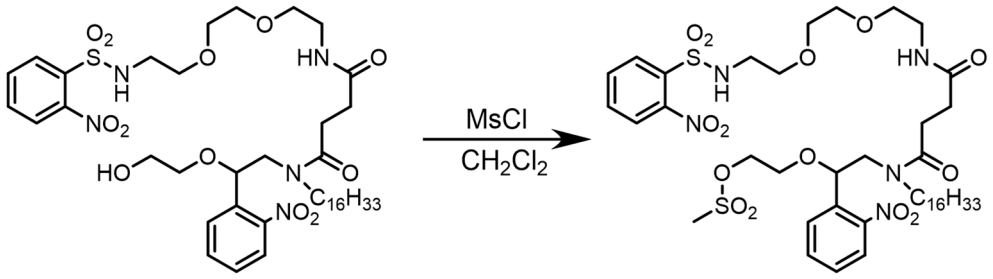

27 **28**

Figure 2-18: Mesylation of 27

To a solution of **27** (1.25 g, 1.44 mmol) in CH_2Cl_2 (10 mL), methanesulfonyl chloride (247 mg, 2.16 mmol) and Et_3N (291 mg, 2.88 mmol) were added sequentially at 0 °C, and the solution was stirred at 0 °C for 4 h. The organic layer was washed with saturated $NaHCO_3$ aq and dried over Na_2SO_4. After removal of the solvent under reduced pressure, the crude product (1.95 g) was developed on a silica gel column chromatography using 10:1 (v/v) EtOAc/MeOH as the eluent to give 1.28 g (87% yield) of **28** as a yellow oil of an isomeric mixture.

Major isomer: ^{1}H-NMR δ($CDCl_3$, 400 MHz): 8.12–8.17 (m, 1H), 8.06 (d, J = 8.2 Hz, 1H), 7.84–7.91 (m, 2H), 7.71–7.78 (m, 3H), 7.53 (t, J = 7.8 Hz, 1H), 6.52 (t, J = 5.2 Hz, 1H), 6.35 (t, J = 5.6 Hz, 1H), 5.18 (dd, J = 9.2 Hz, 2.5 Hz, 1H), 4.25–4.34 (m, 2H), 3.27–3.63 (m, 16H), 3.07 (s, 3H), 2.35–2.78 (m, 3H), 1.48–1.61 (m, 2H), 1.19–1.32 (m, 26H), 0.88 (t, J = 7.0 Hz, 3H).

Minor isomer: ^{1}H-NMR δ($CDCl_3$, 400 MHz): 8.12–8.17 (m, 1H), 7.84–7.91 (m, 2H), 7.71–7.78 (m, 3H), 7.66 (t, J = 7.8 Hz, 1H), 7.47 (t, J = 7.8 Hz, 1H), 6.49 (t, J = 5.2 Hz,

1H), 6.33 (t, *J* = 5.6 Hz, 1H), 5.22 (dd, *J* = 8.2 Hz, 4.1 Hz, 1H), 4.34–4.41 (m, 2H), 3.27–3.63 (m, 16H), 3.07 (s, 3H), 2.35–2.78 (m, 3H), 1.48–1.61 (m, 2H), 1.19–1.32 (m, 26H), 0.88 (t, *J* = 7.0 Hz, 3H).

HRMS(ESI) *m/z* found 966.41848 ($M+Na^+$), $C_{43}H_{69}O_{14}N_5NaS_2$ ($M+Na^+$) requires 966.41746.

2.3.8. Preparation of 13-hexadecyl-11-(2-nitrophenyl)-7-(2-nitrophenyl-sulfonyl)-1,4,10-trioxa-7,13,18-triazacycloicosan-14,17-dione (**29**)

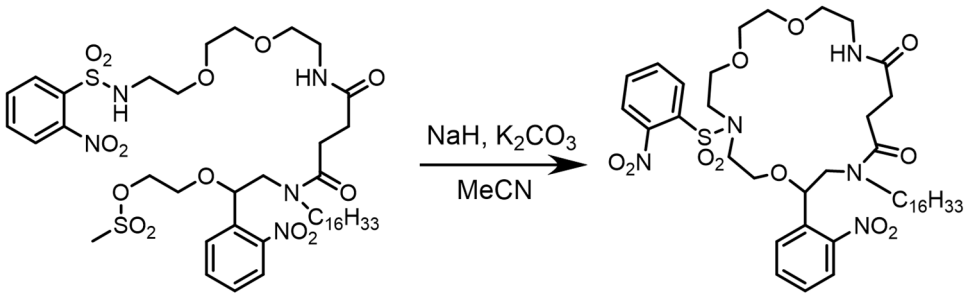

28 **29**

Figure 2-19: Cyclization reaction of 28 to form 29

To a solution of **28** (450 mg, 0.477 mmol) in 300 mL of MeCN, K_2CO_3 (35.0 mg, 0.25 mmol) was added, and then NaH (60% in paraffin oil, 120 mg, 3.00 mmol) was added. After stirring for 20 h at 50 °C under a nitrogen atmosphere, saturated NH_4Cl (aq) was added, and the mixture was extracted with CH_2Cl_2. After washing the organic layer and removal of the solvent under reduced pressure, the crude product (587 mg) was developed on a silica gel column chromatography using 30:1 (v/v) EtOAc/MeOH as the eluent to give 302 mg (75% yield) of **29** as a yellow oil of an isomeric mixture.

Major isomer: ^{1}H-NMR δ($CDCl_3$, 400 MHz): 8.02–8.08 (m, 1H), 7.96–8.01 (m, 1H), 7.60–7.79 (m, 5H), 7.49–7.55 (m, 1H), 6.62 (t, *J* = 5.4 Hz, 1H), 5.06 (dd, *J* = 9.6, 1.6 Hz, 1H), 3.0–3.85 (m, 21H), 2.65–2.80 (m, 1H), 2.50–2.60 (m, 2H), 1.16–1.36 (m, 2H), 1.13–1.39 (m, 26H), 0.88 (t, *J* = 7.0 Hz, 3H).

^{13}C-NMR δ($CDCl_3$, 100 MHz): 173.1, 172.4, 149.0, 148.0, 135.1, 134.5, 133.7, 133.6, 131.9, 130.4, 129.3, 128.3, 125.1, 124.3, 76.6, 70.9, 70.1, 70.1, 69.6, 69.0, 53.0, 49.0, 48.4, 45.6, 39.3, 32.5, 31.9, 29.8-29.3, 27.7, 27.1, 22.7, 14.2.

Minor isomer: ^{1}H-NMR δ($CDCl_3$, 400 MHz): 8.02–8.08 (m, 1H), 7.88 (d, *J* = 8.2 Hz, 1H), 7.60–7.79 (m, 5H), 7.49–7.55 (m, 1H), 7.06 (t, *J* = 5.8 Hz, 1H), 5.10 (dd, *J* = 4.6, 3.6 Hz, 1H), 4.06 (dd, *J* = 13.7, 8.2 Hz, 1H), 3.0–3.85 (m, 20H), 2.65–2.80 (m, 1H), 2.50–2.60 (m, 2H), 1.16–1.36 (m, 2H), 1.13–1.39 (m, 26H), 0.88 (t, *J* = 7.0 Hz, 3H).

^{13}C-NMR δ($CDCl_3$, 100 MHz): 173.1, 172.6, 148.3, 148.0, 134.8, 133.8, 133.7, 133.4, 131.8, 130.7, 128.9, 128.7, 124.3, 124.2, 75.4, 70.9, 70.1, 69.7, 69.5, 68.8, 51.2, 49.0, 48.6, 48.3, 39.1, 32.3, 31.9, 29.8-29.3, 28.7, 26.8, 22.7, 14.2.

HRMS(ESI) *m*/*z* found 870.43016 ($M+Na^+$), $C_{42}H_{65}O_{11}N_5NaS_2$ ($M+Na^+$) requires 870.42935.

2.3.9. Synthesis of 13-hexadecyl-11-(2-nitrophenyl)-1,4,10-trioxa-7,13,18-triazacycloicosan-14,17-dione (**30**)

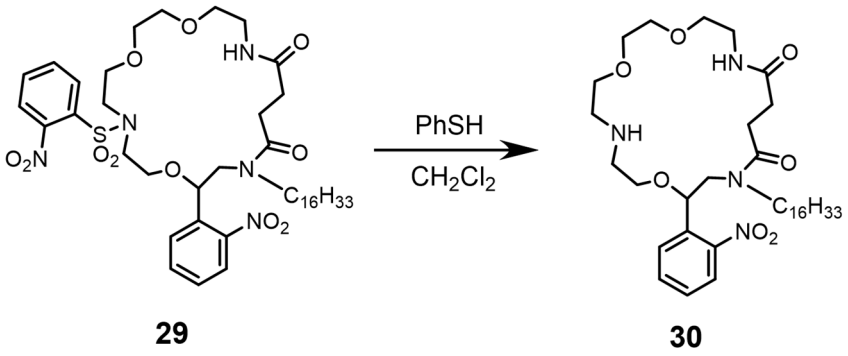

29 **30**

Figure 2-20: Deprotection of Ns group

To a solution of **29** (110 mg, 129 μmol) in 10 mL of MeCN, PhSH (15.7 mg, 143 μmol) and Cs_2CO_3 (84.7 mg, 260 μmol) were added sequentially. After stirring at r.t. for 5 h, the reaction mixture was washed with brine, extracted three times with CH_2Cl_2, and the combined organic layers were dried over Na_2SO_4. After removal of the solvent under reduced pressure, 118 mg of crude product was developed on a silica gel column chromatography with MeOH as the eluent to give 74.2 mg (86% yield) of **30** as a yellow oil.

Major isomer: ^{1}H-NMR δ($CDCl_3$, 400 MHz): 8.01–8.1 (m, 1H), 7.69–7.75 (m, 1H), 7.42–7.60 (m, 1H), 5.00–5.09 (m, 1H), 2.5–4.6 (m, 22H), 2.2–2.45 (m, 4H), 1.5–1.65 (m, 2H), 1.2–1.4 (m, 26H), 0.88 (t, J = 6.8 Hz, 3H).

Minor isomer: ^{1}H-NMR δ($CDCl_3$, 400 MHz): 7.42–7.96 (m, 4H), 4.81–4.98 (m, 1H), 2.5–4.6 (m, 22H), 2.2–2.45 (m, 4H), 1.5–1.65 (m, 2H), 1.2–1.4 (m, 26H), 0.88 (t, J = 6.8 Hz, 3H).

HRMS(ESI) *m*/*z* found 663.46970 ($M+H^+$), $C_{36}H_{63}O_7N_4S_2$ ($M+H^+$) requires 663.46913.

2.3.10. Synthesis of 2,2,5,5-tetramethyl-3-(13-hexadecyl-11-(2-nitrophenyl)-1,4,10-trioxa-7,13,18-triazacycloicosan-14,17-dione-7-yl)carbonylpyrrolidine-*N*-yloxyl radical (**2**)

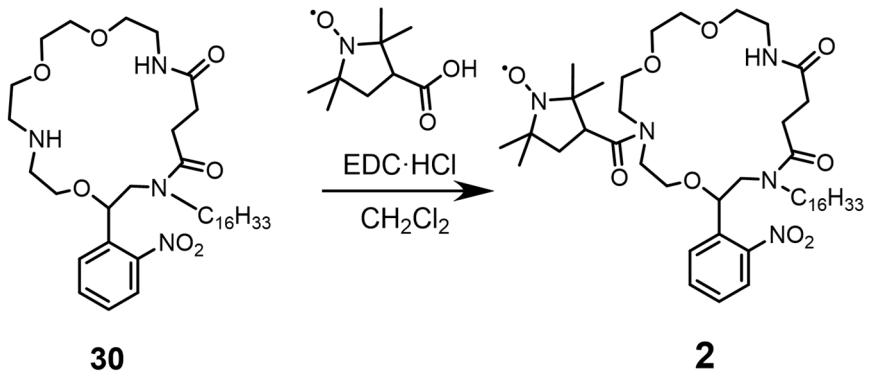

30 **2**

Figure 2-21: Synthesis of radical probe 2

To a solution of 2,2,5,5-tetramethyl-3-carboxypyrrolidinooxy radical (40.9 mg, 0.220 mmol) and **30** (120 mg, 0.181 mmol) in 10 mL of CH_2Cl_2, EDC·HCl (42.1 mg, 0.220 mmol) and DMAP (5.00 mg) were added, and the solution was stirred at r.t. for 20 h. The mixture was washed with saturated $NaHCO_3$ (aq), and the organic layer was dried over Na_2SO_4. The solvent was evaporated under reduced pressure to give 167 mg of crude product, which was developed on a silica gel column chromatography with 15:1 (v/v) EtOAc/MeOH as the eluent to give 98.7 mg (66% yield) of **2** as a yellow oil.

HRMS(ESI) *m/z* found 853.55407 ($M+Na^+$), $C_{45}H_{76}O_9N_5Na$ ($M+Na^+$) requires 853.55352.

2.4. Synthesis of radical probe **3**

2.4.1. Preparation of 18-t-butoxycarbonyl-13-hexadecyl-11-(2-nitrophenyl)-1,4,10-trioxa-7,13,18-triazacycloicosan (**33**)

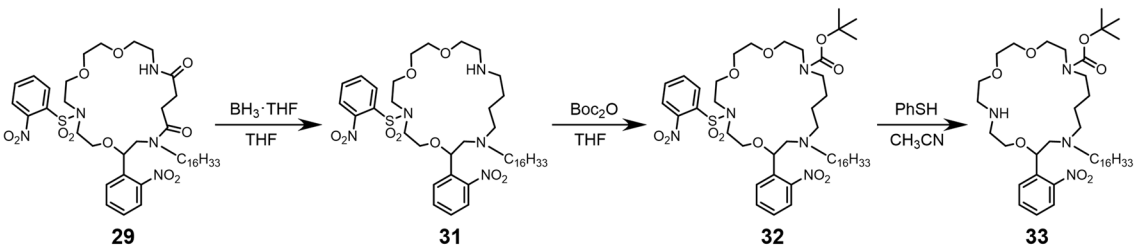

Figure 2-22: Synthesis of 33

To a dry THF solution of **29** (97.0 mg, 114 μmol), a 1.0 M solution of BH_3·THF complex in THF (1.4 mL) was added at r.t., and the solution was heated to 70 °C and was stirred for 2 h. After quenching the reaction by the addition of MeOH (0.5 mL), the solution was concentrated under reduced pressure. CH_2Cl_2 was added to the crude material, and the solution was washed by 2 M NaOH (10.0 mL). The extracted organic layer was dried over Na_2SO_4, and 93.8 mg of **31** was obtained after evaporation of the solvent.

Without further purification, **31** was dissolved in 8 mL of dry THF, and di-*t*-butyl decarbonate (BOC_2O, 46 μL, 200 μmol) and Et_3N (44 μL, 300 μmol) were added to the solution. After stirring at r.t. for 2 h, 10 mL of water was added to the solution, the mixture was extracted with CH_2Cl_2, and the organic layer was dried over Na_2SO_4. After removal of the solvent under reduced pressure, 142 mg of crude product was obtained, which was developed on a silica gel chromatography using 2:1 (v/v) *n*-Hex/EtOAc as the eluent to give 48.5 mg of a mixture of unreacted BOC_2O and **32**. According to the NMR signal intensities, this mixture was predicted to contain 4.9 mg of unreacted BOC_2O and 43.6 mg of **32**. To 5 mL of MeCN, 37 mg of the mixture (5 mL), PhSH (2.44 μL, 24 μmol),

and Cs_2CO_3 (14.1 mg, 43.4 μmol) were added sequentially. After stirring at r.t. overnight, the solution was washed with brine, and the organic layer was dried over Na_2SO_4. The crude product (24.4 mg) was obtained after removal of the solvent under reduced pressure. A silica gel column chromatography with a gradient elution of 5:1 (v/v) EtOAc/MeOH to MeOH afforded **33** (7.7 mg, 10.5 μmol) as a yellow oil. The net yield from **29** via the three steps was 12%.

^{1}H-NMR δ($CDCl_3$, 400 MHz): 7.92 (d, *J* = 7.9 Hz, 1H), 7.78 (d, *J* = 7.5 Hz, 1H), 7.64 (t, *J* = 7.6 Hz, 1H), 7.42 (t, *J* = 7.8 Hz, 1H), 5.10 (br, 1H), 3.55–3.72 (br, 7H), 3.27–3.51 (br, 5H), 2.78–2.94 (br, 4H), 2.62–2.78 (br, 5H), 2.43–2.62 (br, 3H), 1.36–1.74 (m, 15H), 1.2–1.35 (m, 26H), 0.88 (t, *J* = 6.9 Hz, 3H).

^{13}C-NMR δ($CDCl_3$, 100 MHz): 155.9, 148.7, 133.6, 128.8, 128.3, 124.4, 79.3, 77.3, 72.7, 71.0, 70.7, 70.5, 70.2, 68.7, 60.3, 54.8, 54.5, 49.5, 48.8, 47.1, 32.0, 29.8, 29.5, 28.6, 27.6, 22.8, 14.2.

HRMS(ESI) *m*/*z* found 735.56281 ($M+H^+$), $C_{41}H_{75}O_7N_4$ ($M+H^+$) requires 735.56303.

2.4.2. Preparation of 2,2,5,5-tetramethyl-3-(18-t-butoxycarbonyl-13-hexadecyl-11-(2-nitrophenyl)-1,4,10-trioxa-7,13,18-triazacycloicosan-7-yl)carbonylpyrrolidine-*N*-yloxy radical (**34**)

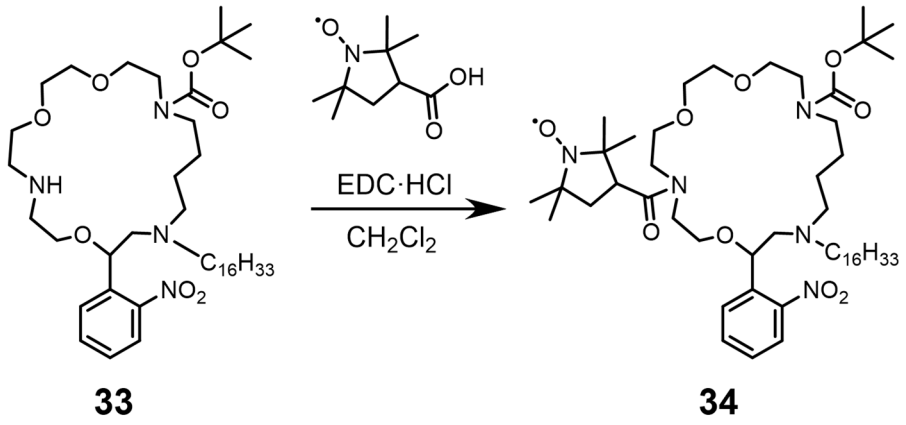

33 **34**

Figure 2-23: amide condensation between 33 and radical

To a solution of 2,2,5,5-tetramethyl-3-carboxypyrrolidinooxy radical (8.37 mg, 45 μmol) and **33** (29.9 mg, 40.7 μmol) in 2 mL of CH_2Cl_2, EDC·HCl (8.63 mg, 45 μmol) and Et_3N (7.00 μL, 50 μmol) were added, and the solution was stirred at 30 °C for 20 h. The solution was washed with saturated $NaHCO_3$ and was dried over Na_2SO_4. The solvent was evaporated under reduced pressure to give 39.2 mg of crude product, which was developed on a silica gel column chromatography with 1:1 (v/v) EtOAc/MeOH as the eluent to give 17.0 mg (46% yield) of **34** as a yellow oil.

HRMS(ESI) *m*/*z* found 903.66557 ($M+H^+$), $C_{50}H_{89}O_9N_5$ ($M+H^+$) requires 903.66548.

2.4.3. Preparation of 2,2,5,5-tetramethyl-3-(13-hexadecyl-11-(2-nitrophenyl)-1,4,10-trioxa-7,13,18-triazacycloicosan-7-yl)carbonylpyrrolidine-*N*-yloxyl radical (**3**)

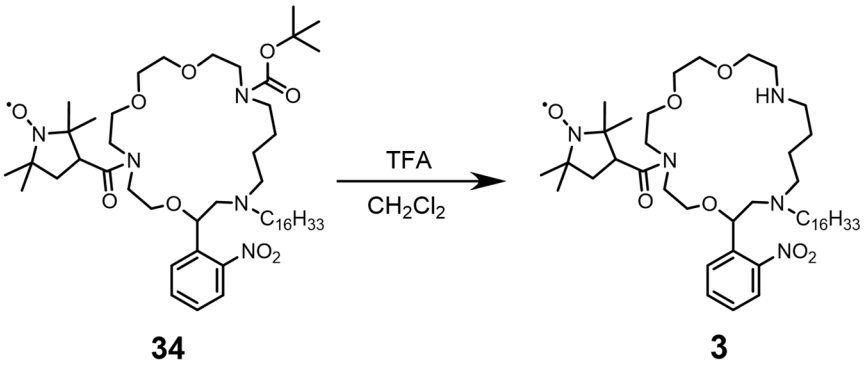

34 **3**

Figure 2-24: Synthesis of radical probe 3

To a solution of **34** (17.0 mg, 18.9 μmol) in 5.0 mL of CH_2Cl_2, 100 μL of TFA was added, and the solution was stirred at r.t. for 1 h. The reaction mixture was washed with sat $NaHCO_3$ aq, and the organic layer was dried over Na_2SO_4. After removal of the solvent under reduced pressure, the crude product (12.3 mg) was developed on a silica gel column chromatography using 1% MeOH in EtOAc as the eluent to give 4.00 mg (27% yield) of **3** as a yellow oil.

HRMS(ESI) *m*/*z* found 803.61512 ($M+H^+$), $C_{45}H_{81}O_7N_5$ ($M+H^+$) requires 803.61512.

2.5. Photolysis of radical probe **1**, **2**, and **3**

2.5.1. Tracking photolysis of radical probe **1**

A 0.07 mM methanolic solution of radical probe **1** was prepared, and 3 mL of the solution was replaced into a quartz cell of 1-cm optical path length. This cell was irradiated by a light (λ = 313 nm) using in an FP-8300 fluorometer (JASCO, Japan) using a xenon lamp as the light source. The change in the UV-vis absorption spectra was measured by a V650 UV-Vis spectrometer (JASCO, Japan), and the product analysis was carried out using a HPLC with an UV and a mass detectors. The measurement was carried out every 5-min until 20-min light irradiation. The eluent used in HPLC was 94:6 (v/v) MeOH/ water (0.05% TFA) and the selected wavelength was 254 nm.

2.5.2. Tracking photolysis of radical probe **2**

2.5.2.1. Tracking using a UV-vis absorption spectrometer

A 0.03 mM methanolic solution of radical probe **2** was prepared, and 3 mL of the solution was placed in a quartz cell of 1-cm optical path length. This cell was irradiated by a light (λ = 313 nm) using a REX-250 high-pressure mercury lamp (Asahi Spectra, Japan) as the light source. The absorption spectrum before and after 30 s of light irradiation was measured by a UV-vis spectrometer.

2.5.2.2. Traciking using a HPLC

The prepared 0.03 mM methanolic solution of radical probe **2** (200 μL) was placed in a quartz cell of 0.2 cm optical path length. This cell was irradiated by a light (λ = 313 and

248 nm) using the REX-250 high-pressure mercury lamp. The product analysis was carried out using HPLC every 5 s until 20 s of light irradiation. The eluent used in HPLC was 90:10 (v/v) MeOH/ water (0.05% TFA), and the selected wavelength was 254 nm.

2.5.3. Tracking photolysis of radical probe **3**

A 0.03 mM methanolic solution of radical probe **3** was prepared, and 200 μL of the solution was placed in a quartz cell of 0.2 cm optical path length. This cell was irradiated by a light (λ = 248 nm) using the REX-250 high-pressure mercury lamp. The product analysis was carried out using HPLC every 5 s until 20 s of light irradiation. The eluent used in HPLC was 1:1 (v/v) MeCN/ water (0.05% TFA), and the selected wavelength was 254 nm.

2.6. Preparation of radical probe incorporated vesicular dispersion

2.6.1 Preparation of DMPC, POPG liposome incorporated with radical probe

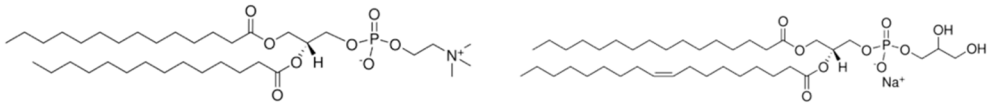

Figure 2-25: Structure of DMPC, POPG

A 60 mM solution of 1,2-dimyristoyl-sn-glycero-3-phosphorylcholine (DMPC) and a 0.60 mM solution of 1-palmitoyl-2-oleoyl-*sn*-glycero-3-phosphoglycerol (POPG) in 1:1 (v/v) MeOH/CH_2Cl_2 were placed in a glass vial; a 0.6 mM methanolic solution of radical probe was then added. Next, the solvent was removed under ambient pressure and the subsequent product was stored in a freezer for 1 day, resulting in a colorless thin film. To the thin film, 3 mL of distilled water was added. The mixture was kept at 40 °C in an ultrasonicator for 1 h, and the resulting dispersion was placed in a 10-mL syringe. A polyimide tube (inner diameter, 0.48 mm; length, 1 m), with one end connected to a glass vial, and the other connected to the syringe, was submerged in the ultrasonicator[36] (40 °C). Finally, the dispersion was allowed to flow into the tube using a syringe pump (YSP-101, YMC, Japan) to obtain the liposomal dispersion (Figure 2-26).

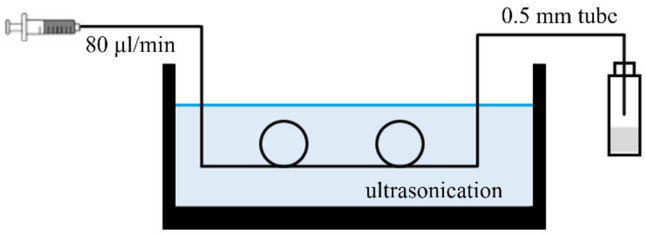

Figure 2-26: Scheme of ultrasonication using micro-channel

2.6.2. Preparation of DOPC, POPG liposome incorporated with a radical probe

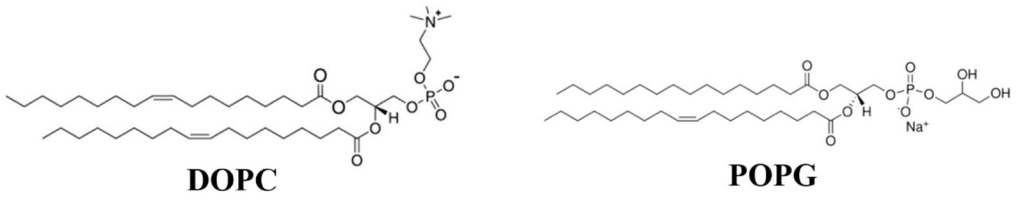

Figure 2-27: Structure of DOPC, POPG

A 45 mM solution of 1,2-dioleoyl-*sn*-glycero-3-phosphocholine (DOPC) in 1:1 (v/v) MeOH/CH_2Cl_2 and a 0.45 mM solution of POPG in 1:1 (v/v) MeOH/CH_2Cl_2 were placed in a glass vial, followed by the addition of a 0.6 mM methanolic solution of radical probe. Next, the solvent was removed under ambient pressure to be stored in a freezer for 1 day, resulting in a colorless thin film. To the thin film, 3 mL of distilled water was added. The mixture was kept at 30 °C in an ultrasonicator for 1 h, and the resulting dispersion was placed in a 10-mL syringe. A polyimide tube, with one end connected to a glass vial, and the other connected to the syringe, was submerged in the ultrasonicator (30 °C). Finally, the dispersion was allowed to flow into the tube using a syringe pump to obtain the

liposomal dispersion.

2.7. ESR and DNP-NMR instrument

2.7.1 ESR spectroscopy

ESR measurements were carried out using an X-band ESR spectrometer (JES-RE2X, JEOL, Japan) and a sample tube, both configured for DNP-NMR spectrometry, as described in this section. The microwave frequency was measured using a 53152A microwave counter (Keysight Technology, USA), and a manganese marker was used as the reference. The shape analysis was carried out using the chili function of EasySpin, an open-source computational toolbox based on Matlab 2021a (Mathworks, USA).

2.7.2 Dynamic nuclear polarization NMR spectroscopy

The DNP-NMR spectrometer was built according to the description by Han.[37, 38] For the microwave irradiation, a microwave generator (E8257D-550, Keysight Technology, USA) and a microwave power amplifier (CA9350BW300-4646R, R&K Co., Ltd., Japan) were connected to the ESR spectrometer using a directional coupler (6194-30, ARRA Inc., USA) and a waveguide switch (WGS-106, NIKOHA, Japan) (Figure 2-28). The incident power and frequency of the microwave were monitored using the 53152A microwave counter, which was connected to the coupled port of the directional coupler (having a coupling factor of 30 dB). For the photolabile reaction, the REX-250 high-pressure mercury lamp unit (equipped with 248 nm and 313 nm bandpass filters), a quartz light guide, and a KLQ-5 high condensing lens (Asahi Spectra, Japan) was employed. For NMR spectrometry, an Apollo series NMR spectrometer with a power amplifier

(Techmag, USA) was used, controlled by NT-NMR software (Techmag, USA).

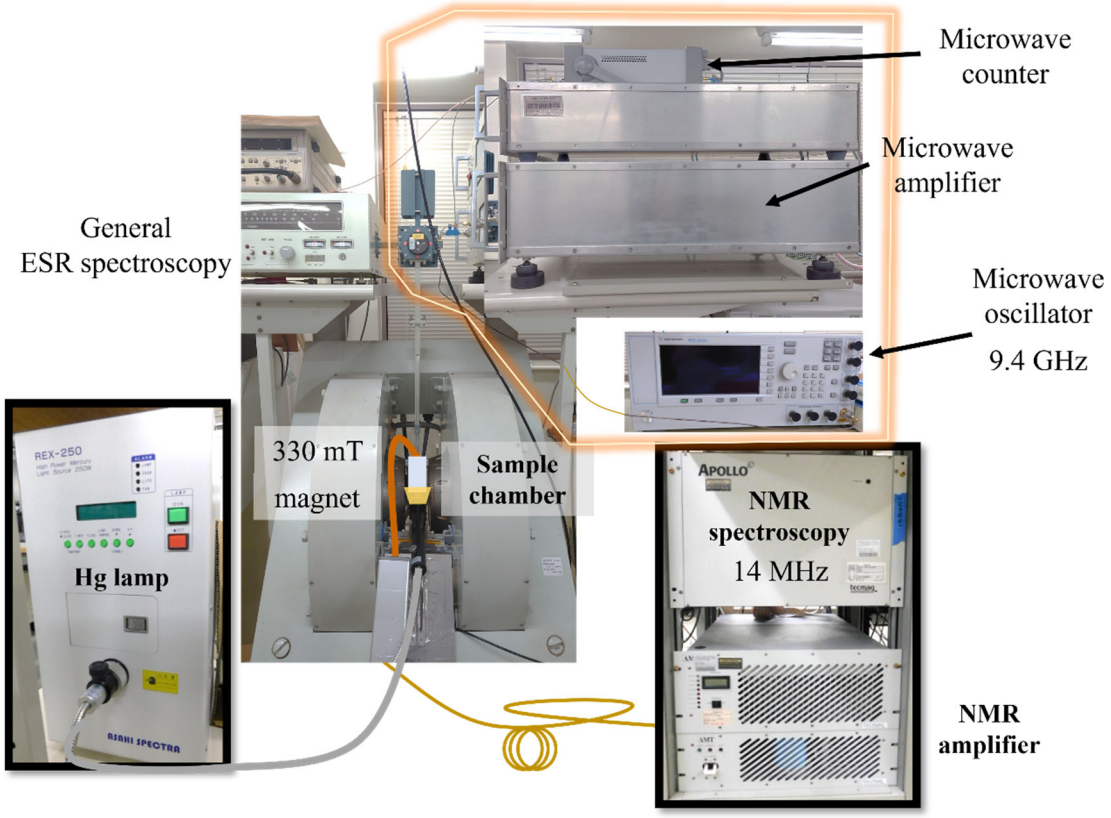

Figure 2-28: Scheme of DNP-NMR equipment

An rf-coil attached to a homemade sample tube holder was connected to a homemade tune-and-match circuit and an NMR circuit for 14-MHz measurements (Figure 2-29). The sample solution was filled up to a height of 0.7 cm in a 1.2-mm-diameter quartz capillary tube, and a heat sink Fluorinert FC-77 (3M, USA) was placed on the sample tube.[39] During the measurement, dried air was passed as a coolant at 10 L/min.

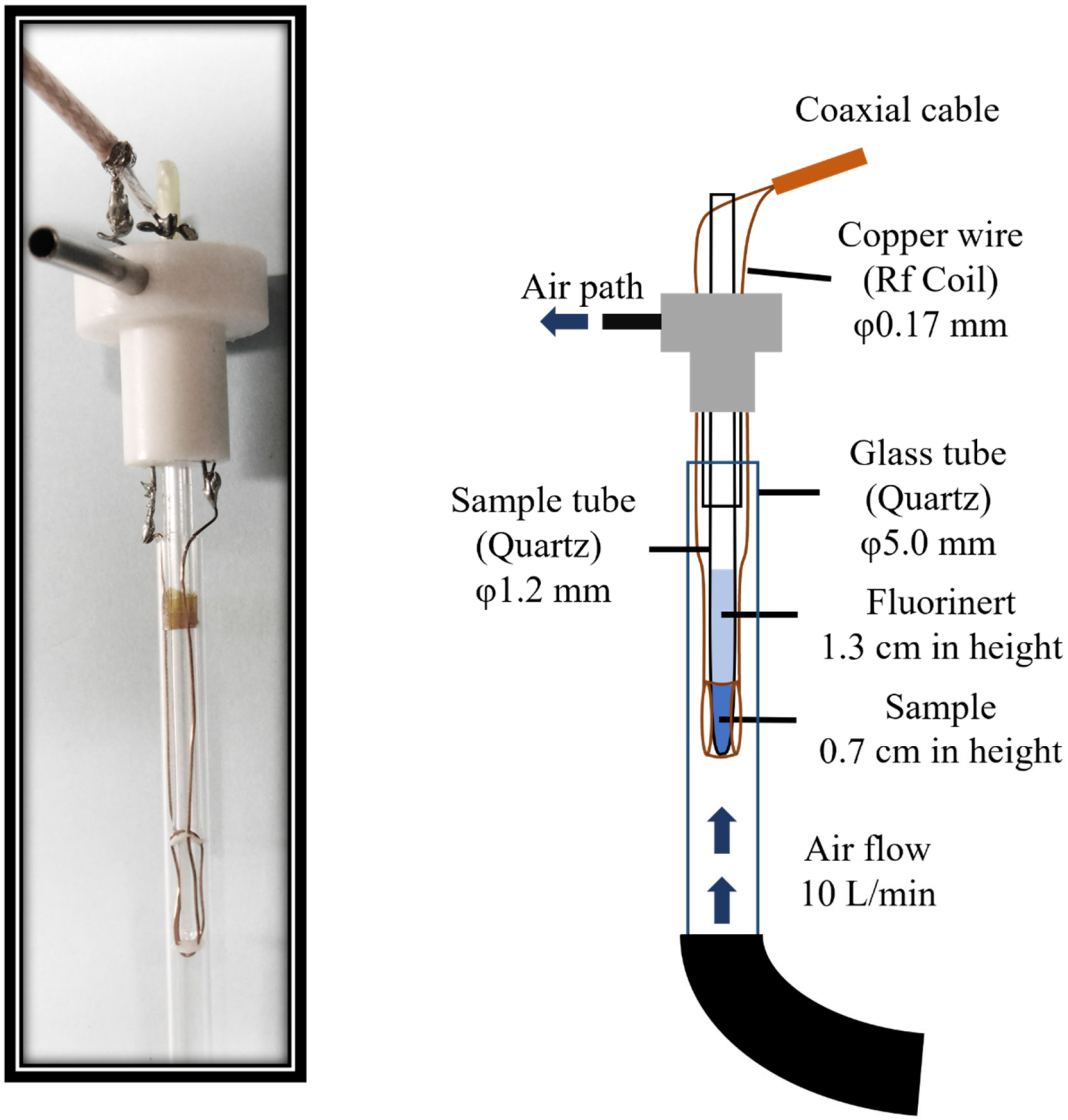

Figure 2-29: Scheme of sample holder

Chapter 3.

Chapter 3. Result & discussion

3.1. Synthesis and photolabile reaction of radical probe **1**

3.1.1. Design of radical probe **1**

For the comparative analysis of water of hydration surrounding the same phospholipid vesicles as those mentioned in our aim to develop the method (introduced in Chapter 1.7), we designed radical probe **1** (Figure 3-1).

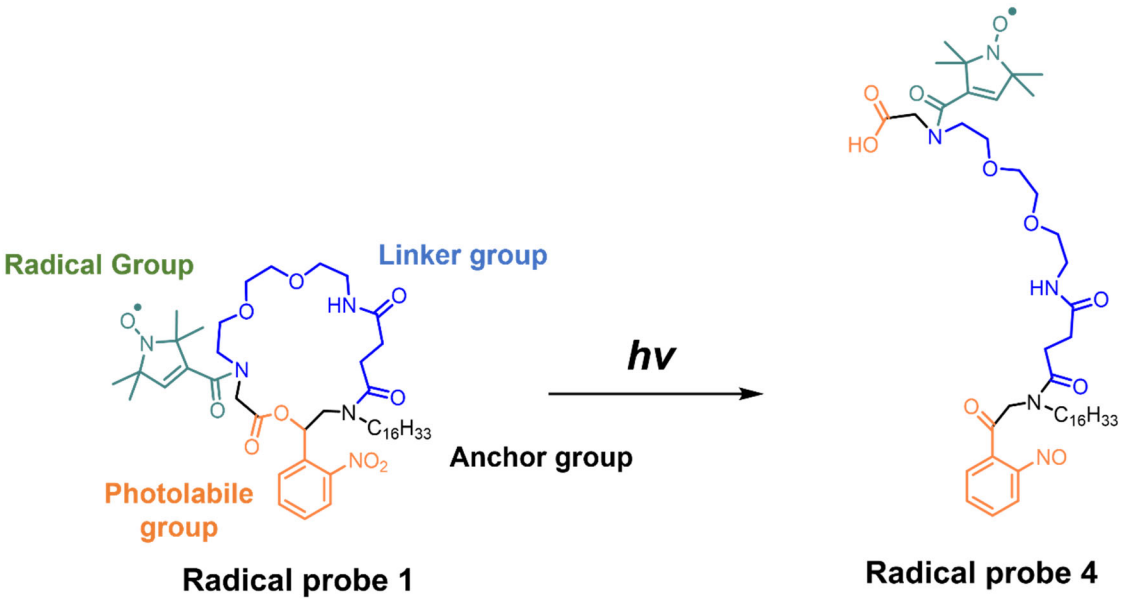

Figure 3-1: Configuration of radical probe 1

For the radical moiety, the 2,2,5,5-tetramethyl-3-carboxy-3-pyrroline-1-oxyl radical was employed because it is chemically stable.[40] The anchor site was designed to be a C16 alkyl chain to modify the radical probe corresponding to the hydrophobic part of its target liposome. The linker site was designed as a 13-member chain. Its length was decided to match the aim of switching the position of the radical moiety significantly relative to that of the anchored site using light irradiation. We also configured the hydrophilic ether and

amide groups in the chain to allow for their contribution to the linker parts in the hydrophilic region of the membrane.

Finally, the authors chose *o*-nitrobenzyl ester as the photocleavage group because carboxylate, which is a highly hydrophilic moiety, was expected to be produced. The photolysis of *o*-nitrobenzyl esters has been used for a moiety of photocaged compounds.[41–45]

3.1.2. Synthesis of radical probe **1**

The synthesis of radical probe **1** using photolabile group *o*-nitrobenzyl ester was carried out as shown in Figure 3-2.

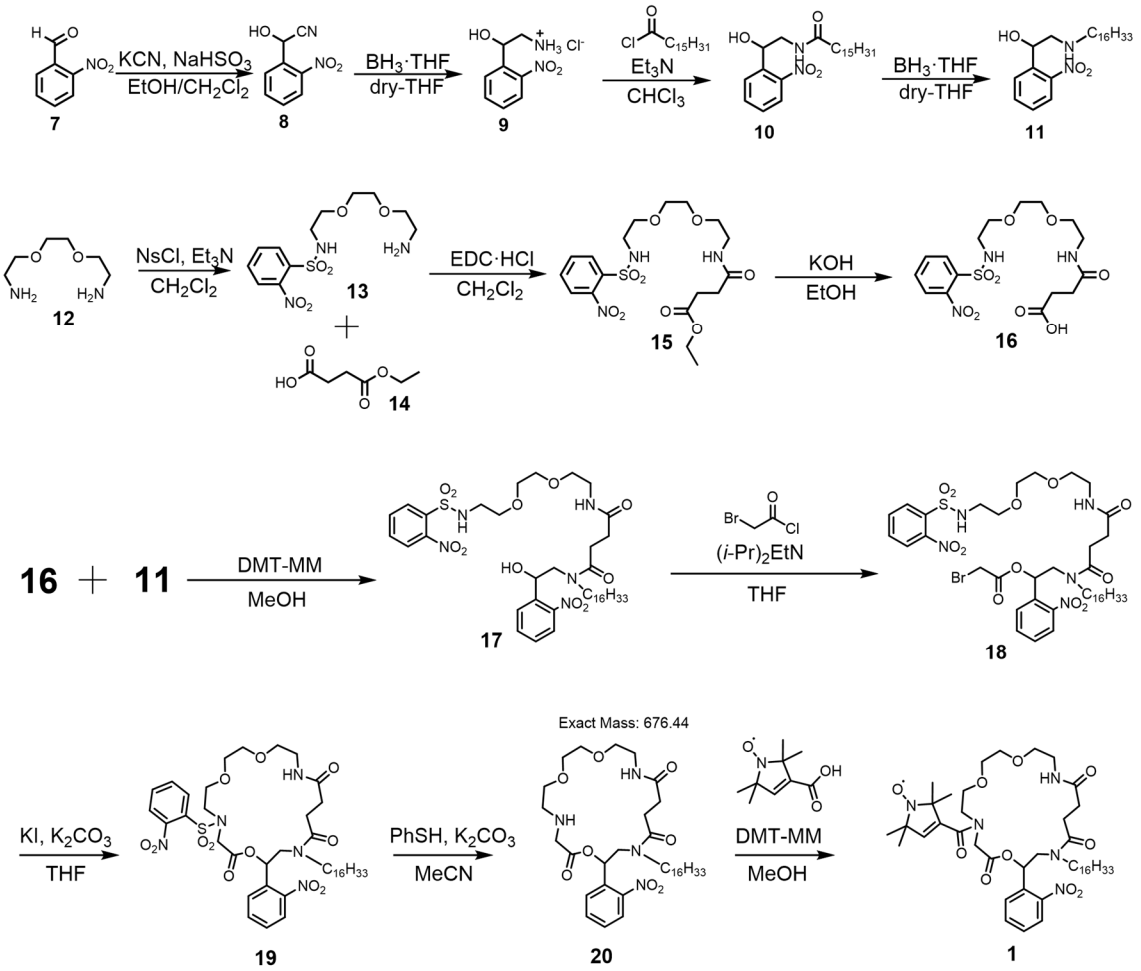

Figure 3-2: Synthesis scheme for radical probe 1

The starting material, *o*-nitrobenzaldehyde (**7**) was treated with potassium cyanide to give *o*-nitromandelonitrile (**8**) in a 93% yield. Subsequently, reduction of the nitrile was carried out using borane-tetrahydrofuran. For selectively reducing nitriles (without reducing nitro groups), borane-THF, a weaker reducing agent than $NaBH_4$, was used. HCl gas was passed over the resulting amine solution to obtain a hydrochloride salt of racemic 2-hydroxy-2-(2-nitrophenyl)ethylamine (**9**) in a 95% yield. Two general methods were considered for the alkylation of **9** to form **11.** One was reductive amination using imine intermediates, whereas the other was reduction post amide formation. Herein, we attempted the method of amide synthesis. The other method is described in Section 3.2.2. *n*-Hexadecenoic chloride was treated with **9** in the presence of triethylamine to obtain **10** in a 99% yield, followed by reduction of the amide with borane-THF to give 1-hexadecyl-2-hydroxy-2-(*o*-nitrophenyl) ethylamine (**11**) in 40% yield (Figure 3-3).

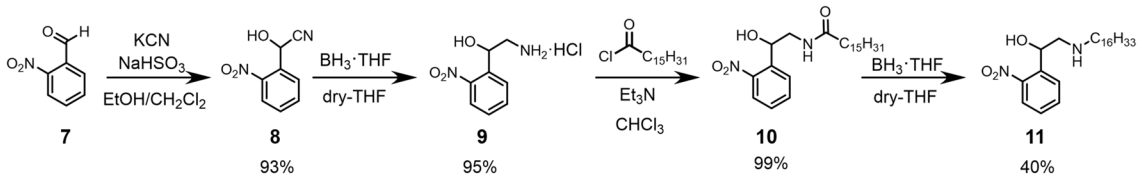

Figure 3-3: Four-step synthesis of 11 from starting material 7

For the preparation of the linker moiety, 1,2-bis(2-aminoethoxy)ethane (**12**) was selected as the starting material. Mono nosyl(Ns)-protected amine (**13**) was prepared by the treatment of *o*-nitrobenzelesulfonyl chloride (NsCl). In the presence of 1-(3-dimethylaminopropyl)-3-ethylcarbodiimide hydrochloride (EDC·HCl), a condensing agent, the condensation between mono-ethylscuccinate and **13** was carried out to give ethyl 13-(2-nitrophenylsulfonylamino)-8,11-dioxa-5-aza-tridecane-4-one-ate (**15**). The yield for the two-step synthesis from **12** was 32%. Next, hydrolysis of the ester of **15** with

potassium hydroxide gave the corresponding carboxylic acid, 13-(2-nitrophenyl-sulfonylamino)-8,11-dioxa-5-aza-tridecane-4-one-ic acid (**16**), in 98% yield (Figure 3-4).

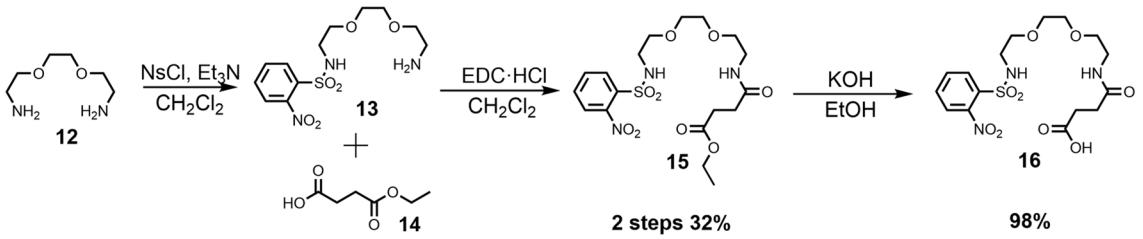

Figure 3-4: Three-step synthesis of 16 from 12

The amide condensation between the synthesized amine derivative **11** and the carboxylic acid derivative **16** was carried out using 4-(4,6-dimethoxy-1,3,5-triazin-2-yl)-4-methylmorpholinium chloride (DMT-MM),[46] and it afforded a 56% yield of *N*-(14-(2-hydroxy-2-(2-nitrophenyl)ethyl)-3,6-dioxa-9,14-diaza-triacontyl-10,13-dione)-2-nitrobenzenesulfon-amide (**17**) (Figure 3-5).

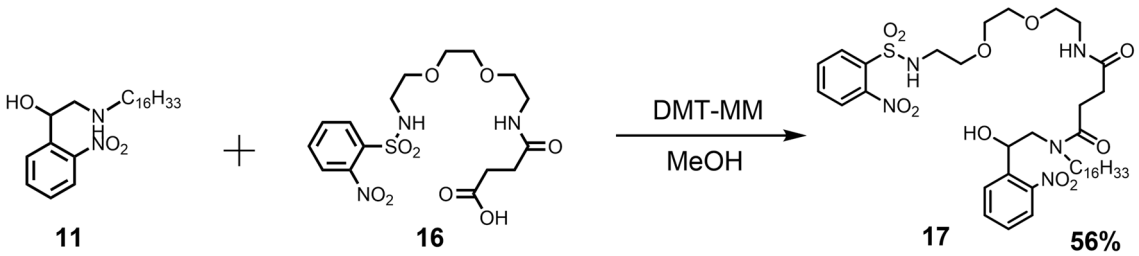

Figure 3-5: Synthesis of 17 using the condensation agent DMT-MM

From the next step, all synthetic experiments were conducted under dark conditions because of the photosensitivity of the compounds. Esterification between **17** and bromoacetyl chloride in the presence of *N*,*N*-diisopropylethylamine afforded a 58% yield of **18**. The cyclization of **18** was carried out using potassium iodide as a catalyst and potassium carbonate as a base. There are two reasons why the author used potassium iodide. The first reason was the expectation that potassium iodide would serve as a

template for cyclization. The nucleophilic substitution reaction between carbon bromide and nosyl-protected amine occurs both intra-molecularly and inter-molecularly, with the latter affording polymeric compounds (Figure 3-7). For the selective formation of **19**, the author added potassium ion as a template for cyclization, and also carried out the reaction at a relatively diluted condition, where the concentration of **18** was 1.5 mM. The second reason was the property of potassium iodide to improve the efficiency of the nucleophilic reaction by replacing the bromide of **18** with iodide, which is the better leaving atom, *in-situ*. As the result, the cyclization took place successfully and 13-hexadecyl-11-(2-nitrophenyl)-7-(2-nitrophenyl-sulfonyl)-1,4,10-trioxa-7,13,18-triazacycloicosane-9,14,17-trione (**19**) was obtained in a good yield of 65% (Figure 3-6).

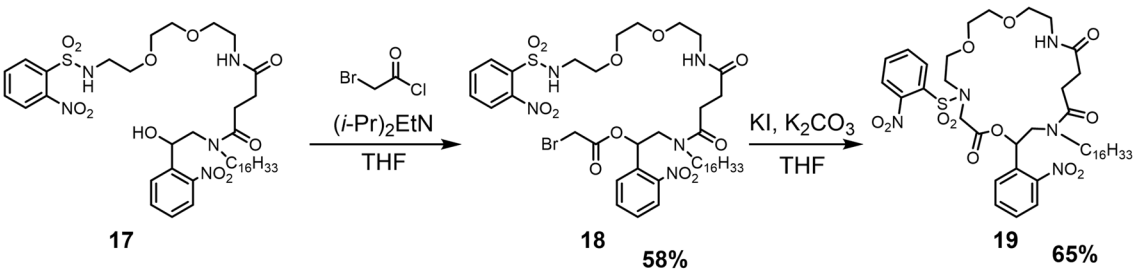

Figure 3-6: Two-step synthesis of compound 19 from 17

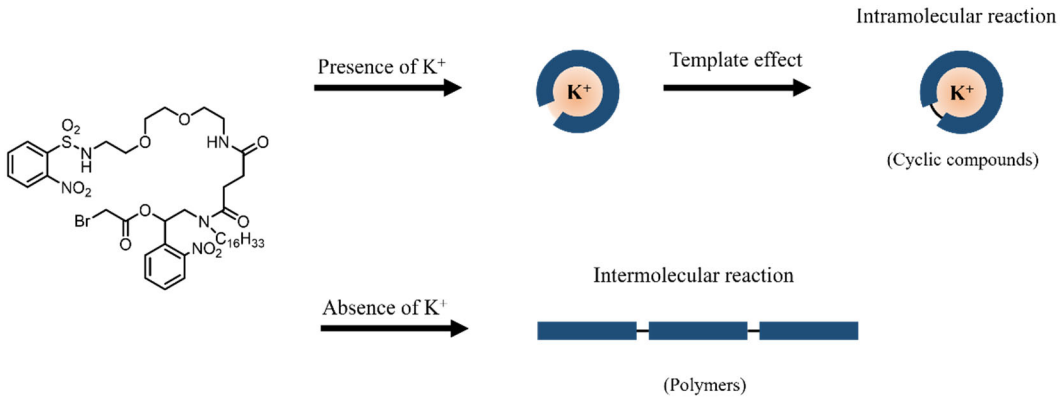

Figure 3-7: Template effect of potassium ions

For the deprotection of Ns group in **19**, benzenethiol was used as similar to the common method, and 13-hexadecyl-11-(2-nitrophenyl)-1,4,10-trioxa-7,13,18-triaza-cycloicosane-9,14,17-trione (**20**) was obtained in a 62% yield.

In the last step, the radical moiety (2,2,5,5-tetramethyl-3-carboxy-3-pyrroline-1-oxyl radical) was condensed to the secondary amines of **20**. Herein, DMT-MM was used as a condensation reagent. As a result, we successfully obtained the target material, 2,2,5,5-tetramethyl-3-(13-hexadecyl-11-(2-nitrophenyl)-1,4,10-trioxa-7,13,18-triazacycloicosan-9,14,17-trione-7-yl)carbonyldi-hydropyrrol-*N*-yloxy radical (**1**) in a 13% yield (Figure 3-8). The lower yield was assumed to be caused by the steric hindrance between DMT-MM and the cyclic substrate.

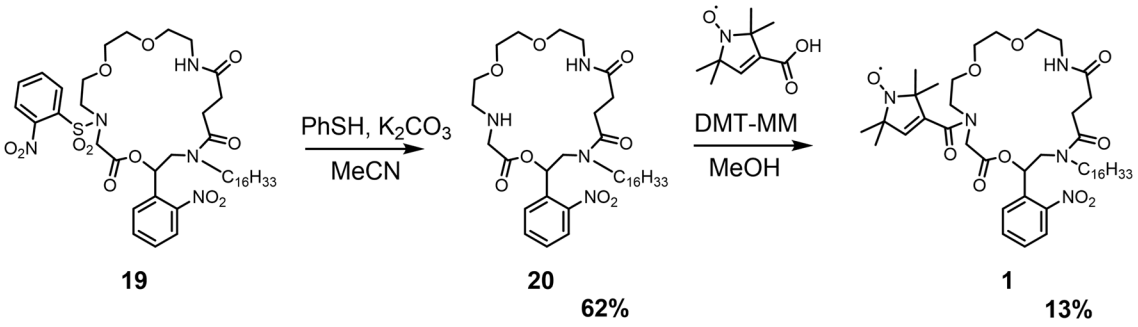

Figure 3-8: Deprotection of nosyl group and amide condensation to connect with the radical moiety

3.1.3 Tracking of photolysis of radical probe **1**

Light irradiation upon radical probe **1** was expected to cause C–O bond cleavage and the formation of radical probe **4**, as shown in Figure 3-9. In this section, we show the result of the photolysis of radical probe **1** upon 313-nm light irradiation.

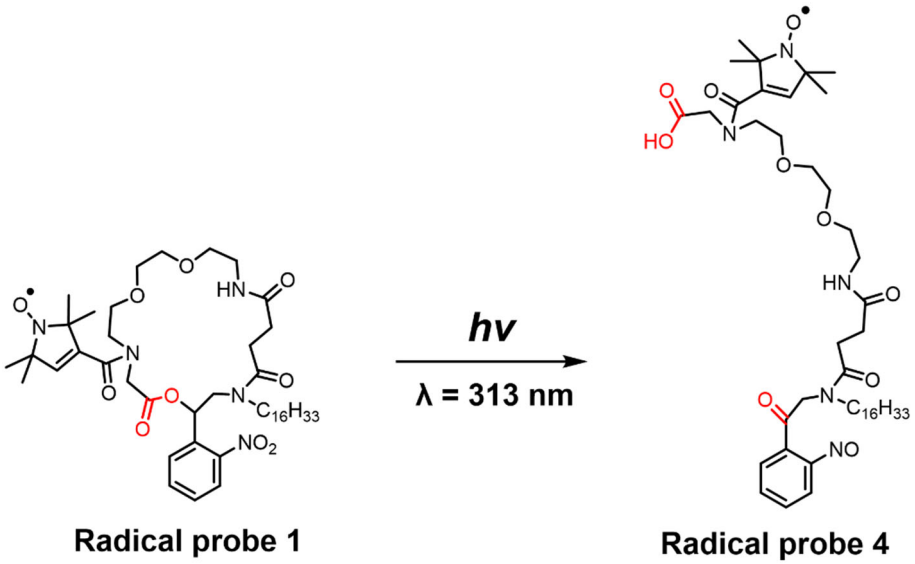

Figure 3-9: Structural change by light irradiation

The photolysis of **1** was tracked using HPLC; the photoconversion ratio was determined by the peak area in the chromatogram, and the products including **4** were determined using LCMS analysis. As shown in Figure 3-10, several byproducts other than **4** were formed upon exposure to the 313-nm light. Radical probe **4** was generated during the initial stage of the reaction; however, the amount of probe did not increase with further light irradiation. The conversion rate for **1** reached 38% and 60% upon 10 min and 20 minutes of irradiation, respectively; however, the peak area for **4** was smaller after 20 minutes compared to that after 10 minutes of irradiation. This suggests that a similar reaction occurred as the recently reported progression of the secondary reaction of *o*-nitrobenzyl ester derivatives by prolonged exposure by Yamaguchi et al.[47]

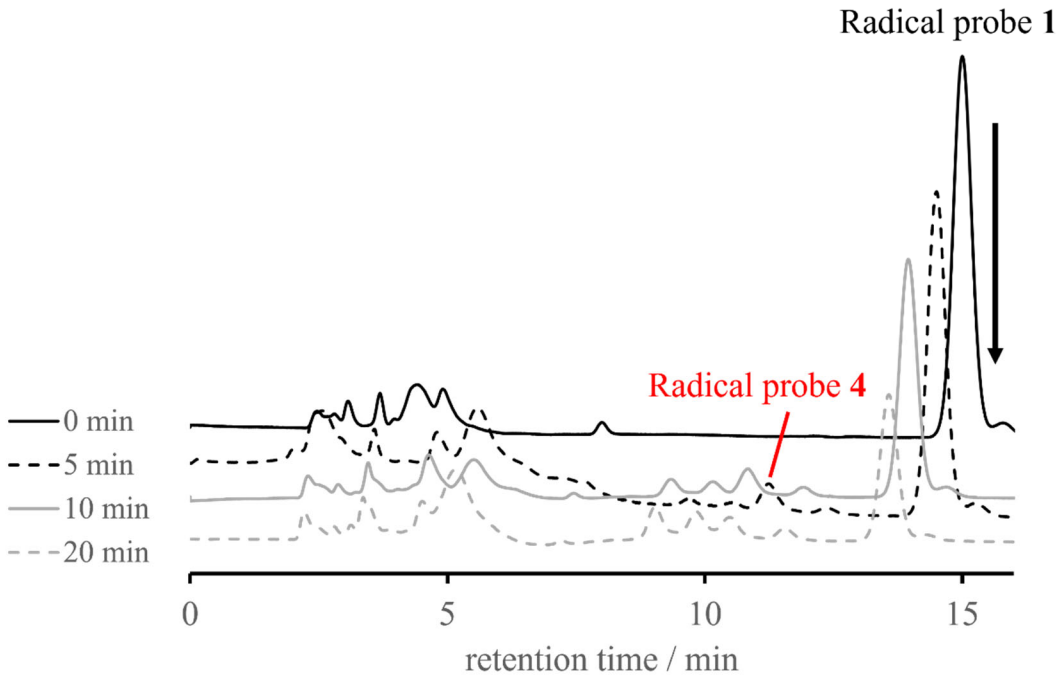

Figure 3-10: HPLC chromatograms of Radical Probe 1 before and after UV irradiation

The UV-vis absorption spectrum of radical probe **1** showed a shoulder at 260 nm; the absorbance decreased upon 313-nm light irradiation.[48] Meanwhile, absorption at 240 nm and 310 nm increased with photo-irradiation. The absence of an isobaric point of photolysis suggest that secondary reactions had occurred.

These experimental results showing the formation of secondary products indicate that radical probe **1** is not suitable for this study because of its insufficient photoreaction efficiency. To prevent the secondary reactions, we also increased the intensity and wavelength of the excitation light. However, the issue could not be resolved.

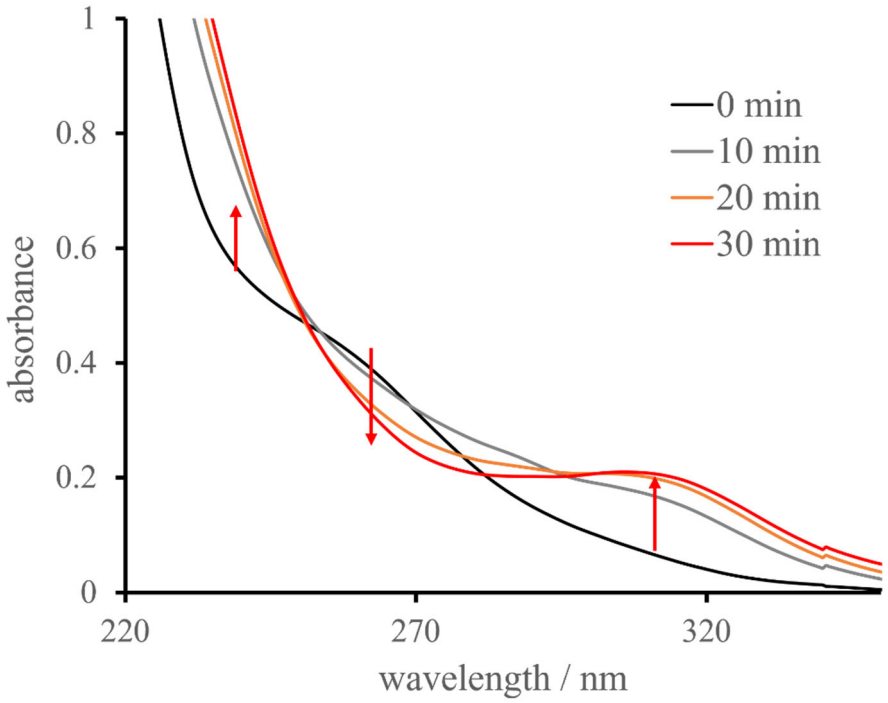

Figure 3-11: UV-Vis spectroscopy of 1 before and after light irradiation

3.1.4 Model experiments to determine a suitable light source and radical probe

Two model experiments were conducted to solve the problem described in Section 3.1.3. The first was to examine the light source for photolysis, and the second was to investigate suitable photolabile groups.

3.1.4.1 Comparison of light sources

The photolysis of 2-nitrobenzyl acetylphenylalaninate (**35**) was investigated to compare light sources for the photoreaction (Figure 3-12). Herein, the author compared a xenon lamp equipped with an FP-8300 fluorometer and a mercury lamp equipped with REX-250.

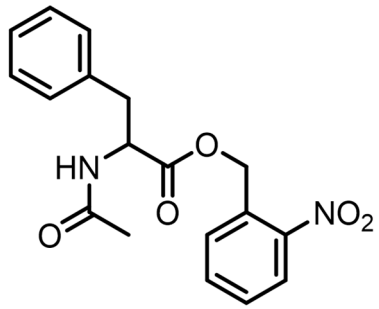

35

Figure 3-12: Model compound 35 with *o*-nitrobenzyl ester

Figure 3-13 shows the HPLC analysis of the photolysis of **35** using a xenon lamp. The results showed that the photoconversion ratio was 35% for 80 min of irradiation upon 313 nm light, and the secondary reaction proceeded similarly as in the case of radical probe **1**. By contrast, using the high-pressure mercury lamp, 55% of **35** was converted upon 313-nm light irradiation for 20 min (Figure 3-14). We expected that the use of a higher intensity light would prevent the secondary photoreaction as then a long-time exposure would not be required. However, the secondary reaction proceeded regardless of the intensity of light. Hence, we concluded that the *o*-nitrobenzyl ester group was not a suitable photolabile group for this research.

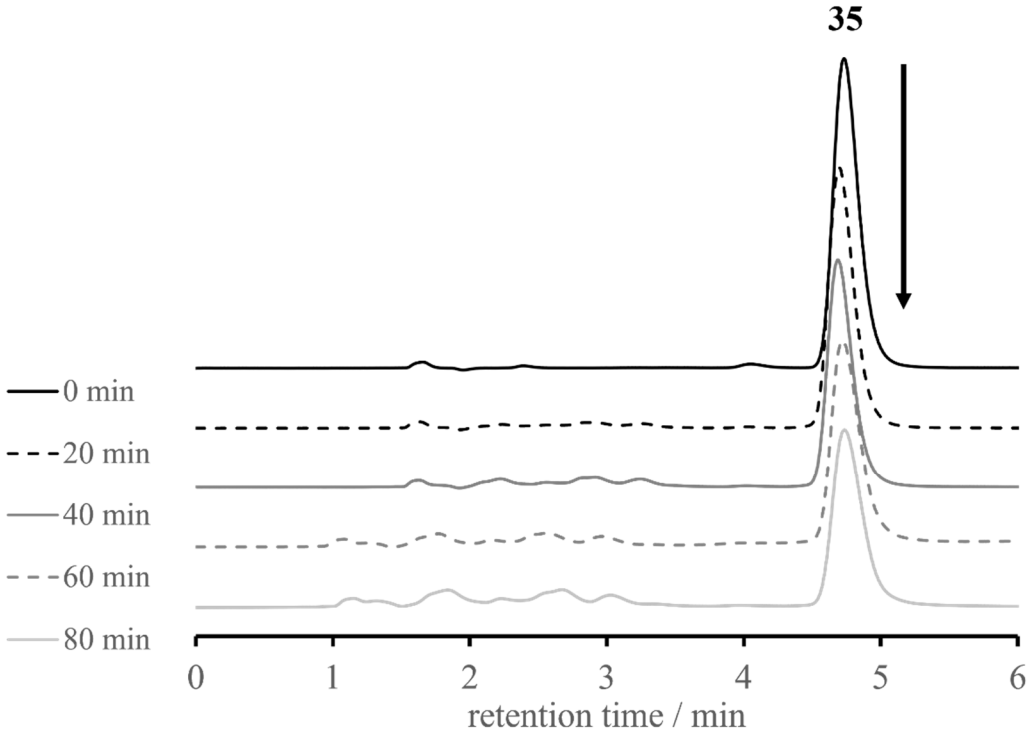

Figure 3-13: Tracking photolysis of 35 using xenon lamp

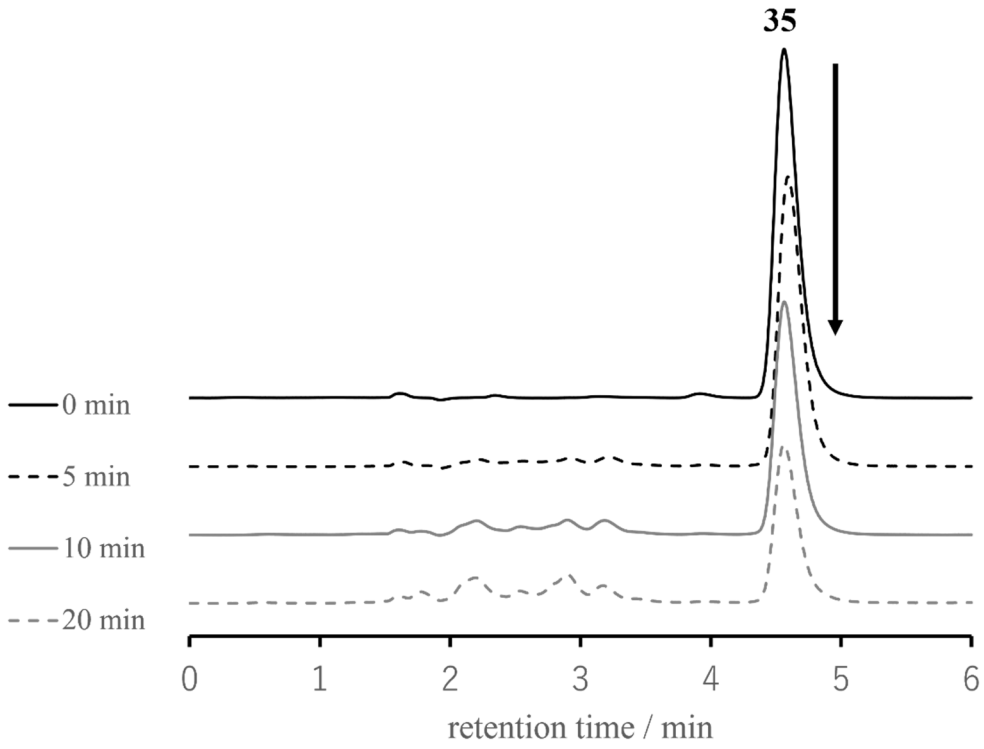

Figure 3-14 : Tracking photolysis of 35 using high-pressure mercury lamp

3.1.4.2 Comparison of photolysis of *o*-nitrobenzyl ester and *o*-nitrobeznyl ether

In addition to *o*-nitrobenzyl ester derivatives, photocleavage compounds incorporated *o*-nitrobenzyl ether derivatives were used in the study.[49–52] To evaluate the photolysis of *o*-nitrobenzyl ether derivatives, we tracked the photolysis of 1-(ethoxymethyl)-2-nitrobenzene (**36**) (Figure 3-15).

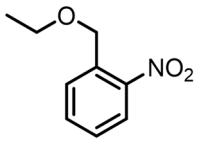

36

Figure 3-15: Model compound 35 with *o*-nitrobenzyl ether

When the mercury lamp was used, 64% of **36** reacted for 1 minute upon 313-nm light irradiation (Figure 3-16). Furthermore, the secondary reactions were suppressed because of the short light irradiation time. Hence, we decided to use *o*-nitrobenzyl ether derivatives as the probe to change the relative position of radicals upon light irradiation and redesigned the radical probe.

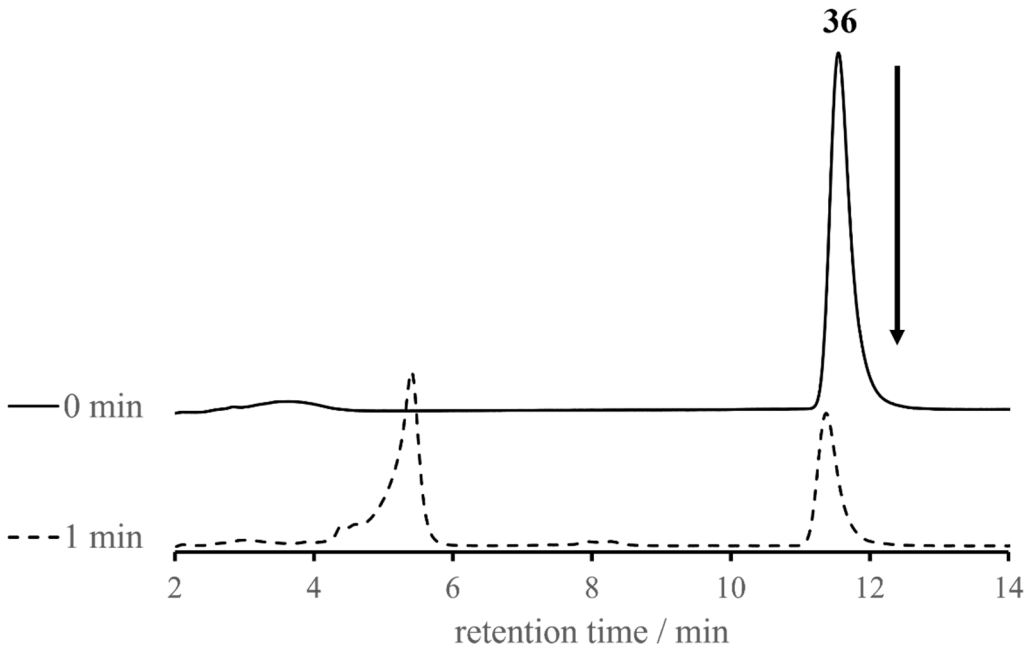

Figure 3-16: Tracking photolysis of 36 using high-pressure mercury lamp

3.2. HD-ODNP NMR measurement of water dynamics sensed with radical probe **2** and its photoproduct incorporated in phospholipid vesicles

3.2.1. Design of radical probe **2**

Based on the results of Section 3.1, the author redesigned the radical probe. A facile photocleavage reaction led to the design of radical probe **2**. Its photolabile group, *o*-nitrobenzyl ester was replaced with *o*-nitrobenzyl ether and its radical moiety, 2,2,5,5-tetramethyl-3-carboxypyrrolidinooxy radical was replaced with 2,2,5,5-tetramethyl-3-carboxy-3-pyrroline-1-oxyl radical (Figure 3-17). The anchor group and the linker group were not redesigned.

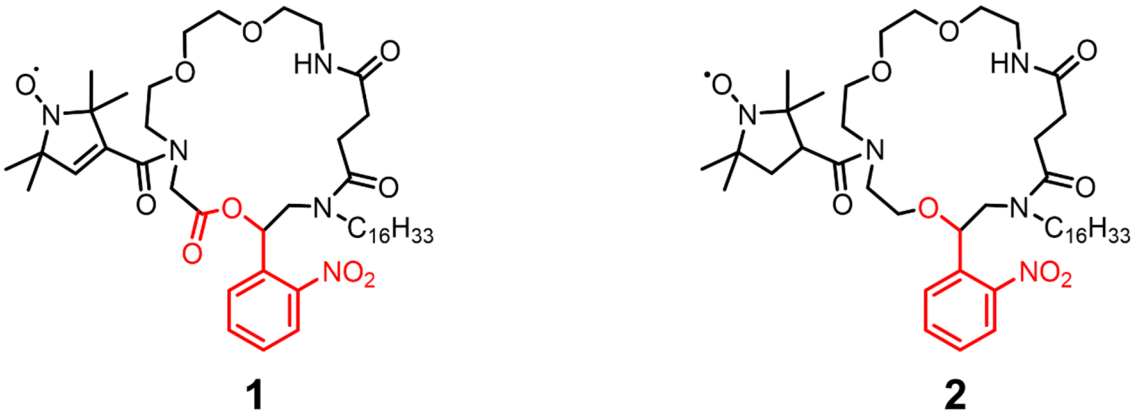

Figure 3-17: Comparison of structure of radical probe 1 and 2

3.2.2. Synthesis of radical probe **2**

For the preparation of an *o*-nitrobenzyl ether derivative, the author initially planned to employ Williamson etherification between an *o*-nitrobenzyl alcohol derivative (specifically, derivative of *o*-nitrobenzyl mandelic acid) and its corresponding bromoalkyl compound. However, presumably because of the acidity of the proton of benzyl position, the corresponding ether was not obtained. Next, the author attempted to prepare an *o*-nitorobenzylbromide derivative for the precursor of etherization with its corresponding alcohol; however, the bromide derivative was not obtained, presumably due to the steric hindrance. The author then investigated the availability of acid-catalyzed etherification between *o*-nitrobenzyl alcohol and aliphatic alcohol. However, the corresponding ether was not obtained. Based on these trials,[53] the author decided to employ acetal formation from *o*-nitrobenzyl aldehyde for the ether bond formation at the *o*-nitrobenzyl position. The overall synthetic route for the preparation of **2** is shown in Figure 3-18.

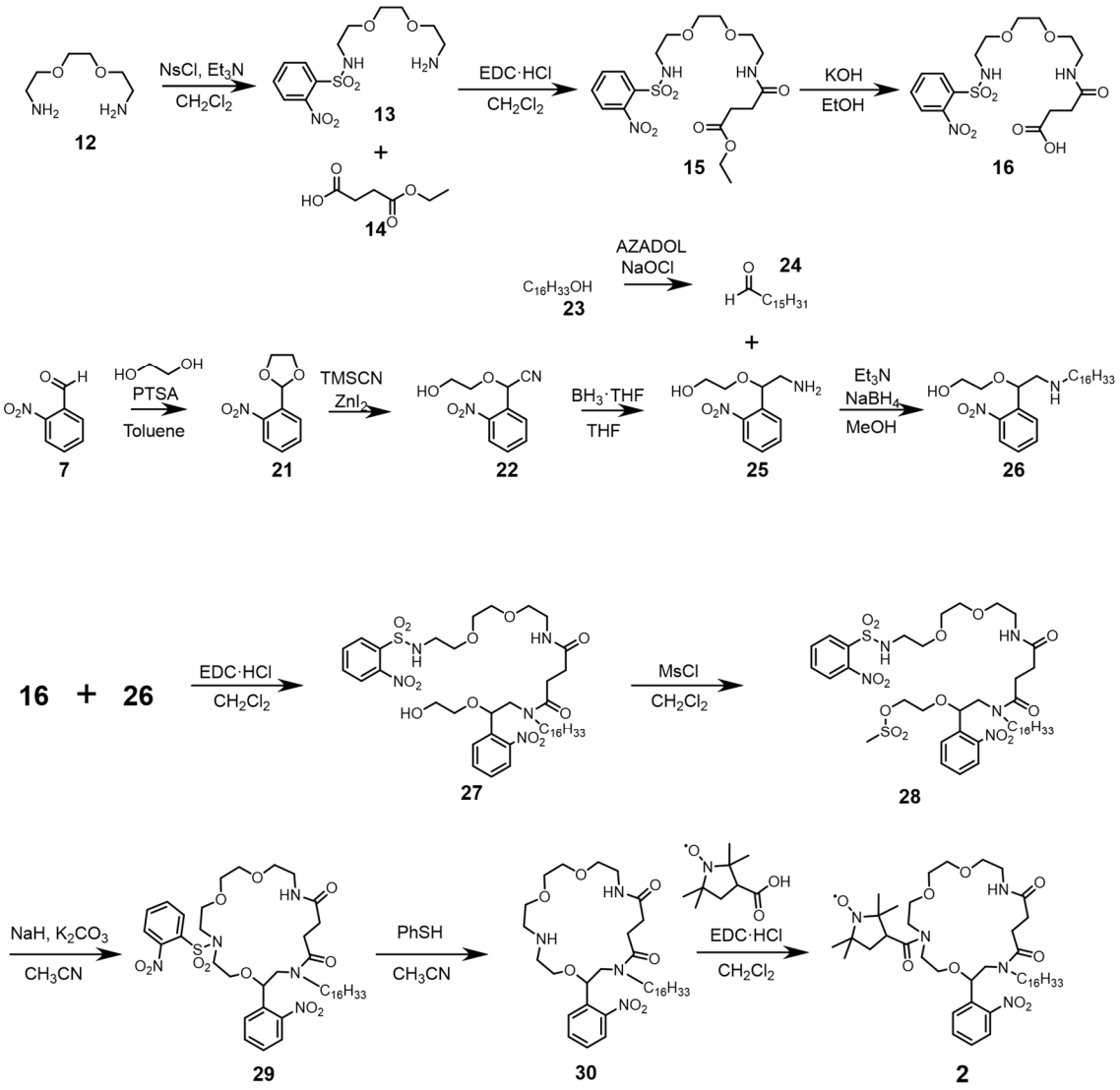

Figure 3-18: Scheme for synthesis of radical probe 2

All syntheses were carried out under dark conditions, except for the preparation of **16** from **12**, as shown in Section 3.1.2. Using compound **7** and ethylene glycol as starting materials, 2-(2-nitrophenyl)-1,3-dioxolane (**21**) was obtained in a 99% yield in the presence of *p*-toluenesulfonic acid as a catalyst.[54] Next, the formation of *o*-nitorobenzyl ether bond successfully resulted in 2-(2-hydroxyethoxy)-2-(2-nitrophenyl)acetonitrile (**22**) in a 96% yield using trimethylsilyl cyanide.[55] Subsequently, the reduction of **22** was carried out to obtain 2-(2-hydroxyethoxy)-2-(2-nitrophenyl)ethylamine (**25**) in a 35% yield (Figure 3-19).

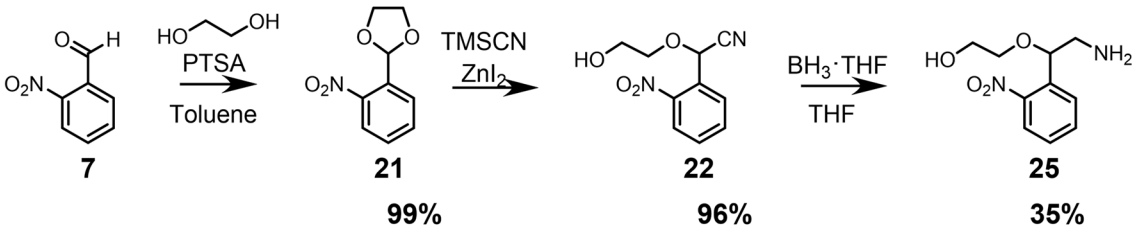

Figure 3-19: Three-step synthesis of 25 from 7

For the preparation of **1**, the alkyl chain of the anchor group was substituted via amide reduction; however, the yield of 40% was lower than what the author had expected. Therefore, reductive amination was employed for the preparation of **2**. For the preparation of 1-hexadecanal (**24**), the author employed 2-hydroxy-2-azaadamantane (AZADOL)[56, 57] mediated oxidation of 1-hexadecanol (**23**) in the presence of NaOCl as an oxidant. As a result, **24** was obtained in a 92% yield. Subsequently, reductive amination was performed between **24** and **25** to obtain *N*-2-(2-hydroxyethoxy)-2-(2-nitrophenyl)ethyl-*N*-hexylamine (**26**) in a 42% yield (Figure 3-20).

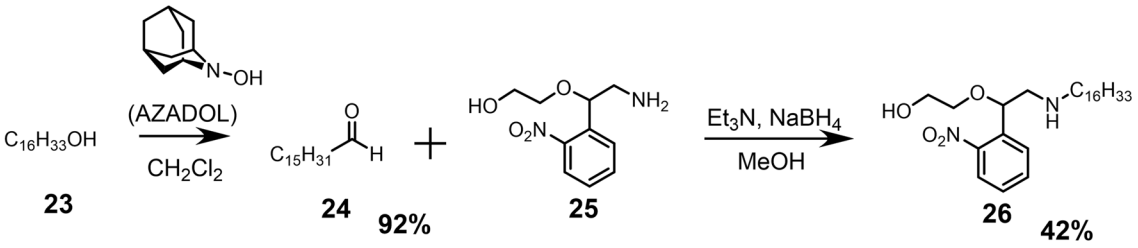

Figure 3-20: Synthesis of 26 by reductive amination

The dehydrocondensation between **16** and **26** was carried out using EDC·HCl as a condensing agent to afford *N*-(14-(2-(2-hydroxyethoxy)-2-(2-nitrophenyl)ethyl)-3,6-dioxa-9,14-diaza-triacontyl-10,13-dione)-2-nitrobenzenesulfonamide (**27**) in a 72% yield (Figure 3-21).

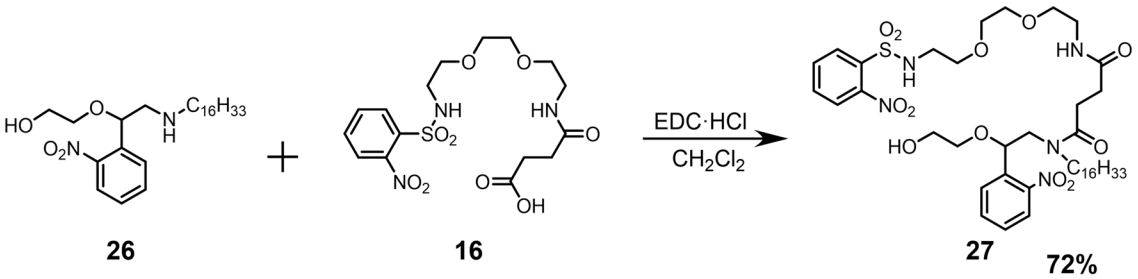

Figure 3-21: Amide condensation between 16 and 26

Before the cyclization, the hydroxy group of **27** was activated by forming methanesulfonyl ester using methanesulfonyl chloride (MsCl).[58] As a result, *N*-(14-(2-methylsulfonyloxyethoxy)-2-(2-nitrophenyl)ethyl)-3,6-dioxa-9,14-diaza-triacontyl-10,13-dione)-2-nitrobenezenesulfoamide (**28**) was obtained in a 87% yield. The intramolecular cyclization of **28** was carried out in the presence of potassium carbonate and sodium hydride. Potassium carbonate was expected to work as a template for the cyclization, as described in Section 3.1.2. As a result of the reaction under relatively low substrate concentration (1.6 mM), the macrocycle, 13-hexadecyl-11-(2-nitrophenyl)-7-(2-nitrophenylsulfonyl)-1,4,10-trioxa-7,13,18-triazacycloicosan-14,17-dione (**29**) was

successfully obtained in a 75% yield (Figure 3-22).

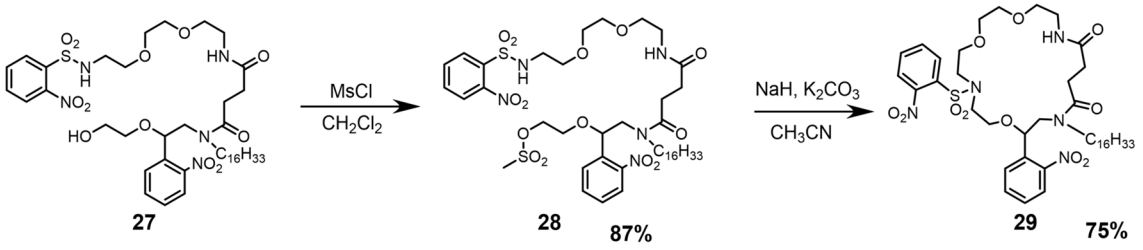

Figure 3-22: Preparation of 29 via intramolecular cyclization

The deprotection of Ns-group was carried out using benzenethiol to obtain 13-hexadecyl-11-(2-nitrophenyl)-1,4,10-trioxa-7,13,18-triazacycloicosan-14,17-dione (**30**) in a 86% yield. Finally, amide condensation between **30** and the stable carboxyl radical, 2,2,5,5-tetramethyl-3-carboxypyrrolidino-1-oxyl radical was carried out using EDC·HCl as the condensation agent instead of DMT-MM. EDC·HCl was assumed to be more suitable for this step because of the lower steric hindrance of its intermediate compared to that of the intermediate formed from DMT-MM. As a result, we succeeded in synthesizing radical probe **2** in a 66% yield (Figure 3-23).

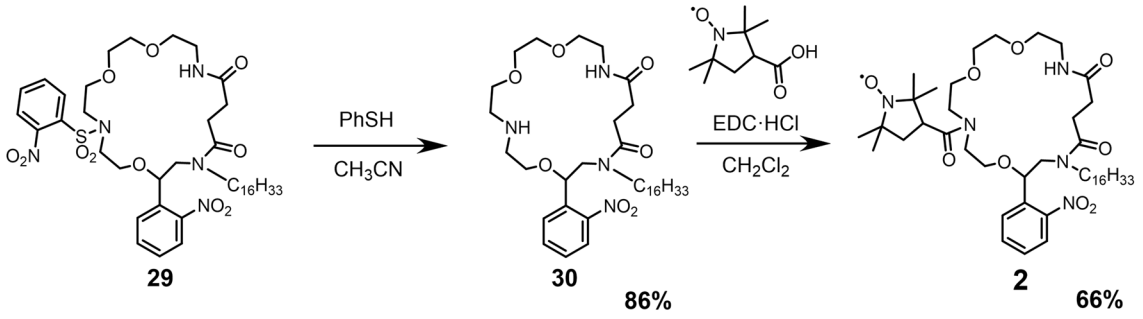

Figure 3-23: Deprotection of Ns group and amide condensation to obtain radical probe 2

3.2.3. Photolysis of radical probe **2**

Light irradiation upon radical probe **2** was expected to cause C–O bond cleavage and form radical probe **5**, as shown in Figure 3-24. In this section, the author analyzed the photolysis of radical probe **2** upon light irradiation of wavelengths 313-nm and 248-nm.

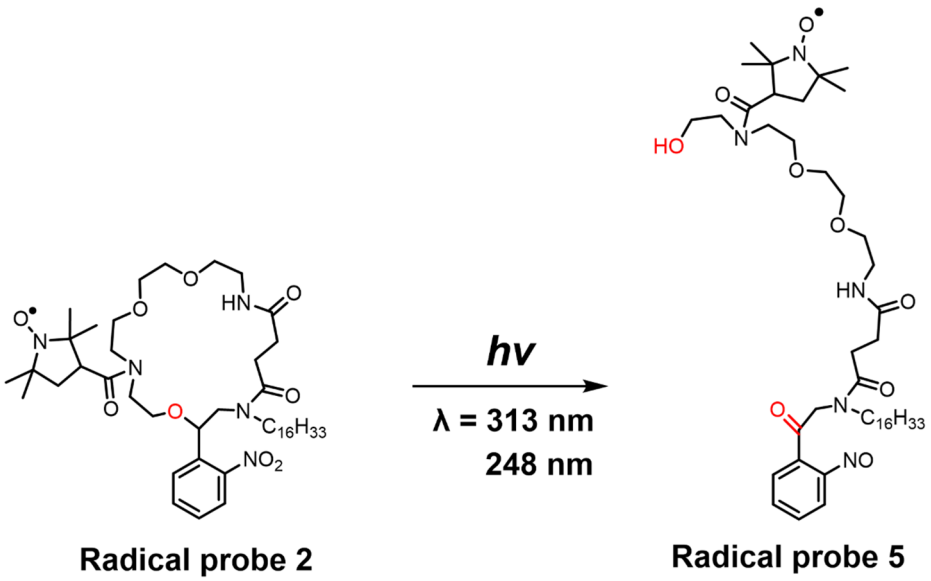

Figure 3-24: Photolysis of probe 2

The photolysis of **2** to form **5** was monitored using HPLC with UV and MS. According to the HPLC chart, the area of the peak of **2** was reduced by 55%, and the peak of **5** was generated in a retention time (RT) of 11 min upon 313-nm light irradiation for 10 s (Figure 3-25). The increase in absorption in the UV-vis spectrum after 30 s of 310 nm light irradiation (Figure 3-26) indicated that the maximum absorption of the product was near 310 nm. As further light irradiation resulted in a decrease in 310 nm absorption, it was necessary to determine the appropriate duration of light exposure. And the fact indicated that the light-irradiation at 313 nm is expected to cause the low efficiency in photolysis. Therefore, the author selected a 248-nm light for the photolysis of **2**, the absorption coefficient of which at 248 nm is larger than that of **5**.

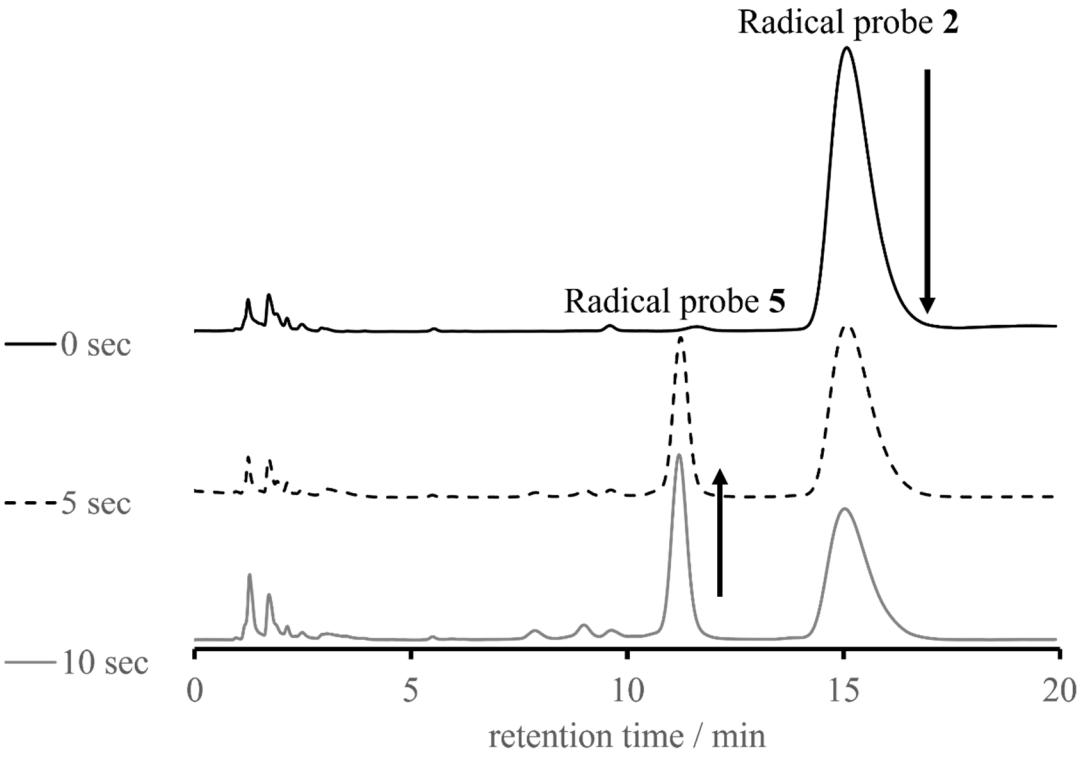

Figure 3-25: Tracking of photolysis 2 upon 313-nm light irradiation

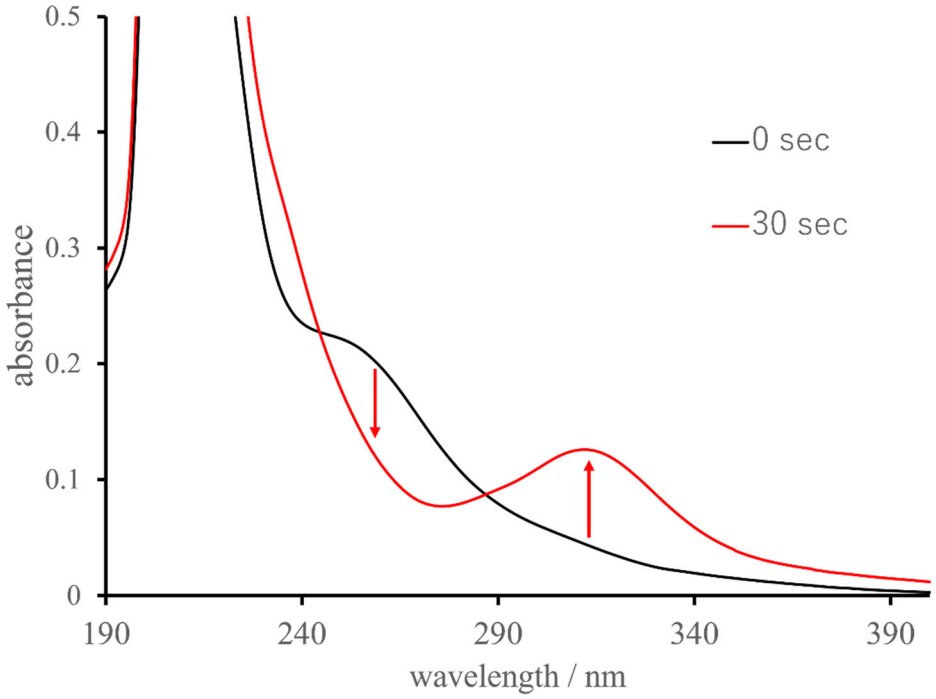

Figure 3-26: Change in UV-vis spectra of radical probe 2 before and after 30 s light irradiation

A 10 s exposure to 248-nm light resulted in a 73% photoconversion of **2** and the generation of a minimal amount of secondary product, according to the HPLC result shown in Figure 3-27. The length of the optical path of the cell for the experiment was 2 mm. The author used a 1.2-mm cell for the *in-situ* photolysis for DNP-NMR measurement (shown later in the thesis). Based on Beer-Lambert's law, it was expected that more than 99% of **2** would be converted upon 10 s of irradiation of 248-nm light.

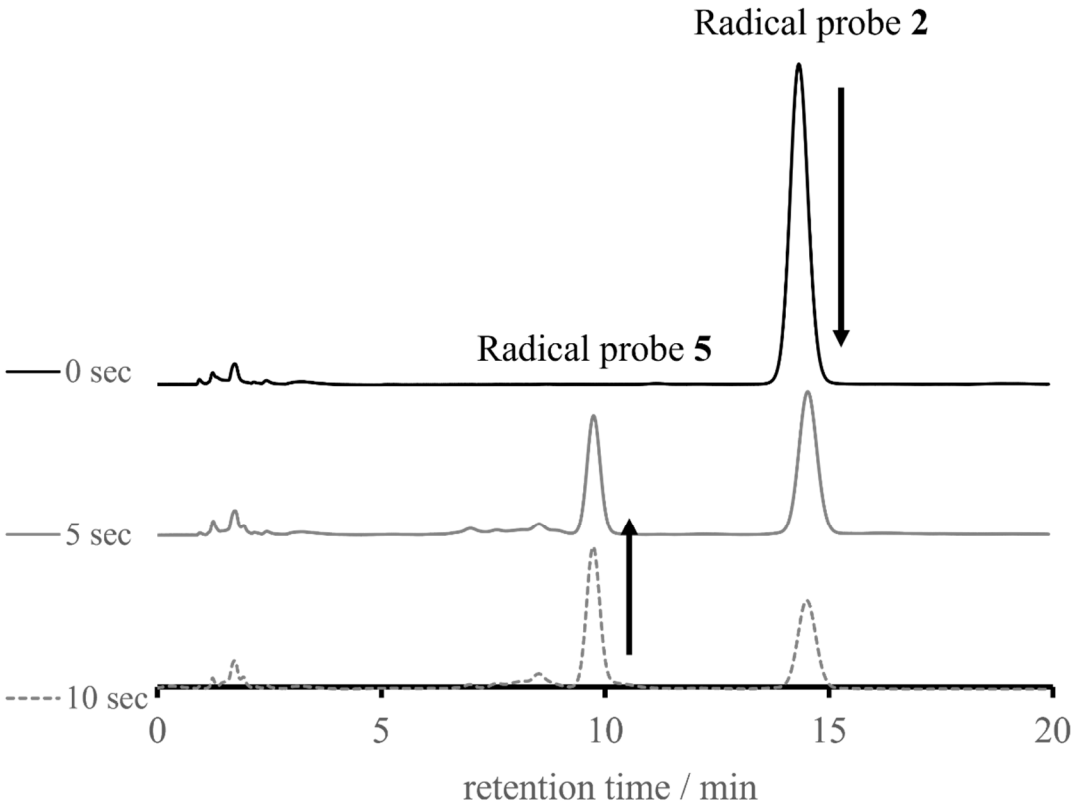

Figure 3-27: HPLC analysis for the photolysis of 2 upon 248-nm light irradiation

3.2.4. ESR spectroscopy for radical probe **2** in phospholipid vesicle

The analysis of the ESR spectra allowed us to determine the rotational correlation time (τ_R) of the radical moiety. τ_R of the radicals in the bulk solvent was reported as 10^{-11} s; this time became longer if the rotation was restricted. In other words, if we knew the correlation time of the radical, we could examine the environment surrounding the radical moiety.

The author expected that **2** was located in the vesicular membrane before light irradiation and its correlation time was longer than that of **5**, whose motility was higher due to its single-strand structure and the slight increase in hydrophilicity.

3.2.4.1 Measurement of radical probe **2** incorporated in DMPC and POPG mixed vesicles

ESR measurement of **2** (0.3 mM against the dispersion) incorporated in the mixed vesicle of 20 mM of DMPC and 0.2 mM of POPG dispersed in pure water was carried out before and after 248-nm light irradiation for 10 s. The reason for the mixing of a small amount of POPG was to prevent the aggregation of the phosphocholine vesicles due to their neutral charge. The results are shown in Figure 3-28. The line-shaped analysis of ESR spectra was carried out using EasySpin on the Matlab platform. The correlation time before light irradiation was determined to be 3.16 ns. The fact that the correlation time was very large compared to that in the bulk water indicated that the radical moiety was buried in the phospholipid vesicle. The correlation time after light irradiation was determined to be 3.47 ns. This value indicated that the radical moiety was still buried in the vesicles, even after light irradiation.

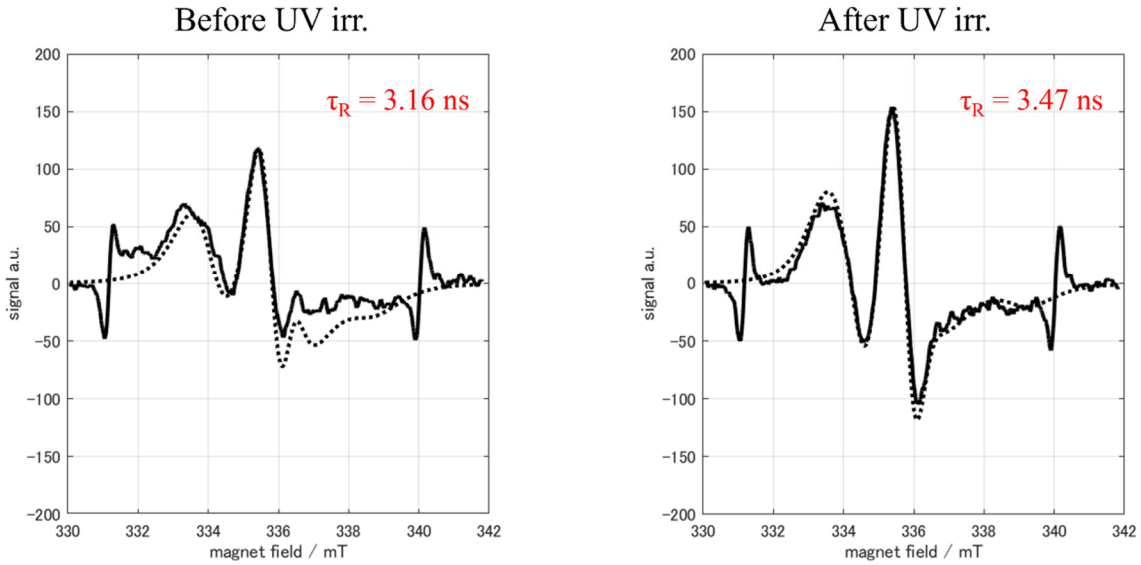

Figure 3-28: ESR spectra of probe 2 incorporated in DMPC, POPG vesicles

3.2.4.2 Measurement of radical probe **2** incorporated in DOPC and POPG mixed vesicle

ESR measurement of **2** (0.3 mM against the dispersion) incorporated in the mixed vesicle of 20 mM of DOPC and 0.2 mM of POPG dispersed in pure water was carried out before and after 248-nm light irradiation for 10 s. The results are shown in Figure 3-29. The correlation times before and after light irradiation were determined to be 3.00 ns and 2.90 ns, respectively. As indicated by the behavior of the DMPC-POPG vesicles, the radical moiety was assumed to be buried in the membrane phase even after photoirradiation. Differences in the correlation times and line shapes between DMPC-POPG vesicles and DOPC-POPG vesicles were observed. The author estimated the reason behind these observations to be the following. Because of the soft hydrophobic part of DOPC vesicles, the two types of probes were averaged in the spectrum. By contrast,

because DMPC was stiffer compared to DOPC, the motion of the radical probe was restricted and appeared as two different spectra.

Overall, the radical moieties of **2** and its photoproduct, **5**, were estimated to be located in the vesicular membrane according to ESR analysis.

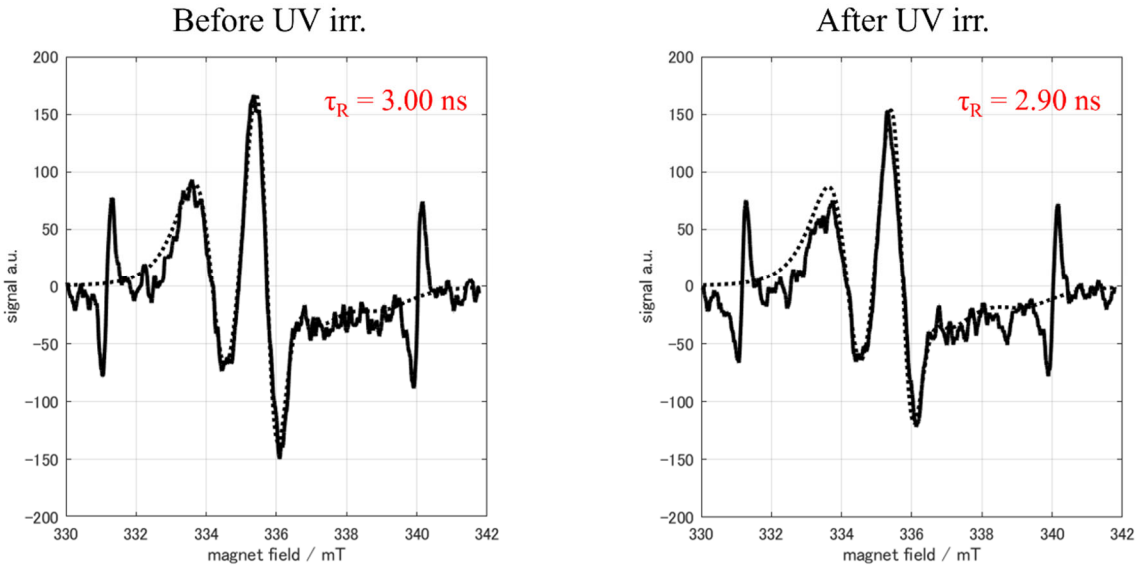

Figure 3-29: ESR spectra of probe 2 incorporated in DOPC, POPG vesicles

3.2.5. Development of sample holder for DNP-NMR measurement for aqueous dispersion of **2**-incorporated phospholipid vesicle

There are three requirements for the sample holder for DNP-NMR measurement. The first is prevention of temperature rise during microwave irradiation. For this purpose, an NMR-inactive hydrophobic heat-sink fluid, Fluorinert, was placed on the sample dispersion, and the coolant air was passed through the sample tube. The second is minimization of the dielectric loss of the incident microwave due to the aqueous sample.

For this purpose, the author prepared an rf-coil, allowing NMR measurement of the micro-litter sample. The third is the transparency of the excitation UV light. For this purpose, the tubes for the chamber were made of quartz. Based on the requirements, the sample holder was initially designed as shown in Figure 3-30.

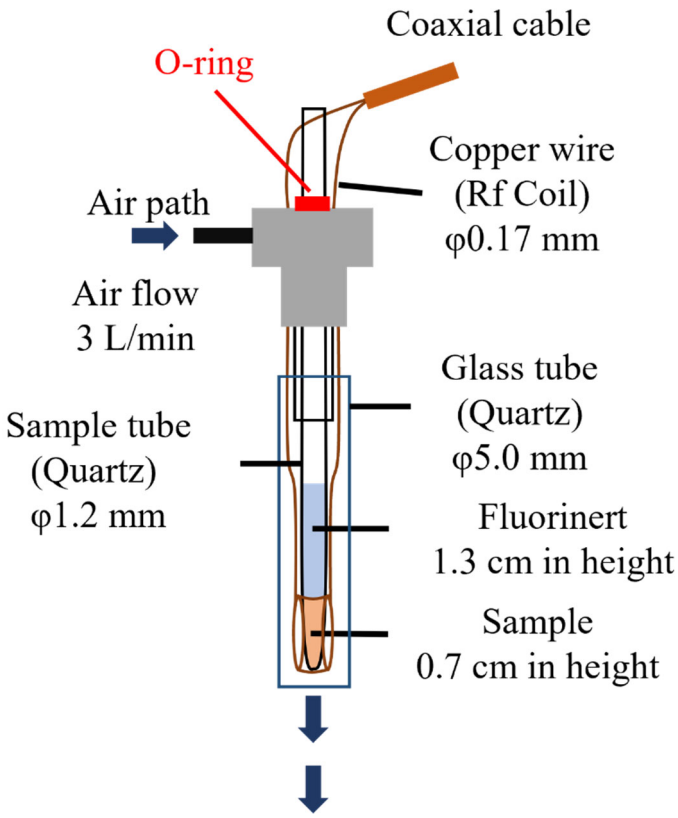

Figure 3-30: Design of sample holder 1

However, the cooling rate of the sample in holder 1 was insufficient for DNP-NMR measurement. The temperature of 4 μL of pure water in the sample chamber was increased up to 47 °C during the measurement (data are shown later in Figure 3-33). The increase in air flow rate could suppress the increase in temperature. However, the flow rate of 3 L/min was the limit for the sample holder. A higher flow rate caused the leakage of the flowing air in the connection between the sample tube and the holder, even though the o-

ring sealed the connection.

Next, the author prepared sample holder 2 (Figure 3-31). A quartz tube containing fluorinert was placed on the outside of the sample tube, and the coolant air was passed directly against the tube. However, it was less effective in cooling the sample than sample holder 1 (Figure 3-31).

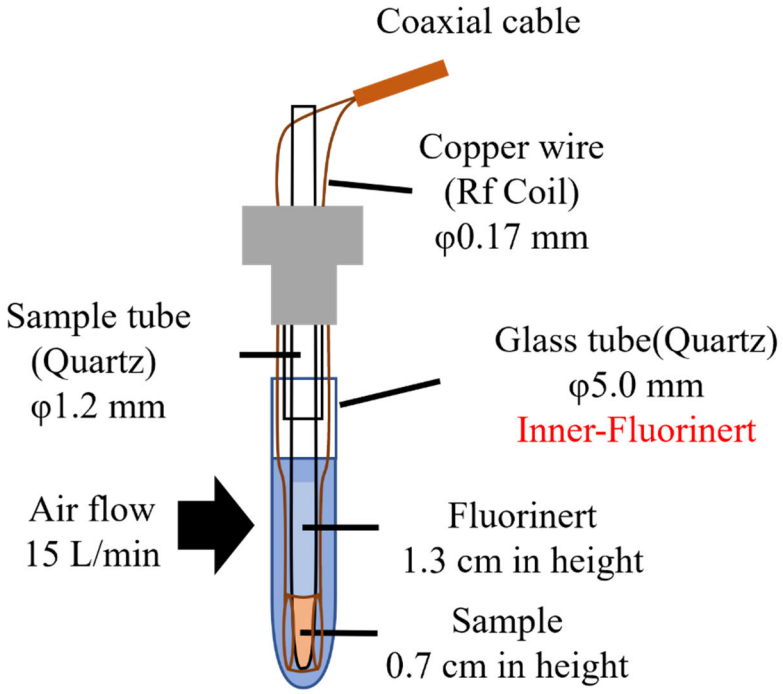

Figure 3-31: Design of sample holder 2

The author then designed and prepared sample holder 3, wherein the flow channel for the coolant air was opposite to that of sample holder 1 (shown in Figure 3-32). The coolant air directly acted on the sample from the bottom of the sample tube, and the flow rate could be increased up to 10 L/min. Further increase in flow rate caused vibration of the sample tube.

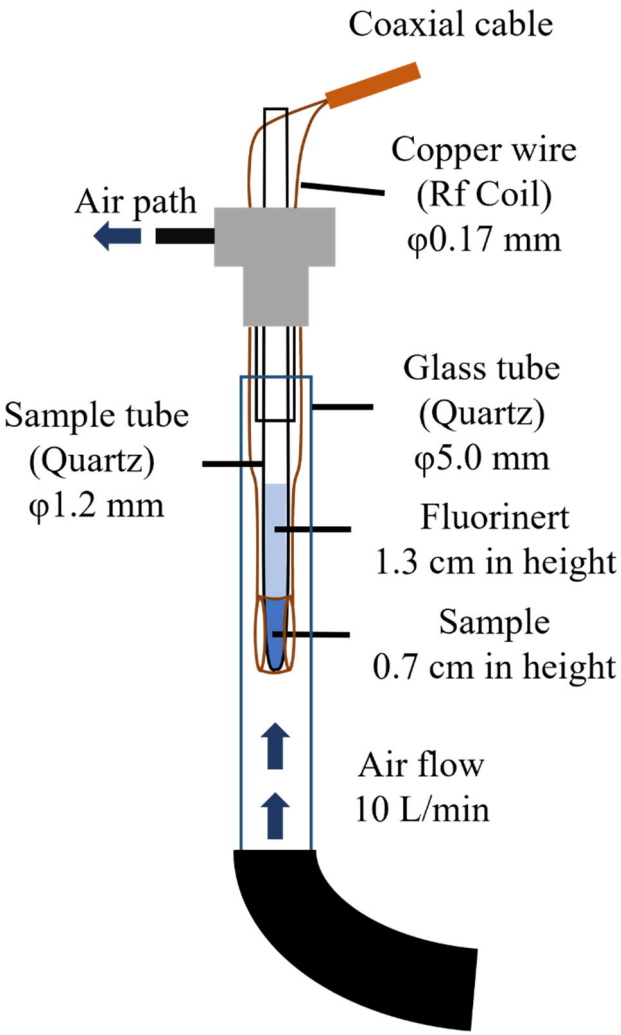

Figure 3-32: Design of sample holder 3

Figure 3-33 shows the increase in T_1 of pure water upon microwave irradiation at r.t. The increase in T_1 indicates an increase in the temperature of the water. According to the data of T_1 and its temperature dependency reported by Hindman,[59] it was revealed that

the temperature of the water set on sample holder 3 increased up to 26 °C, whereas that set on sample holder 1 increased up to 47 °C. From these results, the author decided to use sample holder 3 for HD-ODNP-NMR measurement.

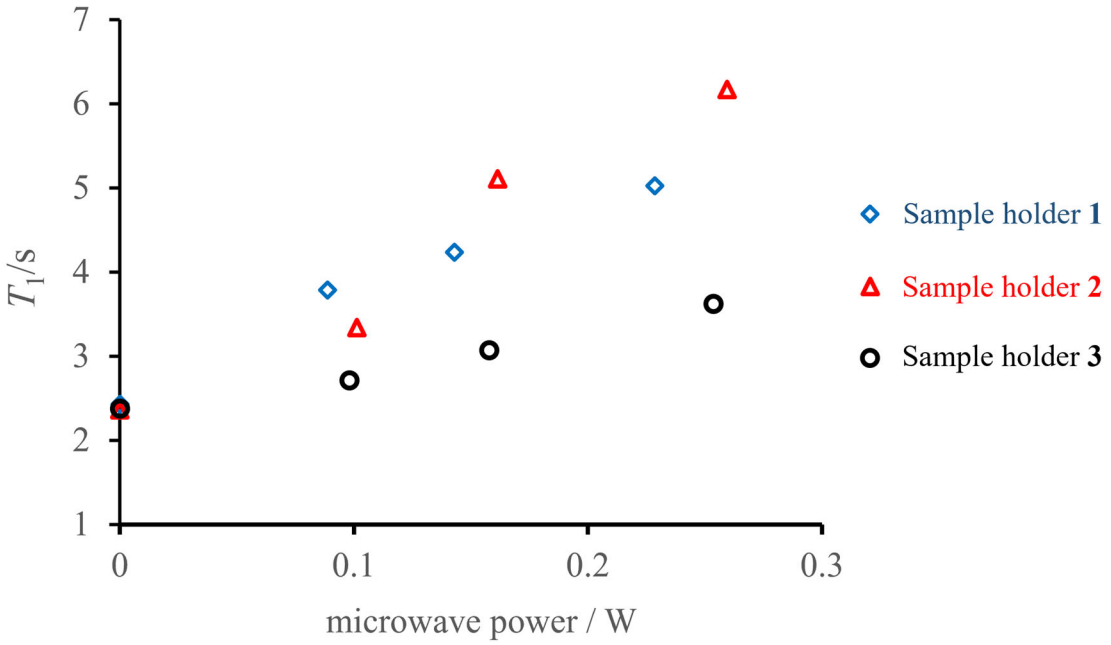

Figure 3-33: Dependence of microwave irradiation on T_1 of proton NMR of ultrapure water

3.2.6. Measurement of water dynamics by DNP-NMR with probe **2**

3.2.6.1 Dynamics of water interacting with DMPC and POPG vesicle

The dynamics of water of hydration at the interface or internal structure of DMPC-POPG mixed vesicle was quantified by DNP-NMR using **2** as a spin probe for DNP-NMR.

First, NMR was measured in the absence of irradiating microwave; subsequently, the pulse sequence of the measurement was determined. The peak intensity at that time was set to -1, which was used as the standard value for the following measurements.

Next, NMR measurements were performed while irradiating the sample with microwave intensities of -18, -16, -14, -12, -10, -8, -6, -5, and -4 dBm. The values of the peak intensities are shown in Figure 3-34-a. The microwave intensities were converted to watts and displayed. In this measurement, the NMR signal was enhanced 7 times when the sample was irradiated with a -4 dBm microwave. The degree of enhancement increased with increasing microwave intensity, but the latter was moderated.

T_1 measurements using the inversion recovery method were carried out under microwave irradiation of -12, -10, -8 dBm and without microwave irradiation. The results are shown in Figure 3-34-b.

Next, the sample was irradiated with 248-nm light for 10 seconds and the set of NMR protocol was measured similar to the aforementioned method. The results are shown as filled circles in Figures 3-34-a and 3-34-b.

Subsequently, by applying Equation (12), $k_\sigma s(p)$ was calculated, as shown in Figure 3-34-c. In the state of saturated electron spin, where $s(p_{max})$ is regarded as 1, k_σ values were quantified as 5.5 $M^{-1}s^{-1}$ and 5.8 $M^{-1}s^{-1}$, before and after photoirradiation, respectively. Moreover, by applying Equation (10) to the result of the T_1 measurement, the k_ρ values

were estimated as 240 $M^{-1}s^{-1}$ and 240 $M^{-1}s^{-1}$, before and after photoirradiation, respectively. From the experimental results, the correlation time (τ_c) of water interacting with DMPC-POPG measured with probe **2** were quantified as 464 ps (ξ = 0.029) before light irradiation and 400 ps (ξ = 0.036) after light irradiation. When we regarded the closest approach of the radical moiety and water proton as 0.34 nm,[26] the measured diffusion coefficients of water around the radical moiety were 0.25 × 10^{-9} m^2/s and 0.29 × 10^{-9} m^2/s, for closed-ring spin probe and opened-ring spin probe, respectively.

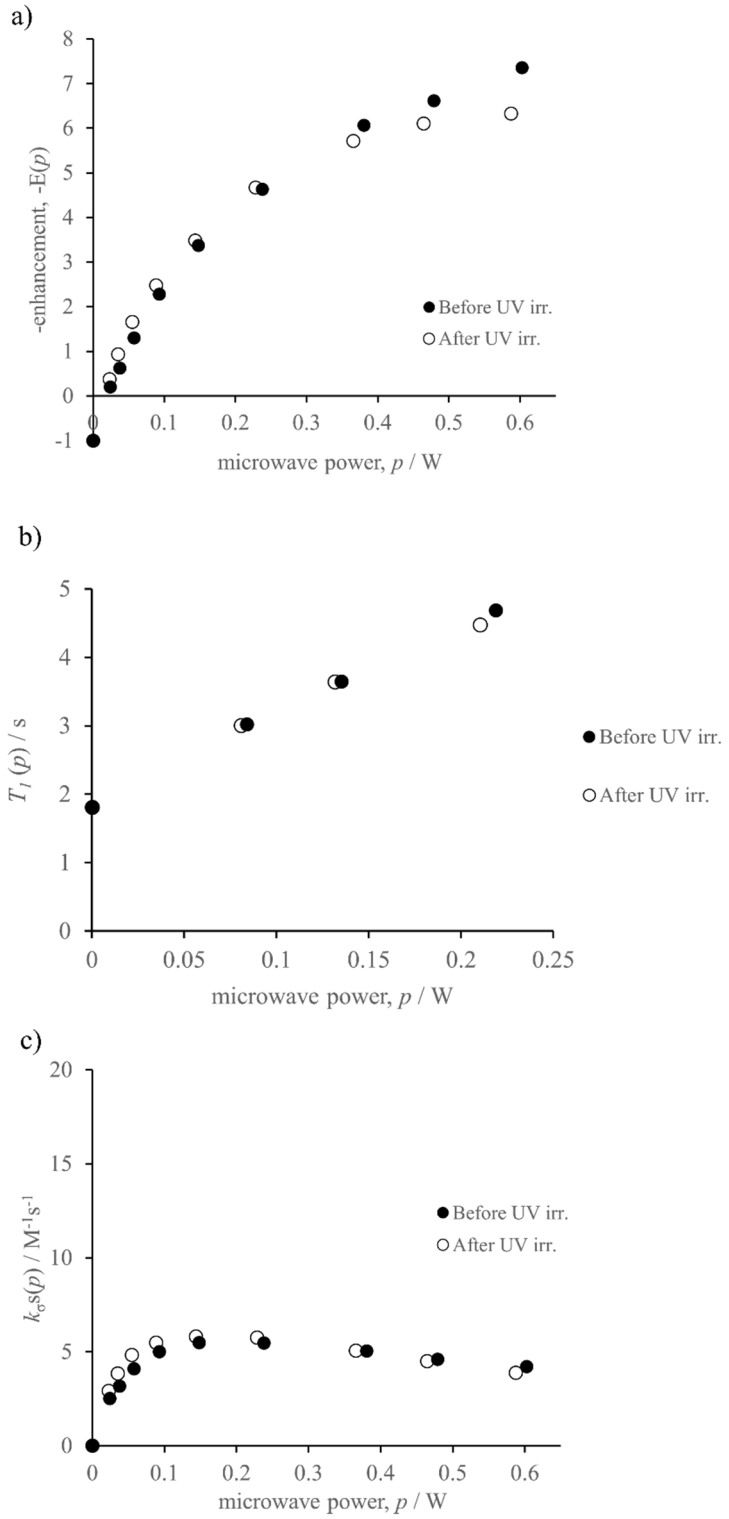

Figure 3-34: Result of DNP-NMR (a) enhancement, (b) T_1 measurement, and (c) $k_\sigma s(p)$ of probe 2 incorporated in DMPC, POPG vesicles

3.2.6.2 Dynamics of water interacting with DOPC and POPG vesicle

Quantification of water dynamics sensed by probe **2** and its photoproduct **5** incorporated in DOPC and POPG vesicle was carried out in a manner similar to that described in Section 3.2.6.1. The results are shown in Figure 3-35-a-c. k_σ values before and after light irradiation were quantified as 18.1 $M^{-1}s^{-1}$ and 17.2 $M^{-1}s^{-1}$, respectively, and k_ρ values before and after light irradiation were estimated as 331 $M^{-1}s^{-1}$ and 341 $M^{-1}s^{-1}$, respectively. From the experimental results, the correlation times (τ_c) of water around DOPC-POPG were quantified as 300 ps ($\xi = 0.055$) before light irradiation and 319 ps ($\xi = 0.050$) after light irradiation. The measured diffusion coefficients of water around the radical moiety were 0.39×10^{-9} m^2/s and 0.36×10^{-9} m^2/s for closed-ring spin probes and opened-ring spin probes, respectively.

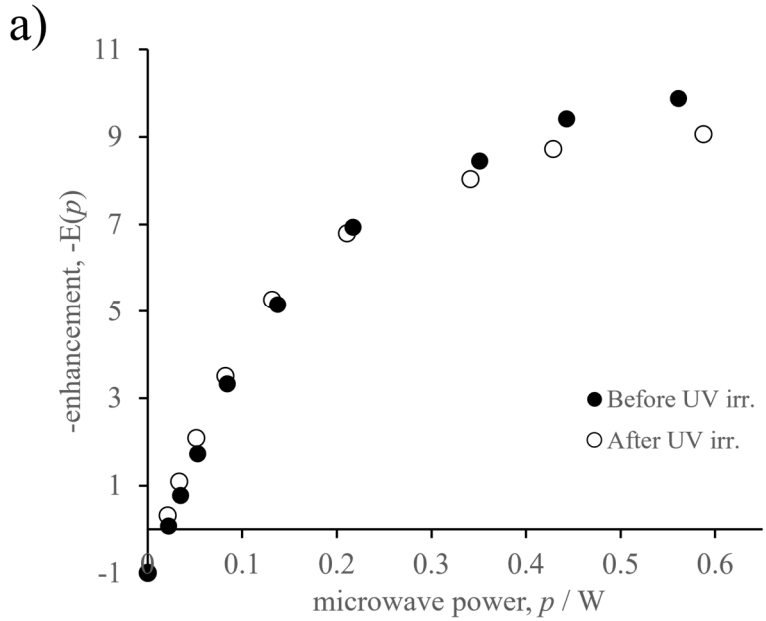

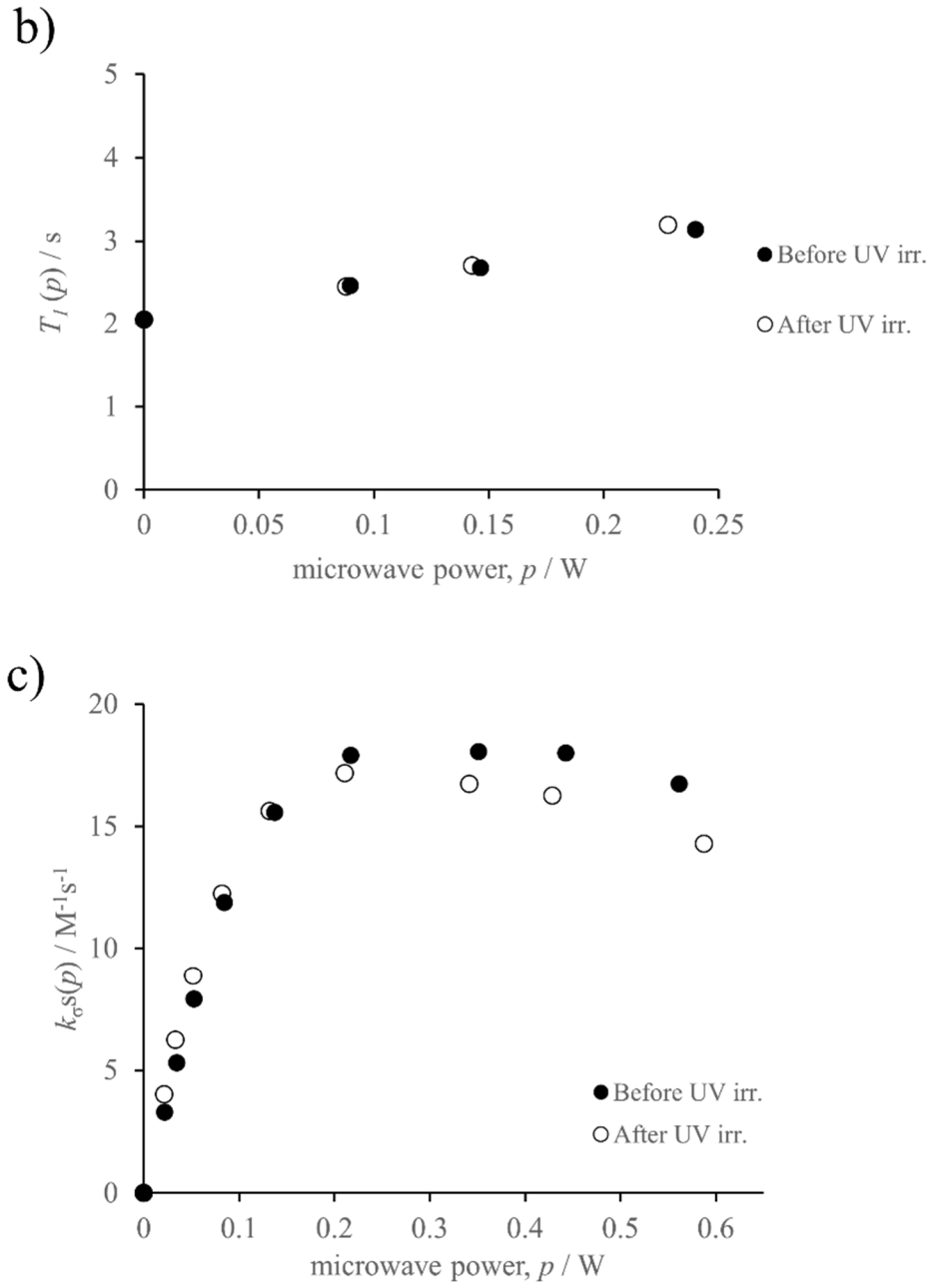

Figure 3-35: Result of DNP-NMR (a) enhancement, (b) T_1 measurement, and (c) $k_\sigma s(p)$ of probe 2 incorporated in DOPC, POPG vesicles

3.2.7 Short summary of DNP-NMR determined dynamics of water sensed by probe **2** in phospholipid vesicles

The ESR measurement of spin probe **2** and its photoproduct in the liposome indicated that the radical moiety remained in the vesicular membrane even after the photolysis of **2**. All the calculated diffusion coefficients of water sensed by the probes were between 0.25×10^{-9} m^2/s and 0.39×10^{-9} m^2/s, which were close to the value 0.32×10^{-9} m^2/s , which was the diffusion coefficient of water determined by Kausik.[21] The results indicated that the radical moieties were buried in the vesicles not only before but also after light irradiation (Figure 3-36).

The slower diffusion in the DMPC-POPG vesicle ($D = 0.25 \times 10^{-9}$ m^2/s, before photolysis) than that in the DOPC-POPG vesicle (0.39×10^{-9} m^2/s) may indicate that the tight molecular interactions between saturated alkyl chains suppress the translation of water molecules. Formation of **5** by photolysis may cause the relocation of the radical moiety to a hydrophilic region inside the vesicular membrane due to the small increase in hydrophilicity around the radical moiety. This behavior indicates that the diffusion of water sensed by **5** was more in comparison to that sensed by **2**, in the DMPC-POPG vesicle. By contrast, in the DOPC-POPG vesicle, the diffusion constant did not change radically because of the originally higher rheology inside the vesicle due to saturated aliphatic chains.

As shown in this chapter, a small difference in the diffusion of water was successfully observed by HD-ODNP-NMR with photolabile radical probe **2**. However, the small difference may not be sufficient to establish the usefulness of the approach of site-switchable measurement. Therefore, the author revised the design of the radical probe again. By further increasing the polarity of the linker group of the radical probe, we

designed radical probe **3**, which allows the radical moiety to exit the vesicular membrane upon light irradiation. Radical probe **3** will be introduced in detail in the next chapter.

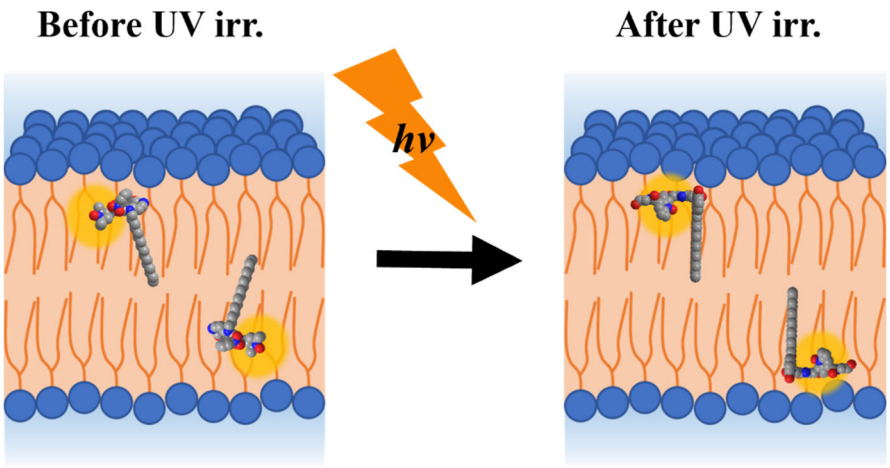

Figure 3-36: Position of the radical probe 2 before and after light irradiation

3.3. Site-selective measurement of water dynamics at the interior and interface of phospholipid vesicles by HD-ODNP NMR sensed by phospholipid-incorporated radical probe **3** and its photoproduct

3.3.1. Design of radical probe **3**

Based on the results of the previous sections, the author aimed to develop a radical probe that can site-specifically sense water located in the hydrophobic region of the membrane, interface of the membrane, and bulk. For this purpose, the amine group was introduced to the linker moiety of the redesigned radical (**3**) by substituting amide bonds of **2** (Figure 3-37). The radical moiety of the closed-ring isomer (**3**) whose radical moiety is near its hydrophobic nitrobenzyl and hexadecyl moieties could be located in the hydrophobic region. By contrast, the radical moiety of the open-ring photoproduct (**6**) could exist at a position far from the hydrophobic anchor moiety, which is beyond the hydrophilic diamine linker.

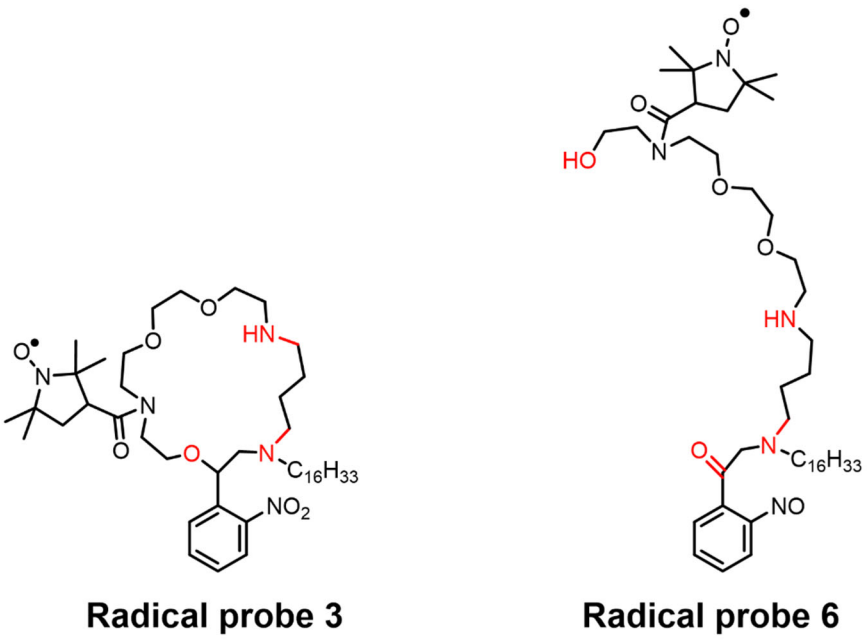

Figure 3-37: Structure of probe 3 and expected ring-opened photoproduct 6

3.3.1. Synthesis of radical probe **3**

The preparation of radical probe **3** was successfully performed by the scheme shown in Figure 3-38. This scheme was designed according to preliminary experiments described in the following paragraphs.

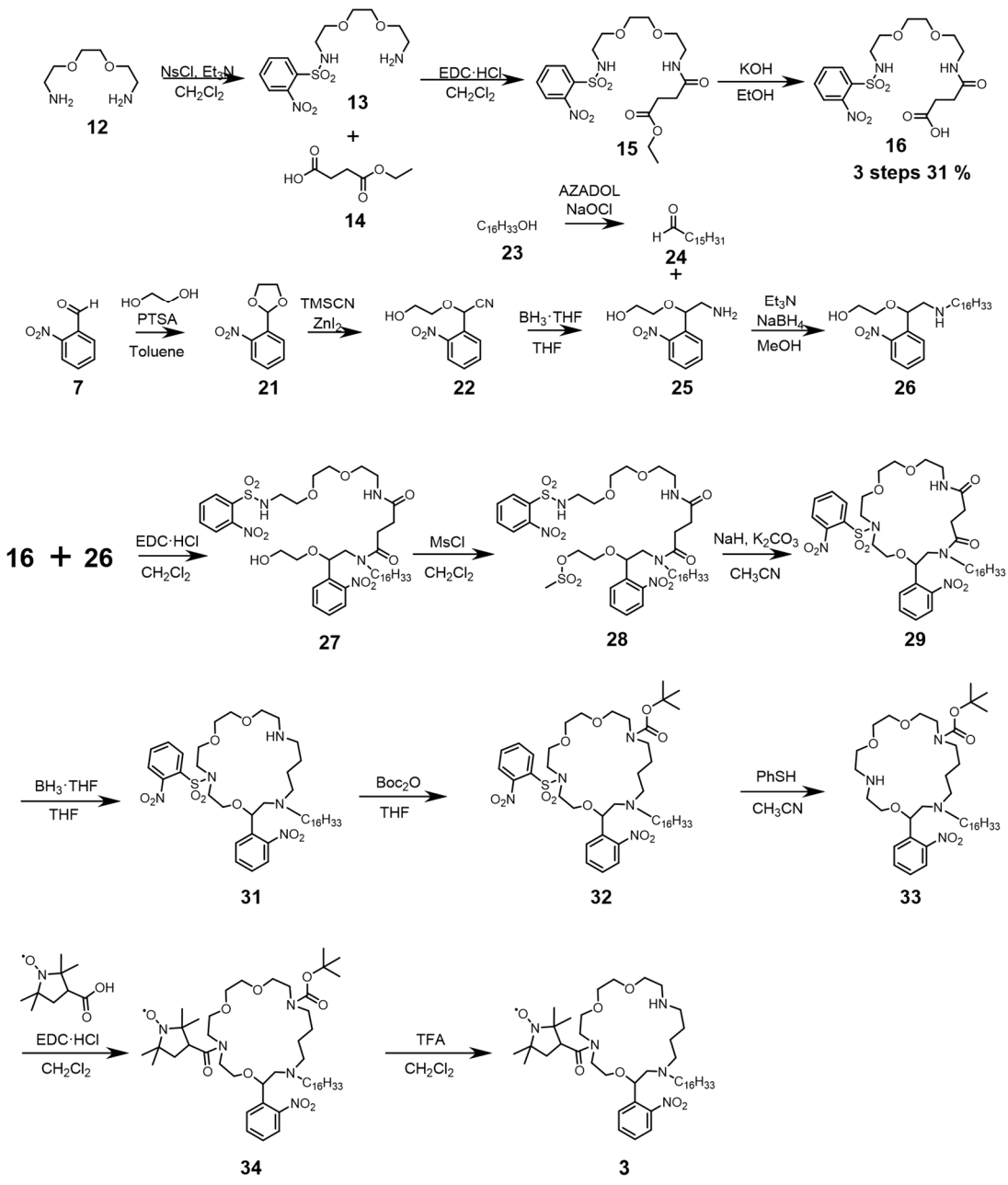

Figure 3-38: Synthesis scheme of radical probe 2

As **3** is the reduced compound of **2**, it can be prepared by inserting a reduction process into the scheme for the preparation of **2**. Borane is frequently employed as the reducing agent for amine formations from its corresponding amide derivatives under mild conditions. It is known that 2,2,5,5-tetramethylpyrrolidinoxy radical is adequately stable against borane-reagent at room temperature. However, the reduction of the amide with borane reagent requires heating up to approximately 80 °C. Therefore, the possibility of decomposition of radical moiety must be considered.

Hence, the reduction of *N*-decyl-1-hydroxy-2,2,5,5-tetramethyl-3-carboxypyrrolidino-oxy radical, which was prepared by the condensation of 2,2,5,5-tetramethyl-3-carboxypyrrolidino-1oxyl radical and *n*-decylamine, was carried out using a borane·THF reagent, as a model experiment for the reduction of **2** to form **3** (Figure 3-39). The reaction was tracked using thin layered chromatography (TLC), and its location was detected by the quenching of a fluorescence plate under an UV illuminator. The fact that no spots were observed after 2 h of reaction indicates that the radical was not stable against the condition. Therefore, the author decided to reduce **29** to form diamines for the preparation of **3** (Figure 3-38).

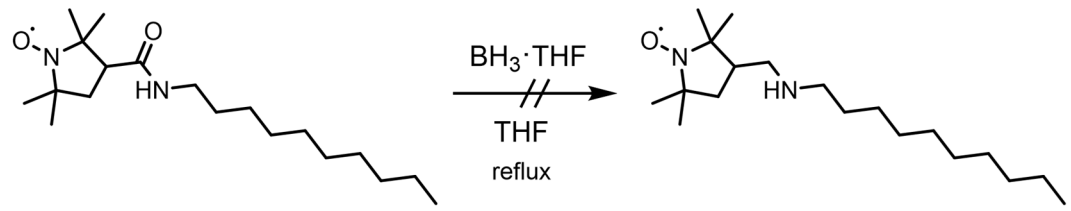

Figure 3-39: Model experiment for reduction of amide

The reduction of **29** was carried out in the presence of 12 equivalents of borane·THF complexes in THF solution under reflux conditions. The corresponding diamine (**31**) was obtained and its secondary amine was protected by the butoxycarbonyl (Boc) group. After

the deprotection of the Ns group in the presence of benzenethiol, 18-*t*-butoxycarbonyl-13-hexadecyl-11-(2-nitrophenyl)-1,4,10-trioxa-7,13,18-triazacycloicosan (**33**) was obtained. The three-step preparation afforded a yield of 12% (Figure 3-40).

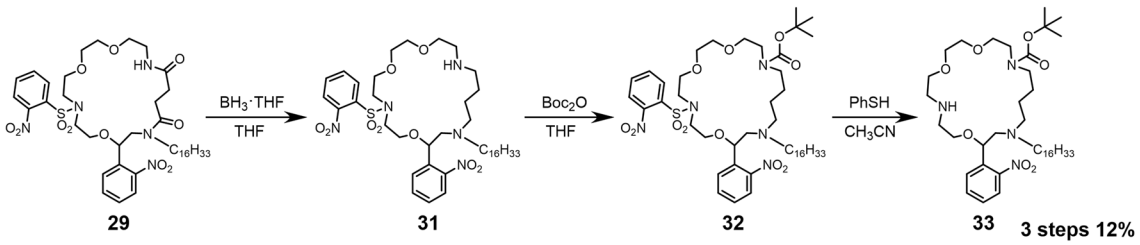

Figure 3-40: Three-step synthesis of 33 from 29

The condensation between the radical moiety and **33** was carried out using EDC·HCl because the reagent is more suitable than DMT-MM for the condensation of a macrocycle with steric hindrance as described in Section 3.2.2. As a result, 2,2,5,5-tetramethyl-3-(18-*t*-butoxycarbonyl-13-hexadecyl-11-(2-nitrophenyl)-1,4,10-trioxa-7,13,18-triaza-cycloicosan-7-yl)carbonylpyrrolidine-*N*-yloxy radical (**34**) was obtained. The radical probe **3** was obtained in a 27% yield after deprotection of the Boc group in the presence of trifluoroacetic acid (Figure 3-41).

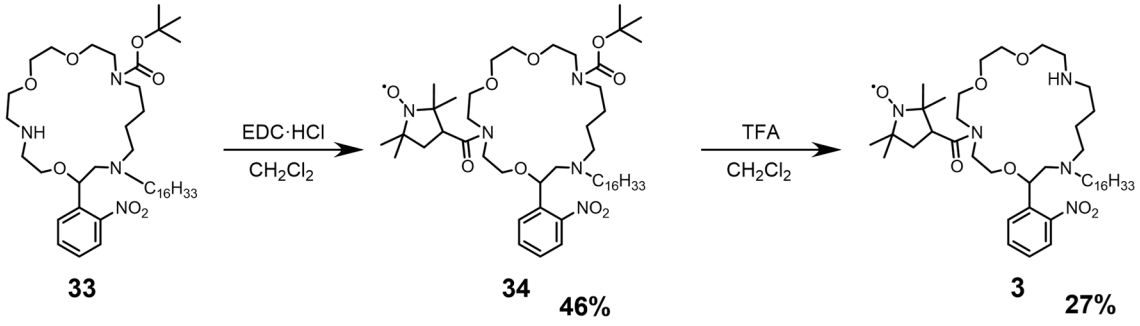

Figure 3-41: Modification of radical moiety and deprotection of Boc group to obtain radical probe 3

3.3.3 Photolysis of radical probe **3**

As per the previous reports, radical probe **3** could convert to radical probe **6** via a photolabile reaction (Figure 3-37). However, the product analysis of the photolysis of **3** revealed that the photoreaction scheme followed in this study is different from those proposed in the previous reports. In this chapter, the finding of the novel C–N bond photolysis of 2-nitrophenylethylamine derivative is described.

The photolysis of **3** was monitored using HPLC equipped with UV and MS. Under the HPLC condition, the peak of probe **3** was split into two as shown in Figure 3-42. The *m*/*z* value of either peak was 803.6, which corresponds to the *m*/*z* value of the protonated **3**. The existence of the diastereomer or the existence of different ionized structures might cause the split of the peak. Based on the former hypothesis, however, the peaks of probes **1** and **2** should also be divided in the HPLC chart; but no peak splitting was observed. Therefore, the assumption that the peak split of **3** was due to differences in the ionized states of **3** is more accurate.

The photoirradiation of a methanolic aqueous solution to **3** with 248-nm light for 5 s results in the generation of two peaks at RT 2.5 min and RT 4.0 min, and a decrease in the peaks of **3** in the chromatogram. The behavior was similar to that upon photoirradiation for 10 s; the conversion of **3** was 62% under experimental conditions.

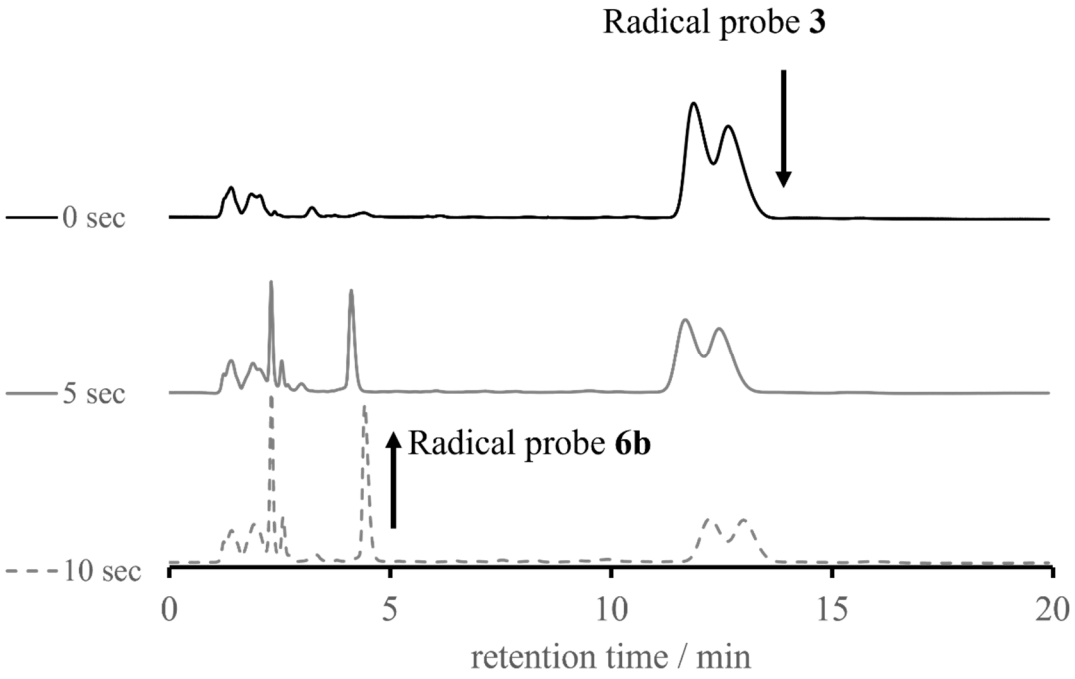

Figure 3-42: Tracking photolysis of 3 upon 248-nm light irradiation

Whereas the *m*/*z* value for the fraction around RT = 2.5 min was uncertain even when it was measured using a high-sensitive ESI-MS system (Exactive, Thermo Scientific, operated by the Global Facility Center at Hokkaido University), the *m*/*z* for the fraction around RT = 4.0 min was 656.6, which can be assigned to $C_{37}H_{75}N_4O_5+H^+$. Considering the nitrogen rule in mass spectrometry, it can be assumed that the second peak was of a radical compound, and according to the *m*/*z* value, the radical species was expected to be **6b**, as shown in Figure 3-43.

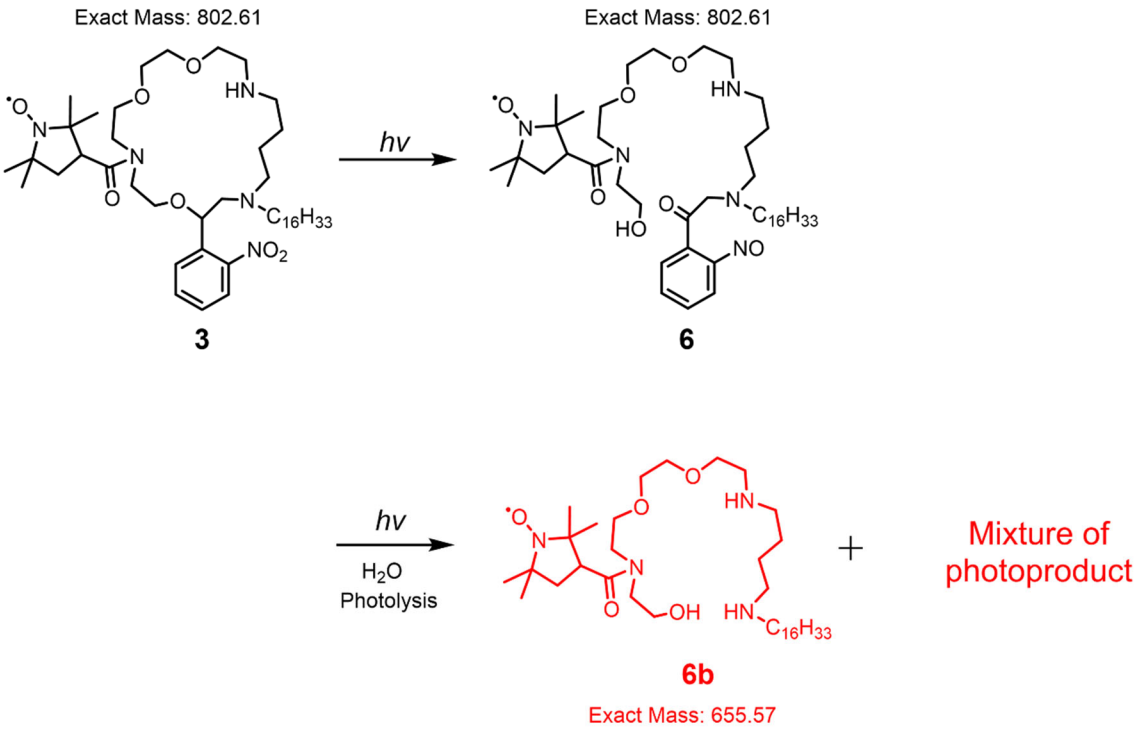

Figure 3-43: Formation of 6b by photolysis of probe 3

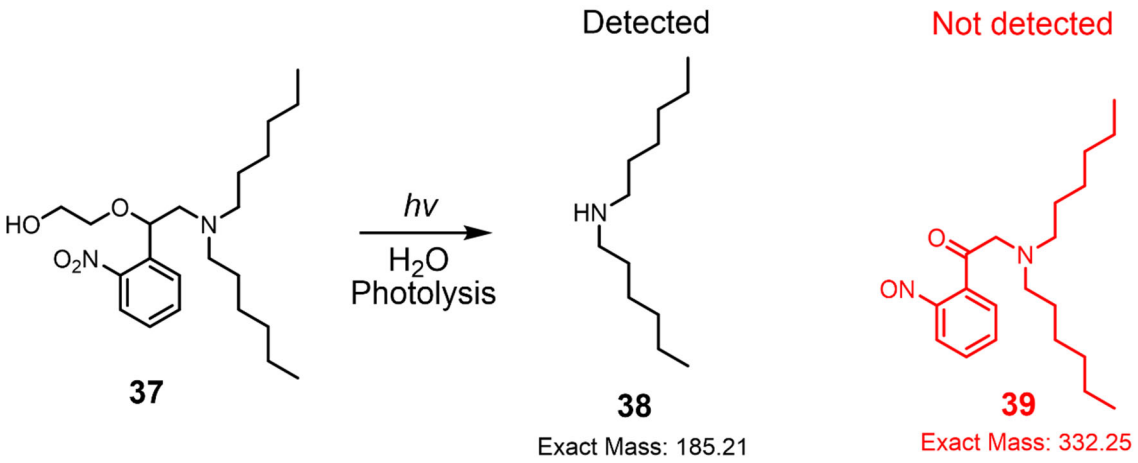

Figure 3-44: Model experiment for analyzing the photolabile reaction

To confirm the hypothesis, the product analysis of the photolysis of **37** was carried out (Figure 3-44). According to HPLC, the *m*/*z* value of 186.2 was sensed by the mass detector at RT 2.5–3.3 min, where UV absorption was not detected. It was assigned to

dihexylamine (**38**). Furthermore, 2-(dihexylamino)-1-(2-nitrosophenyl)ethan-1-one (**39**), which is a C–O bond cleavage compound whose molecular mass is 332.5, was not detected by HPLC analysis. As shown in the chromatograph in Figure 3-45, other specific compounds were formed by the photolysis (Figure 3-45). To identify the compound, the crude material was separated by gel permeation liquid chromatography. However, the photo products were unstable and therefore the separated compounds were different from the component of the crude material.

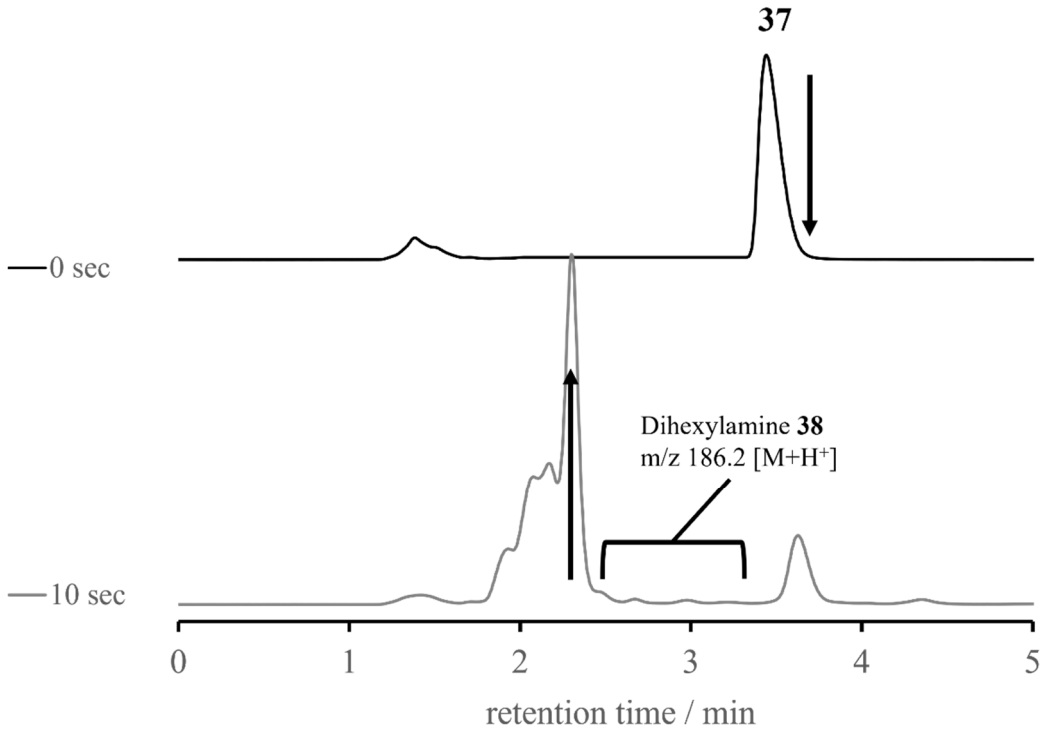

Figure 3-45: Tracking photolysis of 37 upon 248-nm light irradiation

Although the nitrosobenzyl derivatives with aromatic ring could not be identified, the other decomposition product was dihexylamine **38**, indicating that the photo reaction of **3** proceeded along the pathway shown in Figure 3-43. From this result, we concluded that DNP-NMR measurement using radical probe **3** is possible.

3.3.4 ESR spectroscopy of **3** in phospholipid vesicle

3.3.4.1 Measurement of **3** incorporated in DMPC and POPG mixed vesicle

ESR measurement of **3** (0.3 mM against the dispersion) incorporated in the mixed vesicle of 20 mM of DMPC and 0.2 mM of POPG dispersed in pure water was carried out before and after 248-nm light irradiation for 10 s. The correlation time before light irradiation was estimated to be 3.39 ns. The fact that the correlation time was very large compared to that in bulk water indicates that the radical moiety was buried in the phospholipid vesicle. By contrast, the line shape of the ESR spectrum after light irradiation became sharper compared to that before irradiation. The calculated correlation time was 0.45 ns (Figure 3-46). The significant increase in the rotational frequency of the radical moiety after light irradiation indicates that the location of radical moiety shifted to the surface of the vesicular membrane.

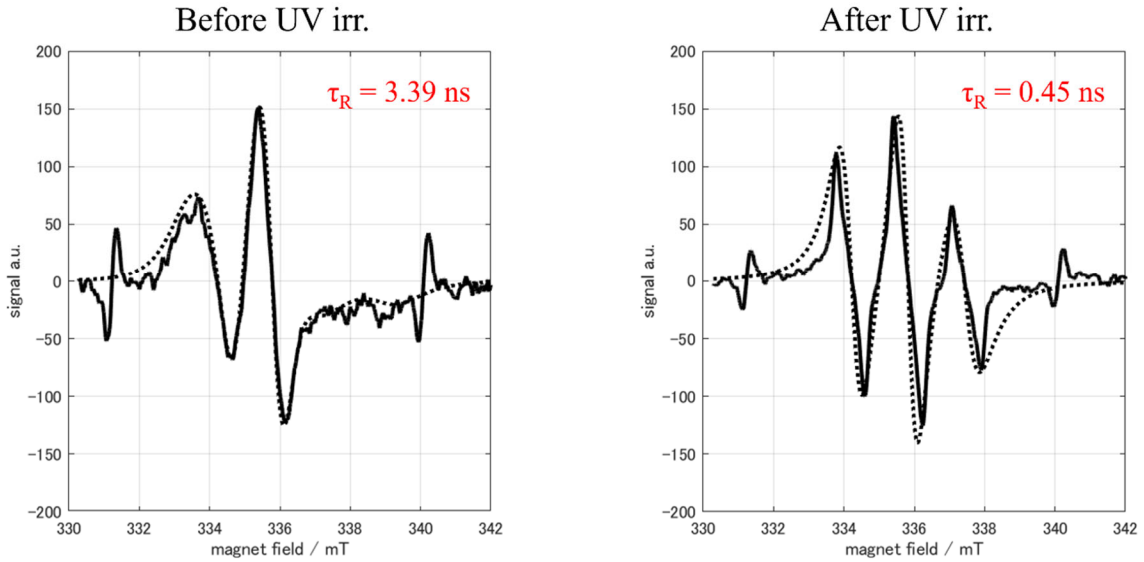

Figure 3-46: ESR spectra of probe 3 incorporated in DMPC, POPG vesicles

3.3.4.2 Measurement of radical probe **3** incorporated in DOPC and POPG mixed vesicle

ESR measurement of **3** (0.2 mM against the dispersion) incorporated in the mixed vesicle of DOPC (15 mM) and POPG (0.2 mM) in pure water was carried out before and after 248-nm light irradiation for 10 s. The correlation time before light irradiation was quantified as 2.81 ns; the value changed to 0.75 ns after light irradiation (Figure 3-47). Similar to the result of **3** in the DMPC-POPG vesicle, the radical moiety was considered to have shifted to the surface of the membrane upon light irradiation.

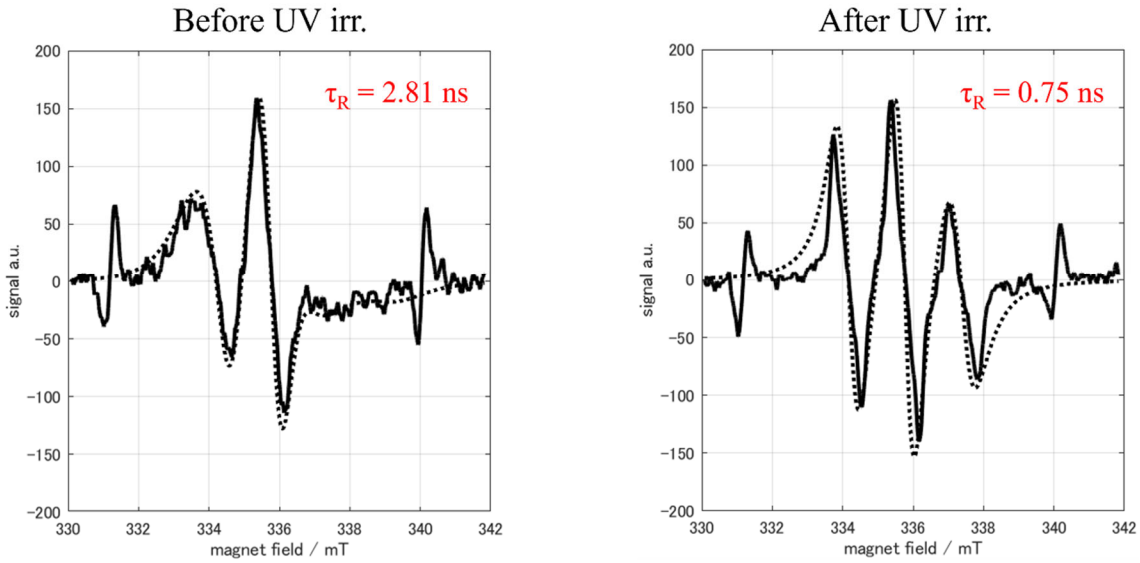

Figure 3-47: ESR spectra of probe 3 incorporated in DOPC, POPG vesicles

3.3.5. Measurement of water dynamics by DNP-NMR with probe **3**

3.3.5.1 Dynamics of water incorporated with DMPC and POPG mixed vesicle

The analysis of water surrounding 20 mM DMPC and 0.2 mM POPG mixed vesicle was carried out using the HD-ODNP NMR method with **3** as the radical probe.

Figure 3-48 shows the HD-ODNP NMR results for the water sensed by **3** in the DMPC-POPG vesicle. The values of k_σ and k_ρ before light irradiation were calculated to be 3.26 $M^{-1}s^{-1}$ and 74.8 $M^{-1}s^{-1}$, respectively, whereas their values after light irradiation were 7.26 $M^{-1}s^{-1}$ and 85.8 $M^{-1}s^{-1}$, respectively. From the results, the correlation times (τ_c) of water sensed by **3** in DMPC-POPG were quantified to be 351 ps (ξ = 0.044) before light irradiation and 215 ps (ξ = 0.085) after light irradiation. The diffusion coefficients of water around the radical moiety were calculated to be 0.33 × 10^{-9} m^2/s and 0.54 × 10^{-9} m^2/s, for the closed-ring spin probe and opened-ring spin probe, respectively. The reproducibility of the measurement is shown with rectangles in Figure 3-48.

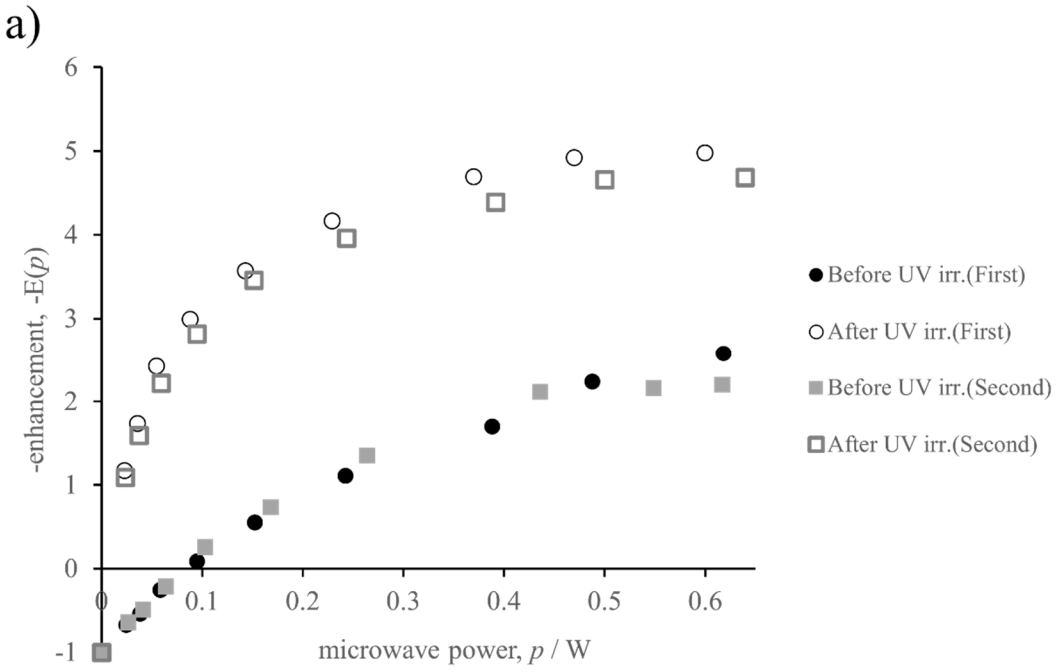

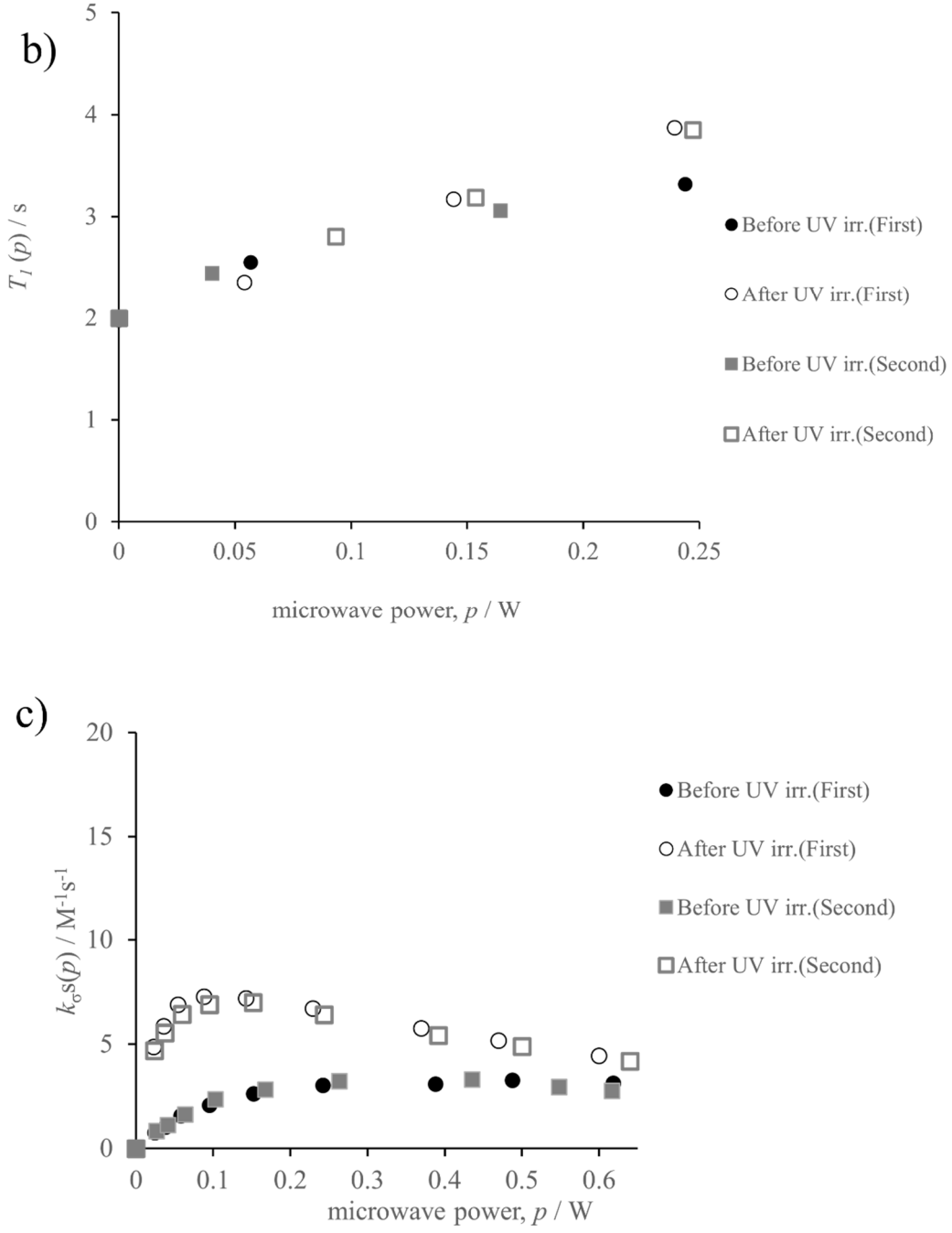

Figure 3-48: Result of DNP-NMR (a) enhancement, (b) T_1 measurement, and (c) $k_\sigma s(p)$ of probe 3 incorporated in DMPC, POPG vesicles

3.3.5.2 Dynamics of water incorporated with DOPC and POPG mixed vesicle

The analysis of the dynamics of water surrounding 20 mM DOPC and 0.2 mM POPG was carried out using HD-ODNP NMR with **3** as a spin probe.

Figure 3-49 shows the HD-ODNP NMR results for the water incorporated with DOPC-POPG vesicles using **3** as a sensing probe for DNP. The values of k_σ and k_ρ before photoirradiation were evaluated to be 6.68 $M^{-1}s^{-1}$ and 141 $M^{-1}s^{-1}$, respectively; their values changed to 10.91 $M^{-1}s^{-1}$ and 128 $M^{-1}s^{-1}$, respectively, after 10 s exposure upon 248-nm light. The correlation times (τ_c) of water around DOPC-POPG were quantified to be 332 ps (ξ = 0.047) before light irradiation and 214 ps (ξ = 0.085) after light irradiation. The diffusion coefficients of water surrounding the vesicle were 0.35 × 10^{-9} m^2/s and 0.54 × 10^{-9} m^2/s for the closed-ring spin probe and opened-ring spin probe, respectively.

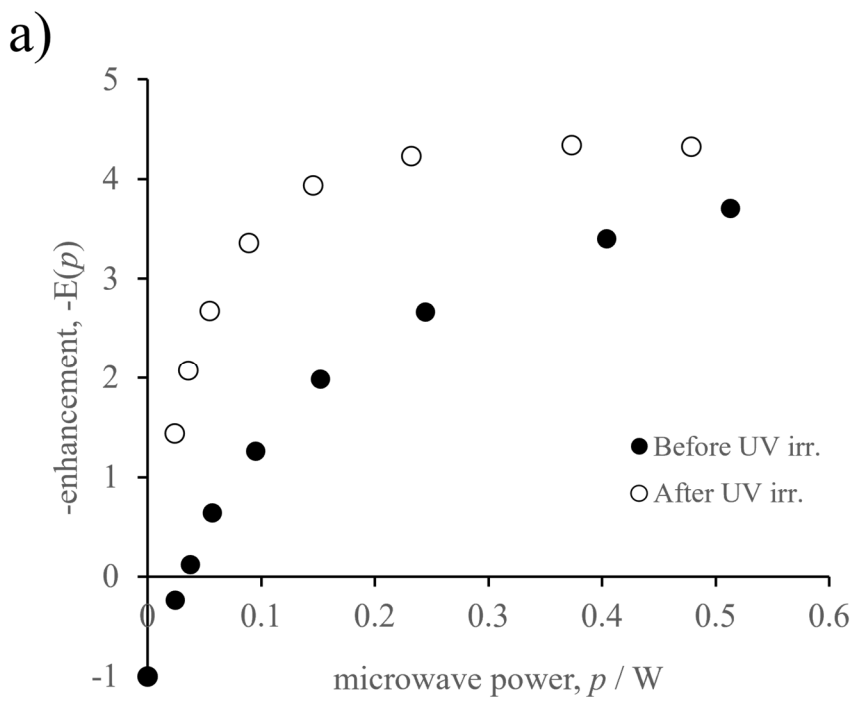

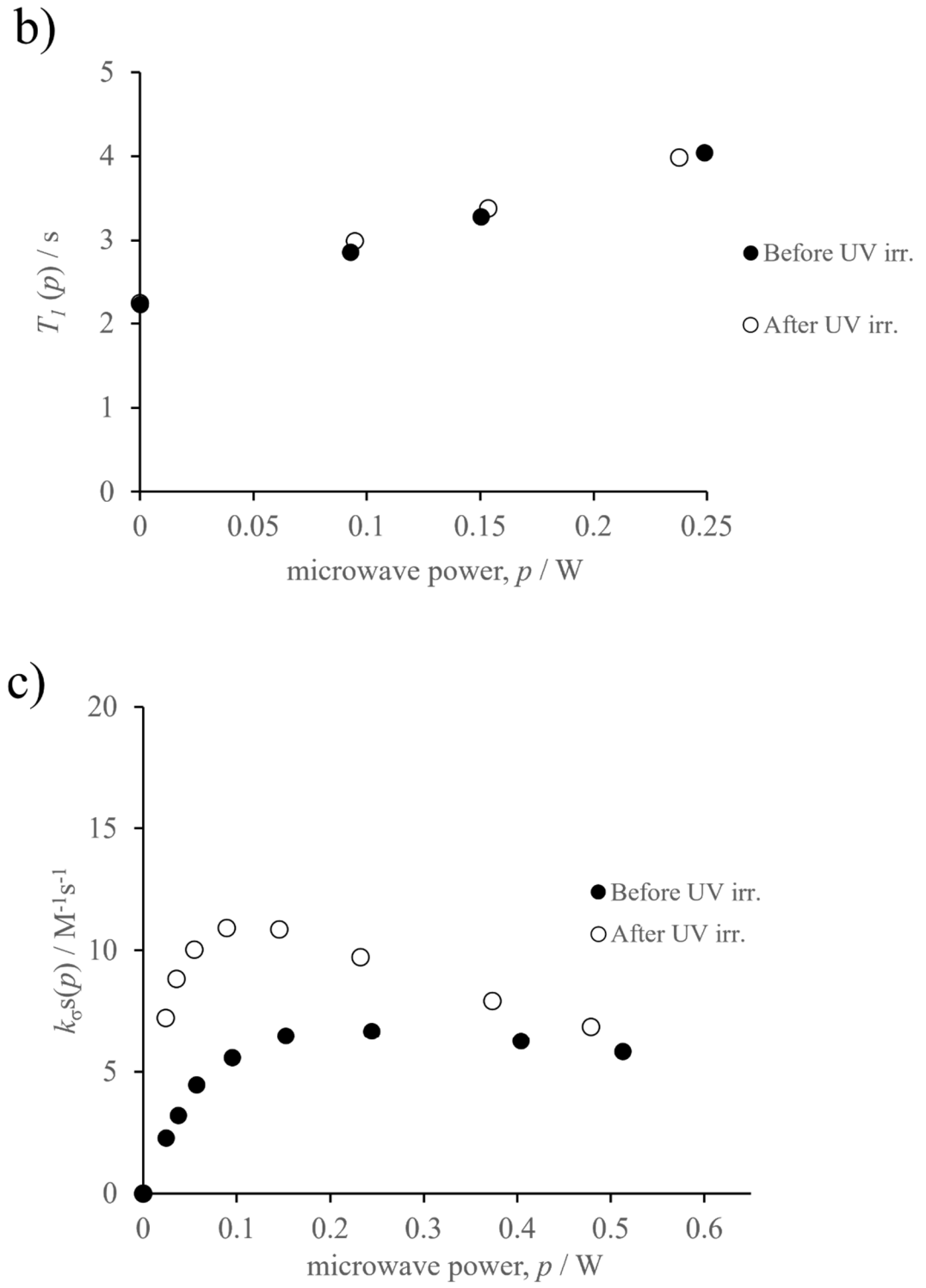

Figure 3-49: Result of DNP-NMR (a) enhancement, (b) T_1 measurement, and (c) $k_\sigma s(p)$ of probe 3 incorporated in DOPC, POPG vesicles

3.3.7 Site-selectivity analysis of water dynamics using radical probe **3**

The clear change in the ESR spectrum of **3** triggered by photolysis indicates that the environment of the radical moiety was changed by the photocleavage reaction. The higher frequency in rotational motion of the radical moiety after the light irradiation indicated that the radical moiety was in a region where molecules can move more freely rather than in the hydrophobic membrane layer, where the radical moiety was located before exposure to light irradiation.

In the DNP-NMR measurement, significant changes in the values of k_ρ and k_σ were observed by photolysis. The increments in the relaxations of the spin magnetization of aqueous proton were due to the increase in the frequency of contacts between water and the radical moiety after light irradiation (Figure 3-50). The diffusion coefficient of water sensed by probe **3** in the DMPC-POPG vesicle (0.33×10^{-9} m^2/s) was almost same to that of water sensed by probe **3** in DOPC-POPG vesicle (0.35×10^{-9} m^2/s). This fact indicates the circumstances of probe **3** were same each other in DMPC-POPG vesicle and DOPC-POPG vesicle.

There were also no difference in water dynamics sensed by the probe after photoirradiation between in DMPC-POPG vesicle (0.54×10^{-9} m^2/s) and DOPC-POPG vesicle (0.54×10^{-9} m^2/s). The values were larger than the values before light irradiation and lower than the calculated diffusion efficient of water in a system composed of 1 : 44 ratio of DMPC-POPC and water molecule by a MD simulation reported by Nilimoni.[60, 61]

This indicated that the radical moiety of **6b** was located at the vesicular surface, where the diffusion coefficients of the waters of hydration are expected to be equal even though the vesicular components are different. The linker of probe **6b**, which behaves as divalent

ammonium in water in the hydrophilic phase, is sufficiently hydrophilic to pull the radical moiety away from the hydrophobic layer. In this state, the radical moiety of **6b** is at the membrane surface, the hydrophobic alkyl chain is anchored to the membrane, and the divalent ammonium linker is attracted to water. The reason for the remaining radical moiety of **6b** at the surface of the vesicle is the hydrophobicity of the moiety itself.

In summary, site-selective measurement was successfully conducted. The dynamics of water inside vesicles were measured before light irradiation, whereas the dynamics of water outside the vesicular membrane were measured after light irradiation.

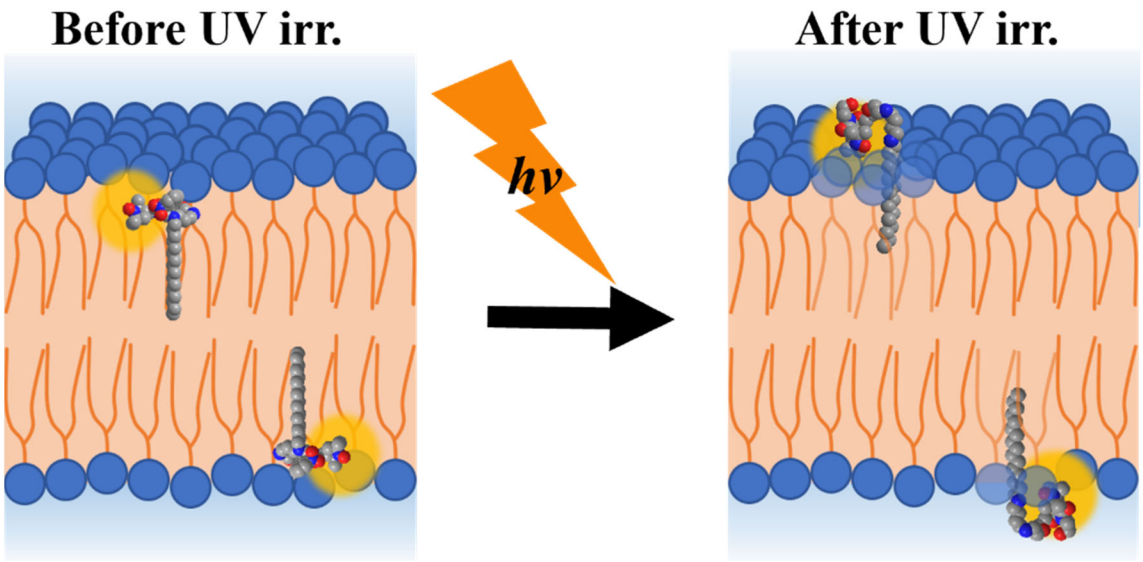

Figure 3-50: Position of the radical probe 3 before and after light irradiation

Chapter 4.

Chapter 4. Conclusions

4.1 Summary of results and discussion

In this thesis, three photolabile radical probes were designed and synthesized to develop a quantitative comparison analysis of water surrounding the same soft matter (Figure 4-1). From the photolysis experiment, it was observed that secondary reactions of radical probe **1** occurred with prolonged light irradiation due to its low photoreaction efficiency. By carrying out model experiments on photolabile groups, the author selected *o*-nitrobenzyl ether as a candidate for photolabile group. The ether bond cleavage occurred more efficiently than in *o*-nitrobenzyl ester, and therefore, secondary reactions were suppressed. Hence, radical probe **2** with *o*-nitrobenzyl ether was designed and prepared.

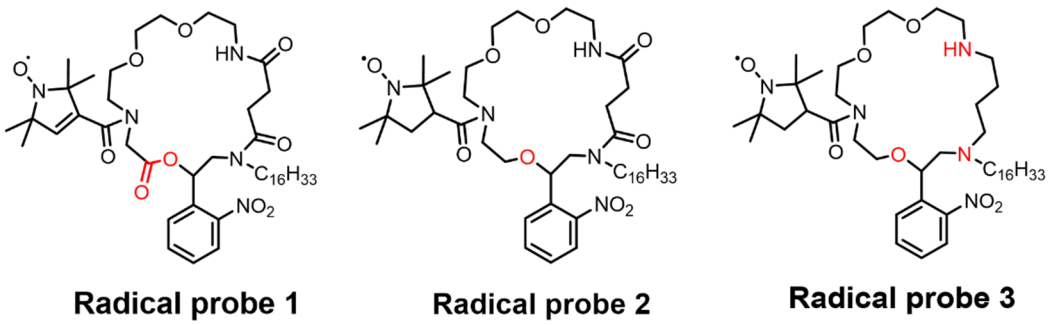

Figure 4-1: Candidate for photolabile radical probes

The photoreaction of radical probe **2** proceeded as efficiently as expected by the result of the model experiment. ESR spectra suggested that probe **2** in phospholipid vesicle dispersion remained buried in the vesicle even after light irradiation.

DNP-NMR results showed that the diffusion coefficients were 0.25 and 0.39 × 10^{-9} m^2/s before light irradiation, and 0.29 and 0.36 × 10^{-9} m^2/s after light irradiation (Figure 4-2). The small changes in the diffusion coefficients were reflected by the fact that the radical moiety remained inside the vesicular membrane even after photo-irradiation, as

expected by the ESR analysis. The difference in their values may reflect the difference in their circumstances.

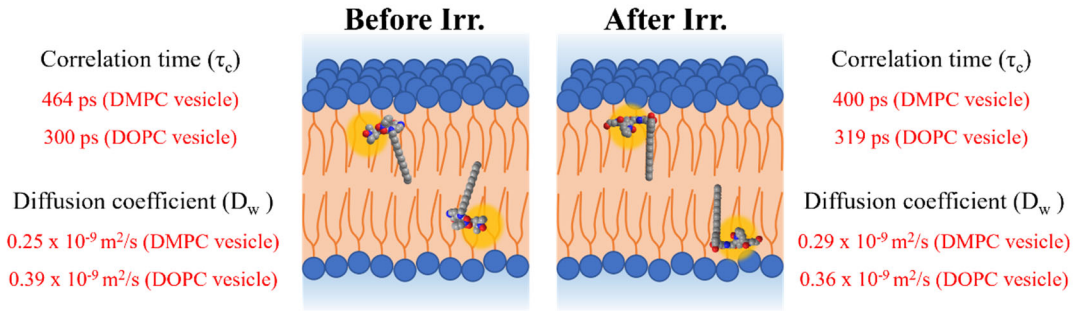

Figure 4-2: Dynamics of water near phospholipid vesicle determined using probe 2

To demonstrate a clearer photo-triggered site-switchable measurement of the water dynamics, the author designed and prepared probe **3**, the linker of which consists of a hydrophilic amino moiety. The radical moiety of probe **3** in phospholipid vesicle dispersion was measured by ESR. The clear change in line shape of the spectrum indicated the relocation of the radical moiety after light irradiation. Increase in the diffusion coefficient from 0.34 × 10^{-9} m^2/s to 0.54 × 10^{-9} m^2/s indicated that the probe sensed waters at different positions on site: before light irradiation, the probe sensed the water present in the interior of the membrane, whereas after light irradiation, the probe sensed the water on the surface of the membrane (Figure 4-3).

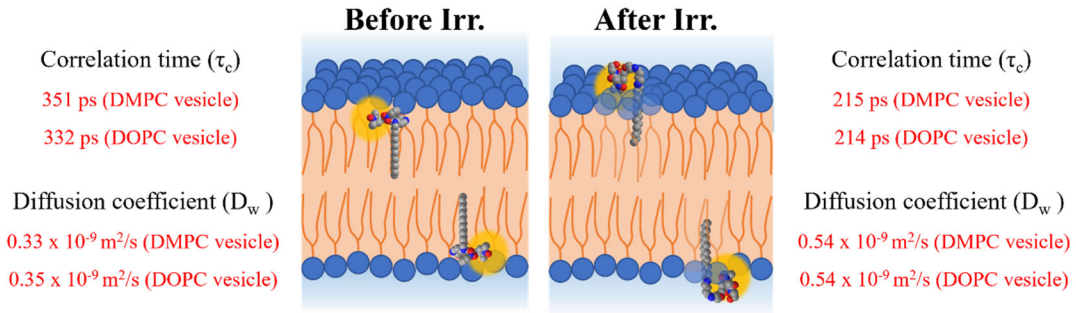

Figure 4-3: Dynamics of water near phospholipid vesicle determined using probe 3

The difference between the radical probes **2** and **3** in terms of the molecular structure is the presence of two amide groups and two amino groups. A small difference in polarity and steric structure may slightly alter the average position inside the membrane. It can be assumed that the small diffusion coefficient of **2**-sensed water in DMPC-POPG vesicle is due to the fact that **2** only sensed the water at the middle of the hydrophobic layer: **3** in DMPC-POPG vesicle sensed water in a rather hydrophilic area, and **2** and **3** in DOPC-POPG vesicle sensed water in the hydrophobic layer in the liquid crystalline phase. The molecular structure of **5** and **6b**, which correspond to the photoproduct of **2** and **3**, were very different to each other due to the unexpected photolysis of **3**. Probe **6b**, which is expected to be a diamine structure under hydrophobic conditions and a diammonium structure under aqueous conditions is more hydrophilic than **5**. As a result, **6b** sensed water on the surface of the vesicular membrane, whereas **5** still sensed water in the hydrophobic layer. This result indicates the fine design in polarity of each moiety in a molecule, which is important for developing custom probes for DNP-NMR.

This study made *in-situ* site-switchable measurement of water dynamics in different environments around and inside a biological membrane possible by developing photolabile radical probes for site-specific NMR relaxometry, namely DNP NMR. Due to the elimination of the sample exchange, the measurement can be taken at the same resonance condition for the incident microwave; this fact contributes to minimizing experimental errors. It also allows the fine quantitative comparison of water dynamics at two difference sites of a heterogeneous matter in the same sample. As evident in this study, the designing and synthesis of custom spin probes makes possible the physical analysis of the dynamics of water, a fundamental molecule in the construction of biological matter.

Considering the fact that life-like behavior is now being promoted in terms of efficiency and softening, miniaturization, and hydrospheric functionalities in the research and development of artificial molecular devices, such as molecular robots and molecular calculators, it is becoming increasingly important to understand the behavior of water molecules. However, we chemists tend to consider every object as a hard body, and our perception of chemical systems are generally constructed by the classical static understandings. To develop our understanding about the intrinsic feature of the biological system and the prospected artificial molecular devices, the development in analytical methods for dynamics of molecules, especially water, is a significant requirement. Considering this requirement, the development of site-selective measurement of water dynamics in this study is a step toward a new stage in chemistry where molecules are in motion.

Acknowledgments

The studies described in this thesis have been carried out at condensed matter chemistry laboratory. The author would like to thank people who have supported him in Ph.D life at Hokkaido University.

The author would like to express the deepest appreciation to Professor Sadamu Takeda, Assistant Professor Yoshiyuki Kageyama and Goro Maruta for giving opportunities to study in laboratory, for their kind guidance and discussion.

The author appreciates to Professor Takanori Suzuki for supporting about applying doctoral degree. The author also would like to express deep acknowledgement to Professor Koichiro Ishimori, Professor Kazuki Sada and Associate Professor Shin-ichiro Sato for their valuable discussion and helpful suggestions.

The author is much grateful to Professor Masako Kato, Associate Professor Atsushi Kobayashi, and Assistant Professor Masaki Yoshida for maintain the high-resolution NMR spectrometer.

Finally, the author would like to thank his family for encouragement and financial assistance.

References

[1] W. J. Fei, Y. Gu, K. J. M. Bishop, *Curr. Opin. Colloid Interface Sci.*, **2017**, *32*, 57–68.

[2]C. Park, J. Yoon, E. L. Thomas, *Polymer*, **2003**, *44*, 6725–6760.

[3] S. R. Bhatia, A. Mourchid, M. Joanicot, *Curr. Opin. Colloid Interface Sci*., **2001**, *6*, 471–478.

[4] M. C. Bellissent-Funel, A. Hassanali, M. Havenith, R. Henchman, P. Pohl, F. Sterpone, D. van der Spoel, Y. Xu, A. E. Garcia, *Chem. Rev*., **2016**, *116*, 7673–7697.

[5] Y. Yin, X. S. Zhao, *Acc. Chem. Res*., **2011**, *44*, 1172–1181.

[6] C. Chmelik, J. Kärger, *Chem. Soc. Rev*., **2010**, *39*, 4864–4884.

[7] K. K. Dey, A. Sen, *J. Am. Chem. Soc*., **2017**, *139*, 7666–7676.

[8] E. Lauga, T. R. Powers, *Rep. Prog. Phys*., **2009**, *72*, 096601.

[9] K. Obara, Y. Kageyama, S. Takeda, *Small*, **2022**, *18*, 2105302.

[10] A. Chakraborty, F. Deligey, J. Quach, F. M. Vigier, P. Wang, T, Wang, *Biochem. Soc. Trans*., **2020**, *48*, 1089–1099.

[11] A. C. Fogarty, D. Laage, *J. Phys. Chem. B*, **2014**, *118*, 7715–7729.

[12] F. Perakis, L. De Marco, A. Shalit, F. Tang, Z. R. Kann, T. D. Kühne, R. Torre, M. Bonn, Y. Nagata, *Chem. Rev*., **2016**, *116*, 7590–7607.

[13] B. Bagchi, *Chem. Rev*., **2005**, *105*, 3197–3219.

[14] D. I. Svergun, S. Richard, M. H. J. Koch, Z. Sayers, S. Kuprin, G. Zaccai, *Proceedings of the Nat'l Acad. Sci. U.S.A*., **1998**, *95*, 2267–2272.

[15] K. S. Singwi, A. Sjolander, *Phys. Rev*., **1960**, *119*, 863–871.

[16] J. Monroe, M. Barry, A. DeStefano, P. Aydogan Gokturk, S. Jiao, D. Robinson-Brown, T. Webber, E. J. Crumlin, S. Han, M. S. Shell, *Annu. Rev. Chem. Biomol. Eng*., **2020**, *11*, 523–557.

[17] J. G. Krummenacker, V. P. Denysenkov, M. Terekhov, L. M. Schreiber, T. F. Prisner, *J. Magn. Reson.*, **2012**, *215*, 94–99.

[18] H. Eto, F. Hyodo, N. Kosem, R. Kobayashi, K. Yasuka, M. Nakao, M. Kiniwa, H. Utsumi, *Free Radic. Biol. Med.*, **2015**, *89*, 1097–1104.

[19] M. Jansen, A. Blume, *Biophys. J*., **1995**, *68*, 997–1008.

[20] K. Gawrisch, H. C. Gaede, M. Mihailescu, S. H. White, *Eur. Biophys. J*., **2007**, *36*, 281–291.

[21] R. Kausik, S. Han, *Phys. Chem. Chem. Phys.*, **2011**, *13*, 7732–7746.

[22] R. Gruetter, S. A. Weisdorf, V. Rajanayagan, M. Terpstra, H. Merkle, C. L. Truwit, M. Garwood, S. L. Nyberg, K. Ugurbil, *J. Magn. Reson.*, **1998**, *135*, 260–264.

[23] T. L. Peck, R. L. Magin, P. C. Lauterbur, *J. Magn. Reson.*, **1995**, *108*. 114–124.

[24] I. Solomon, *Phys. Rev*., **1955**, *99*, 559–565.

[25] J. M. Franck, A. Pavlova, J. A. Scott, S. Han, *Prog. Nucl. Magn. Reson. Spectrosc*., **2013**, *74*, 33–56.

[26] R. Kausik, S. Han, *J. Am. Chem. Soc.*, **2009**, *131*, 18254–18256.

[27] J. M. Franck, Y. Ding, K. Stone, P. Z. Qin, S. Han, *J. Am. Chem. Soc*., **2015**, *137*, 12013–12023.

[28] Y. Akdogan, W. Wei, K. Y. Huang, Y. Kageyama, E. W. Danner, D. R. Miller, N. R. Martinez Rodriguez, J. H. Waite, S. Han, *Angew. Chem. Int. Ed*., **2014**, *53*, 11253–11256.

[29] K. G. Valentine, G. Mathies, S. Bédard, N. V. Nucci, I. Dodevski, M. A. Stetz, T. V. Can, R. G. Griffin, A. J. Wand, *J. Am. Chem. Soc*., **2014**, *136*, 2800–2807.

[30] R. Barnes, S. Sun, Y. Fichou, F. W. Dahlquist, M. Heyden, S. Han, *J. Am. Chem. Soc*., **2017**, *139*, 17890–17901.

[31] O. Fisette, C. Päslack, R. Barnes, J. M. Isas, R. Langen, M. Heyden, S. Han, L. V. Schäfer, *J. Am. Chem. Soc*., **2016**, *138*, 11526–11535.

[32] E. R. McCarney, B. D. Armstrong, R. Kausik, S. Han, *Langmuir*, **2008**, *24*, 10062–10072.

[33] A. N. Smith, U. T. Twahir, T. Dubroca, G. E. Fanucci, J. R. Long, *J. Phys. Chem. B*, **2016**, *120*, 7880–7888.

[34] J. Song, J. Franck, P. Pincus, M. W. Kim, S. Han, *J. Am. Chem. Soc*., **2014**, *136*, 2642–2649.

[35] J. H. Ortony, B. Qiao, C. J. Newcomb, T. J. Keller, L. C. Palmer, E. Deiss-Yehiely, M. Olvera de la Cruz, S. Han, S. I. Stupp, *J. Am. Chem. Soc*., **2017**, *139*, 8915–8921.

[36] K. Yamashita, M. P. B. Nagata, M. Miyazaki, H. Nakamura, H. Maeda, *Chem. Eng. J*., **2010**, *165*, 324–327.

[37] B. D. Armstrong, M. D. Lingwood, E. R. McCarney, E. R. Brown, P. Blumler, S. Han, *J. Magn. Reson*., **2008**, *191*, 273–281.

[38] I. Kaminker, R. Barnes, S. Han, *Methods Enzymol*., **2015**, *564*, 457–483.

[39] P. J. M. van Bentum, G. H. A. van der Heijden, J. A. Villanueva-Garibay, A. P. M. Kentgens, *Phys. Chem. Chem. Phys*., **2011**, *13*, 17831–17840.

[40] G. Sosnovsky, N. U. M. Rao, J. Lukszo, *Z. Naturforsch*, **1986**, *41b*, 1293–1305

[41] M. Kim, S. L. Diamond, *Bioorganic Med. Chem. Lett.*, **2006**, *16*, 4007–4010.

[42] Z. Tajmoradi, H. R. Mamaqani, M. S. Kalajahi, *J. Polymer*, **2020**, *205*, 122859.

[43] H. Shen, Y. Xia, Z. Qin, J. Wu, L. Zhang, Y. Lu, X. Xia, W. Xu, *J. Polym. Sci. A Polym. Chem.*, **2017**, *55*, 2770–2870.

[44] Y. Yang, F. Liu, X. Liu, B. Xing, *Nanoscale*, **2013**, *5*, 231–238.

[45] Y. Lin, M. M. Mazo, S. C. Skaalure, M. R. Thomas, S. R. Schultz, M. M. Stevens, *Chem. Sci*., **2019**, *10*, 1158–1167.

[46] M. Kunishima, C. Kawachi, K. Hioki, K.Terao, S. Tani, *Tetrahedron*, **2001**, *57*, 1551–1558.

[47] N. C. Kasuga, Y. Saito, N. Okamura, T. Miyazaki, H. Satou, K. Watanabe, T. Ohta, S. Morimoto, K. Yamaguchi, *J. Photochem. Photobiol. A*, **2016**, *321*, 41–47.

[48] W. Yao, C. Liu, N. Wang, H. Zhou, F. Shafiq, S. Yu, W. Qiao, ***J***. *Mol. Liq.*, **2021**, *334*, 116016.

[49] P. Klán, T. Šolomek, C. G. Bochet, A. Blanc, R. Givens, M. Rubina, V. Popik, A. Kostikov, J. Wirz, *Chem. Rev*., **2013**, *113*, 119–191.

[50] S. Cheawchan, H. Sogawa, T. Takata, *Macromol. Chem. Phys*., **2021**, *222*, 2000459.

[51] N. Madhavan, M. S. Gin, *Chem. Commun*., **2004**, 2728–2729.

[52] N. F. König, A. A. Ouahabi, L. Oswald, R. Szweda, L. Charles, J. F. Lutz, *Nature Commun*., **2019**, *10*, 3774.

[53] Gyeorye Lee, Master's Thesis, Hokkaido Univ., **2018**.

[54] Z. A. De los Santos, C. Wolf, *J. Am. Chem. Soc*., **2016**, *138*, 13517–13520.

[55] L. Peng, M. Goeldner, *J. Org. Chem*., **1996**, *61*, 185–191.

[56] M. Shibuya, M. Tomizawa, I. Suzuki, Y. Iwabuchi, *J. Am. Chem. Soc.*, **2006**, *128*, 8412–8413.

[57] Y. Iwabuchi, *J. Syn. Org. Chem.*, **2008**, *66*, 1076.

[58] X. Lei, A. Jalla, M. A. A. Shama, J. M. Stafford, B. Cao, *Synthesis*, **2015**, *47*, 2578–2585.

[59] J. C. Hindman, A. Svirmickas, M. Wood, *J. Chem. Phys*., **1973**, *59*, 1517–1522.

[60] D. Mondal, S. Malik, P. Banerjee, N. Kundu, A. Debnath, N. Sarkar, *Langmuir*, **2020**, *36*, 12423–12434.

[61] B. Choi, N, Katoch, H. Kim, J. Park, I. Ko, O. Kwon, E. Woo, *BioMed. Eng.*, **2020** *19*, 35.

Supplementary section (^{1}H,^{13}CNMR, MS data)

Radical probe **1**

HRMS (Crude **1**)

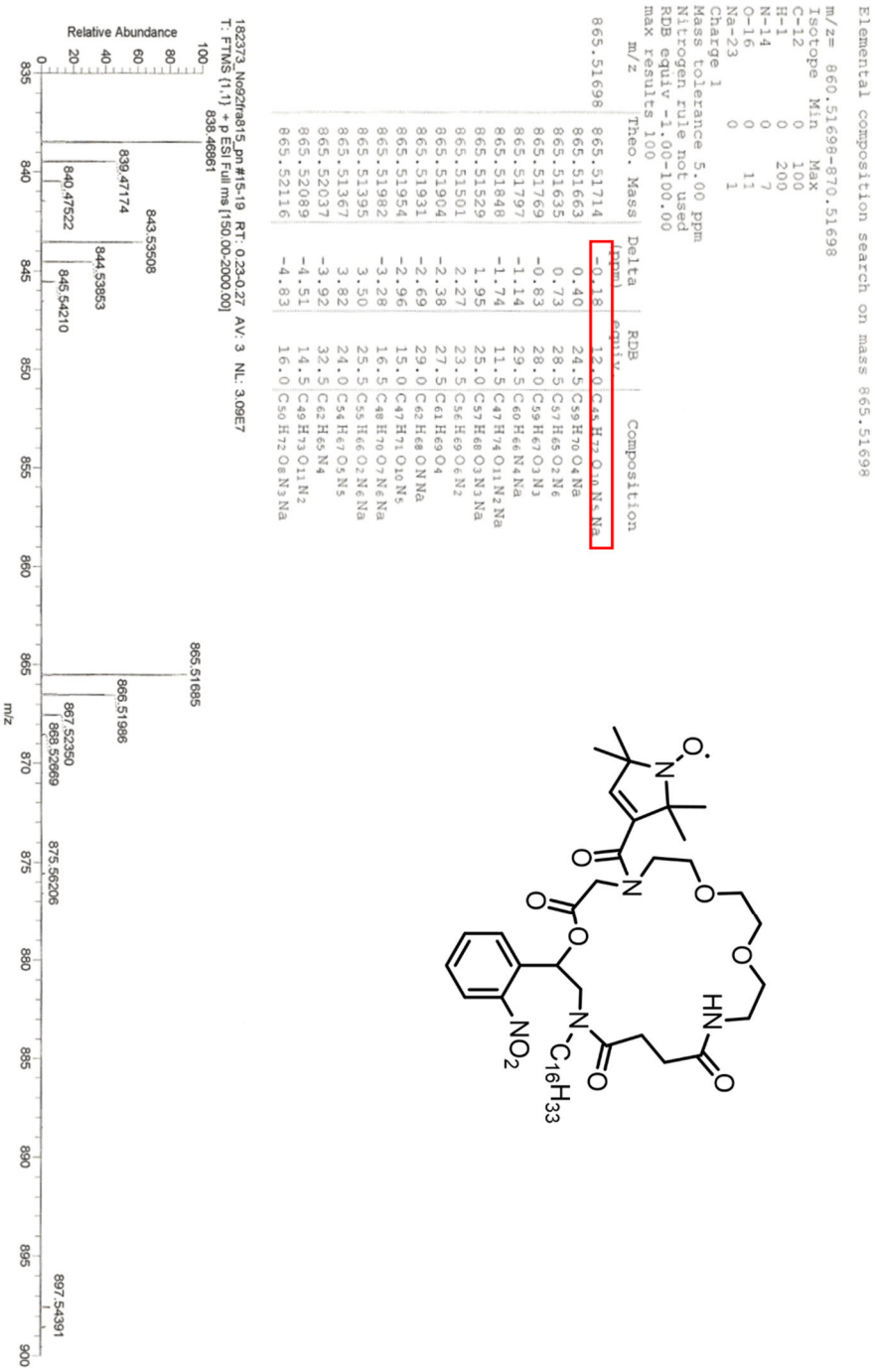

LRMS (Pure **1**)

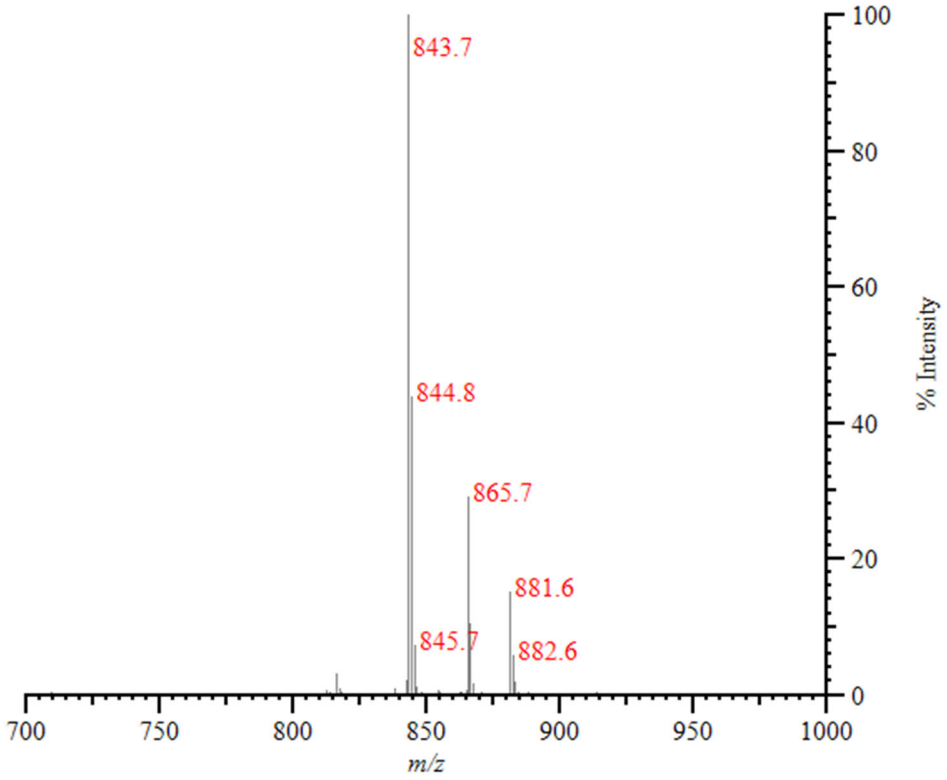
843.7
844.8
865.7
881.6
845.7
882.6
100
80
60
40
20
0
% Intensity
700
750
800
850
900
950
1000
m/z

Radical probe **2**

HRMS (ESI)

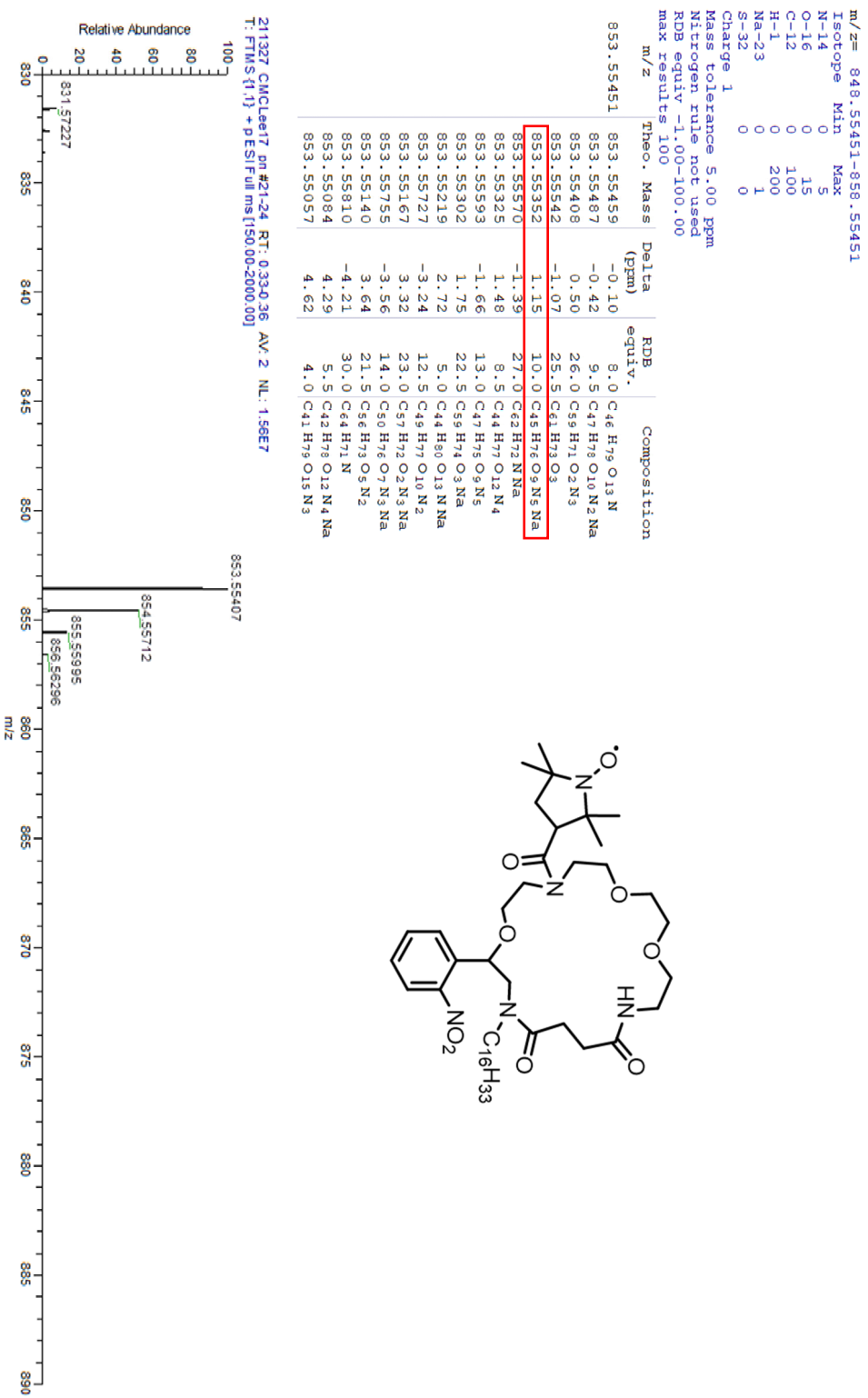

Radical probe **3**

HRMS (ESI)

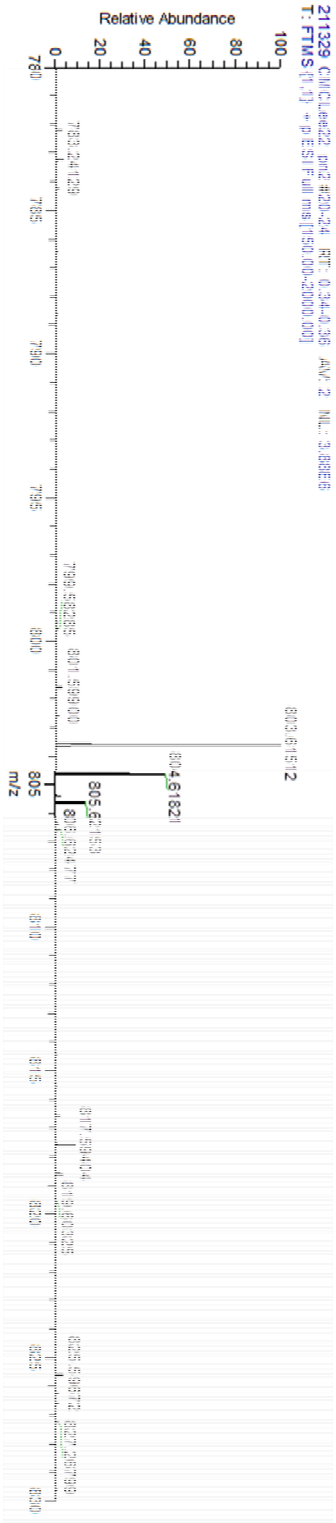

m/z= 798.61466-808.61466
Isotope Min Max
N-14 0 5
O-16 0 15
C-12 0 100
H-1 0 200
Na-23 0 1
S-32 0 0
Charge 1
Mass tolerance 5.00 ppm
Nitrogen rule not used
RDB equiv -1.00-100.00
max results 100

m/z	Theo. Mass	Delta (ppm)	RDB equiv.	Composition
803.61466	803.61467	-0.01	9.0	$C_{48}H_{82}O_5N_3Na$
	803.61439	0.33	7.5	$C_{47}H_{83}O_8N_2$
	803.61601	-1.68	8.5	$C_{50}H_{84}O_6Na$
	803.61305	2.00	8.0	$C_{45}H_{81}O_7N_5$
	803.61254	2.63	20.5	$C_{59}H_{79}O$
	803.61707	-3.00	12.0	$C_{50}H_{81}O_5N_3$
	803.61199	3.32	4.5	$C_{45}H_{84}O_8N_2Na$
	803.61735	-3.35	13.5	$C_{51}H_{80}O_2N_4Na$
	803.61171	3.67	3.0	$C_{44}H_{85}O_{11}N$
	803.61120	4.30	21.0	$C_{57}H_{77}N_3$
	803.61842	-4.67	11.5	$C_{52}H_{83}O_6$
	803.61065	4.99	5.0	$C_{43}H_{82}O_7N_5Na$

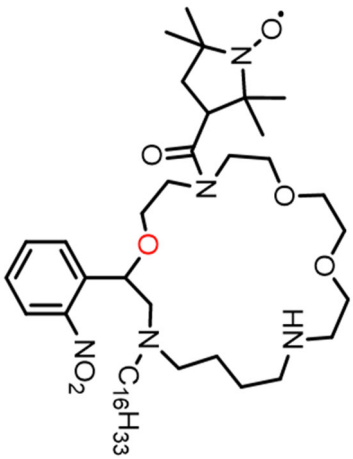

Compounds **8**

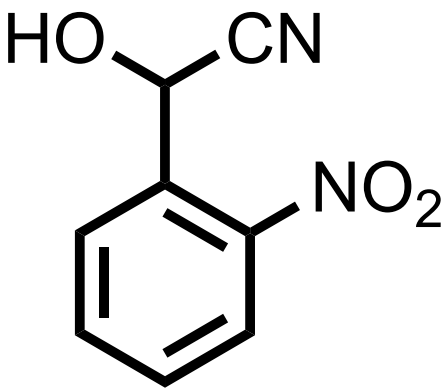

^{1}H-NMR

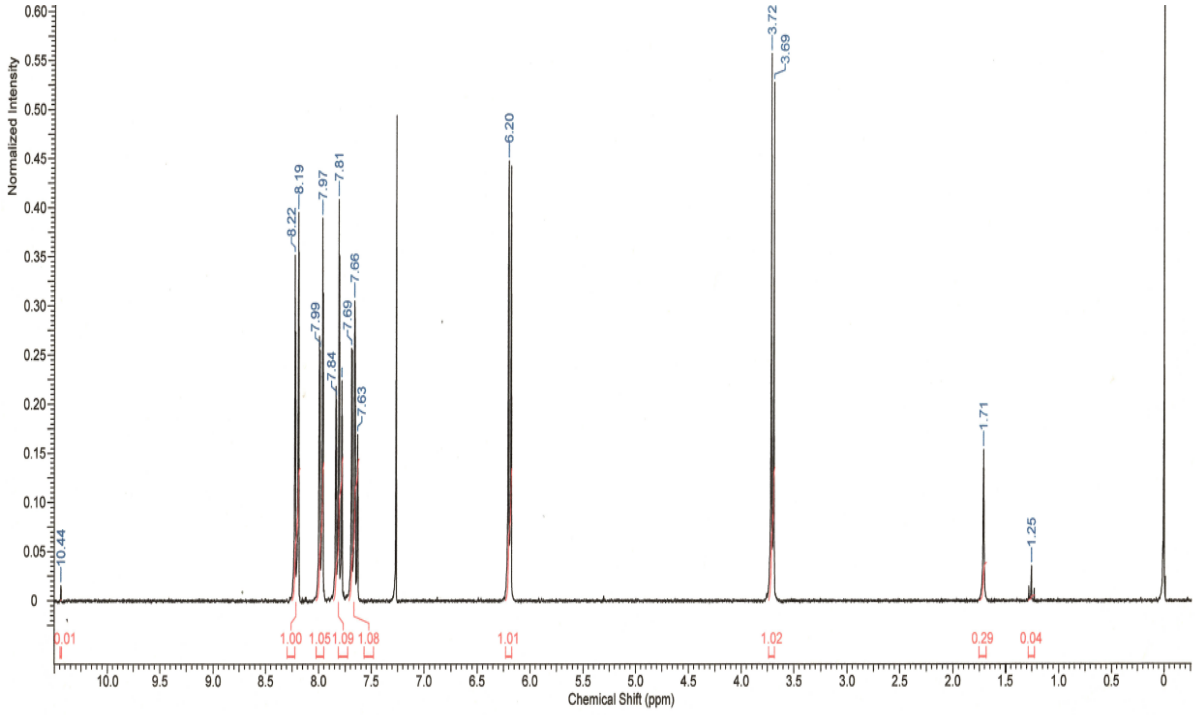

Compounds **9**

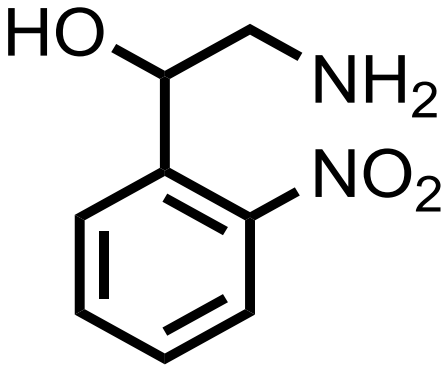

^{1}H-NMR

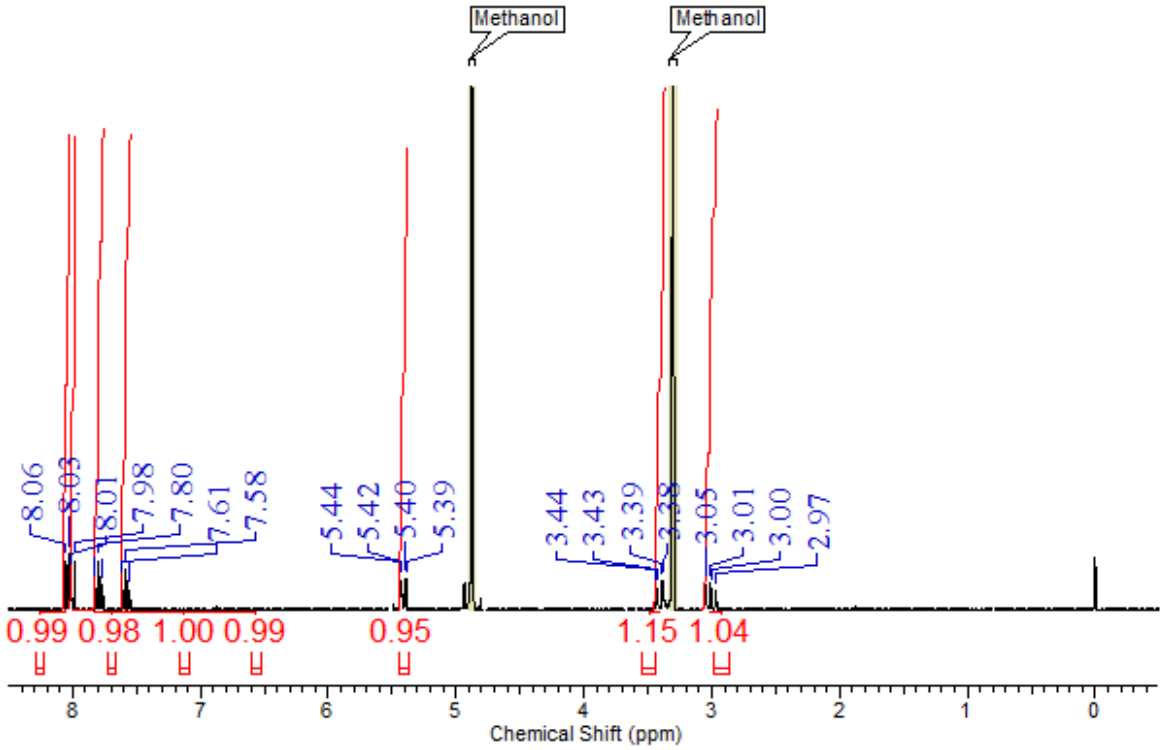

Compounds **10**

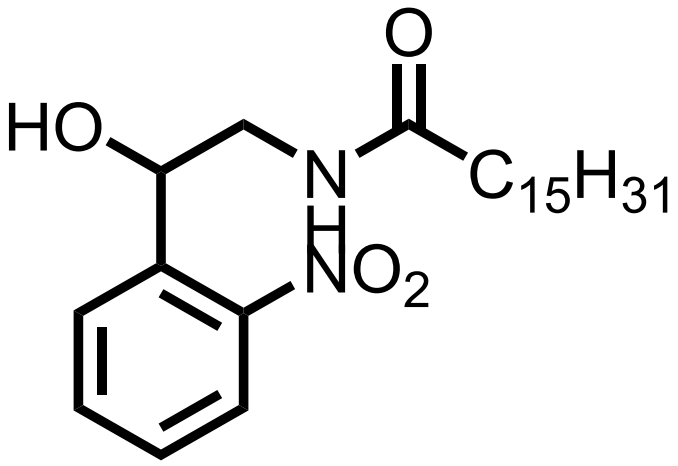

^{1}H-NMR

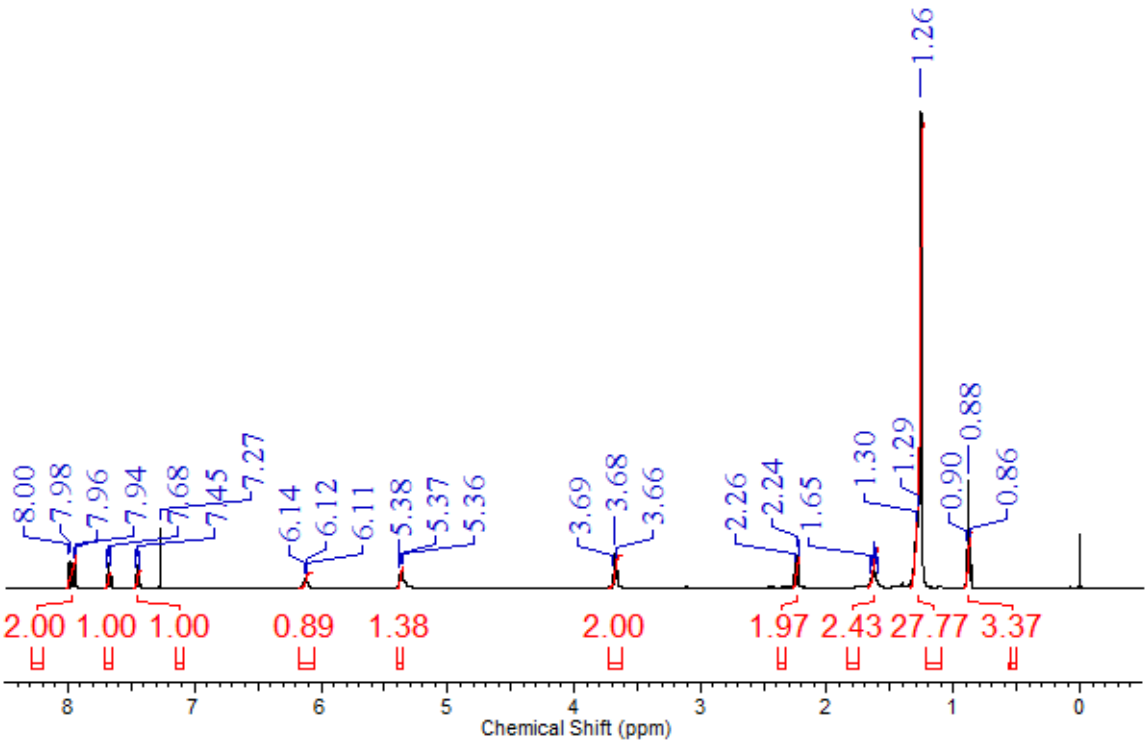

Compounds **11**

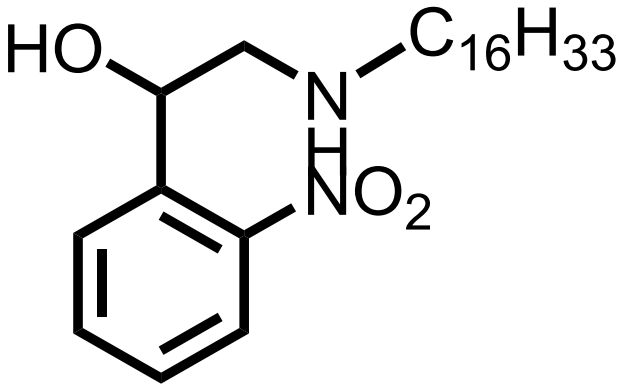

^{1}H-NMR

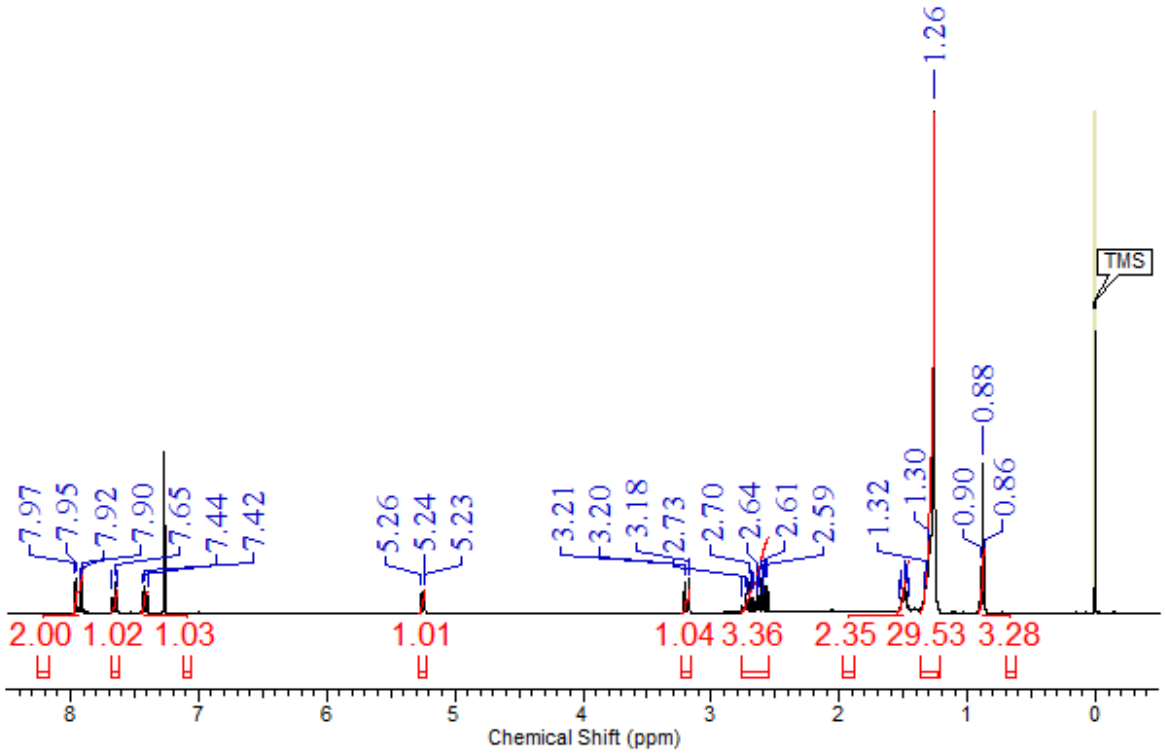

Compounds **15**

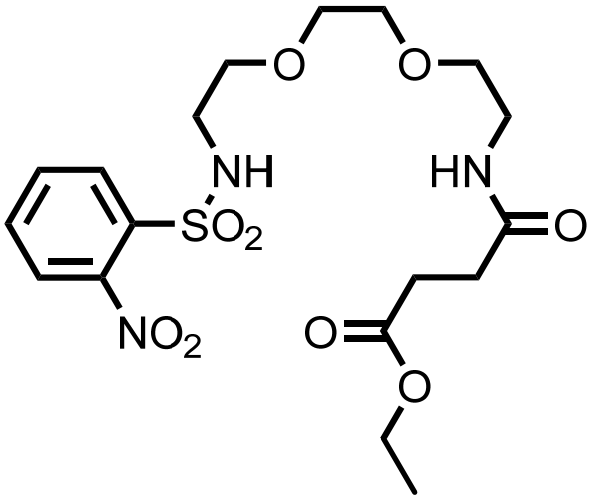

^{1}H-NMR

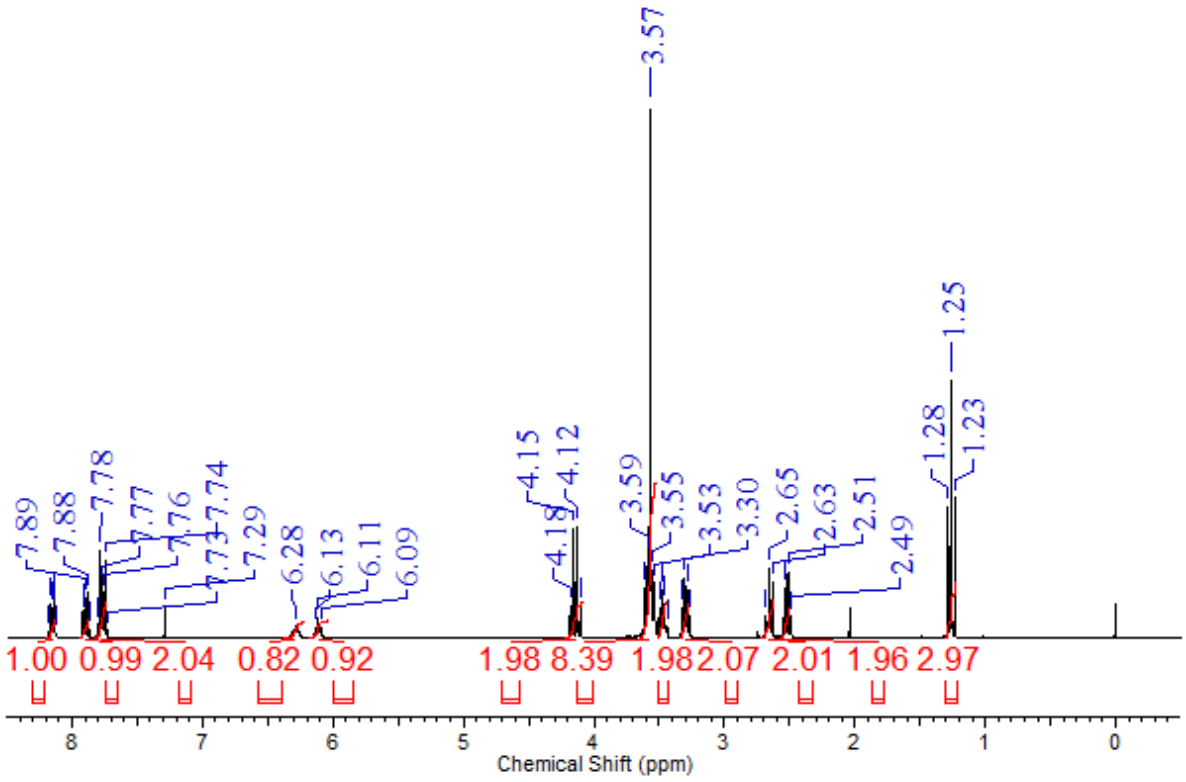

^{13}C-NMR

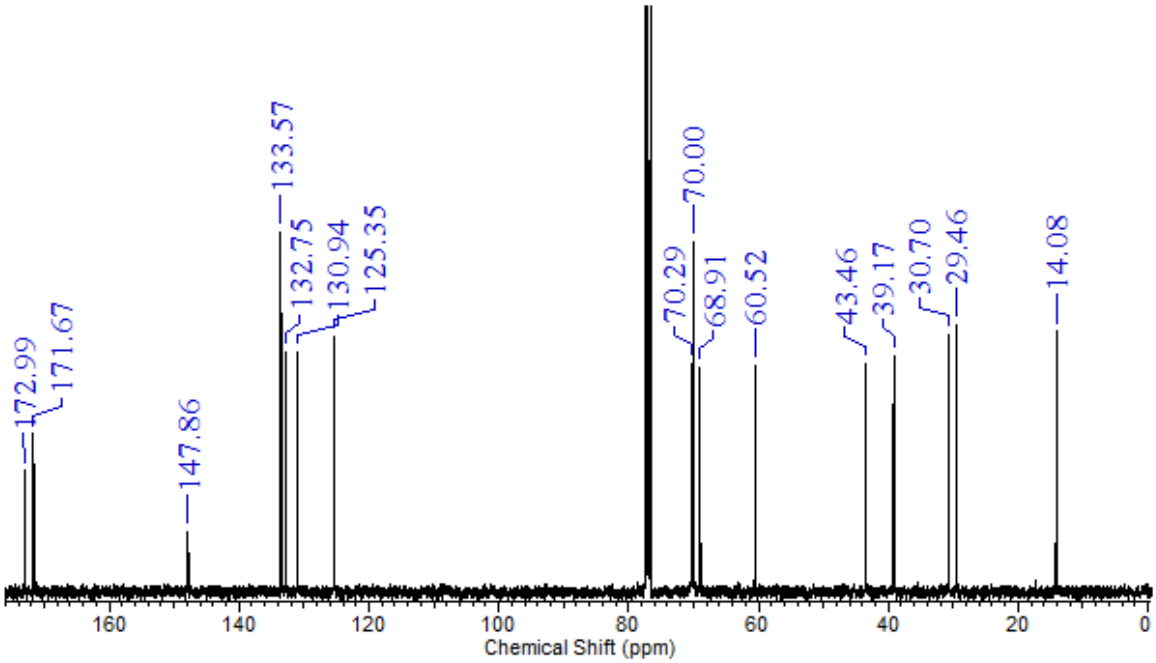

HRMS (ESI)

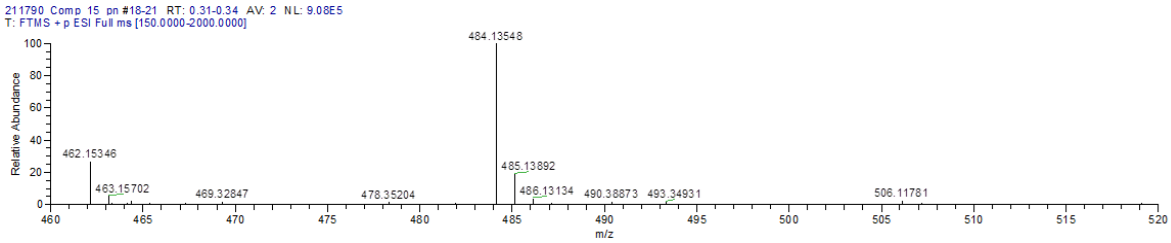

m/z	Theo. Mass	Delta (ppm)	RDB equiv.	Composition
484.13544	484.13575	-0.63	5.0	$C_{17}H_{28}O_{12}N_2S$
	484.13506	0.79	14.5	$C_{23}H_{22}O_9N_3$
	484.13602	-1.20	6.5	$C_{18}H_{27}O_9N_3NaS$
	484.13640	-1.98	14.0	$C_{25}H_{24}O_{10}$
	484.13658	-2.35	22.5	$C_{32}H_{22}O_2NS$
	484.13667	-2.55	15.5	$C_{26}H_{23}O_7NNa$
	484.13417	2.62	19.5	$C_{30}H_{23}O_2NNaS$
	484.13399	2.99	11.0	$C_{23}H_{25}O_{10}Na$
	484.13390	3.19	18.0	$C_{29}H_{24}O_5S$
	484.13736	-3.97	6.0	$C_{20}H_{29}O_{10}NaS$
	484.13334	4.34	2.0	$C_{15}H_{29}O_{12}N_2NaS$
	484.13321	4.62	27.5	$C_{35}H_{18}O_2N$
	484.13307	4.90	0.5	$C_{14}H_{30}O_{15}NS$

Compounds **16**

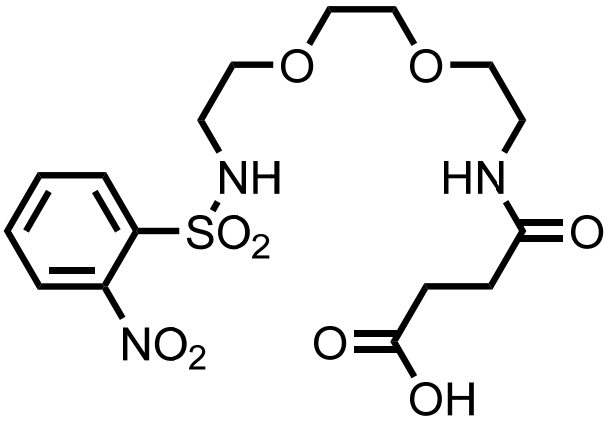

^{1}H-NMR

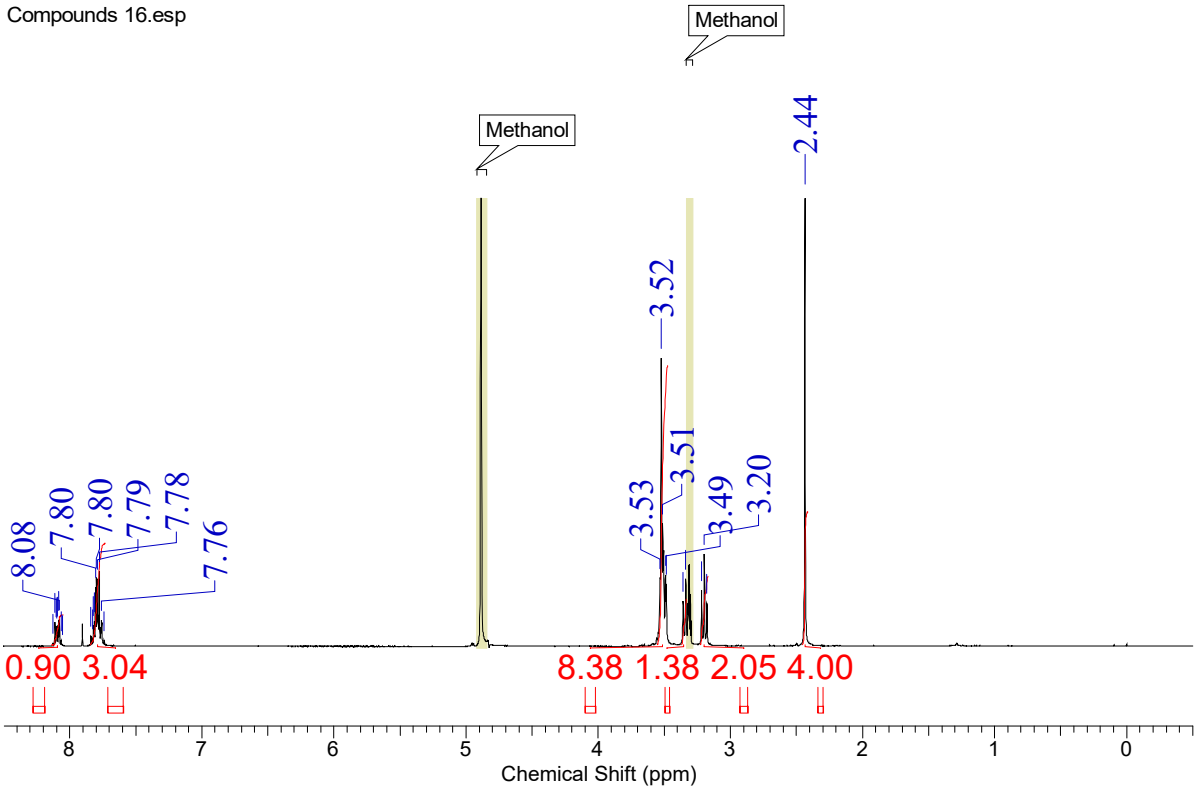

^{13}C-NMR

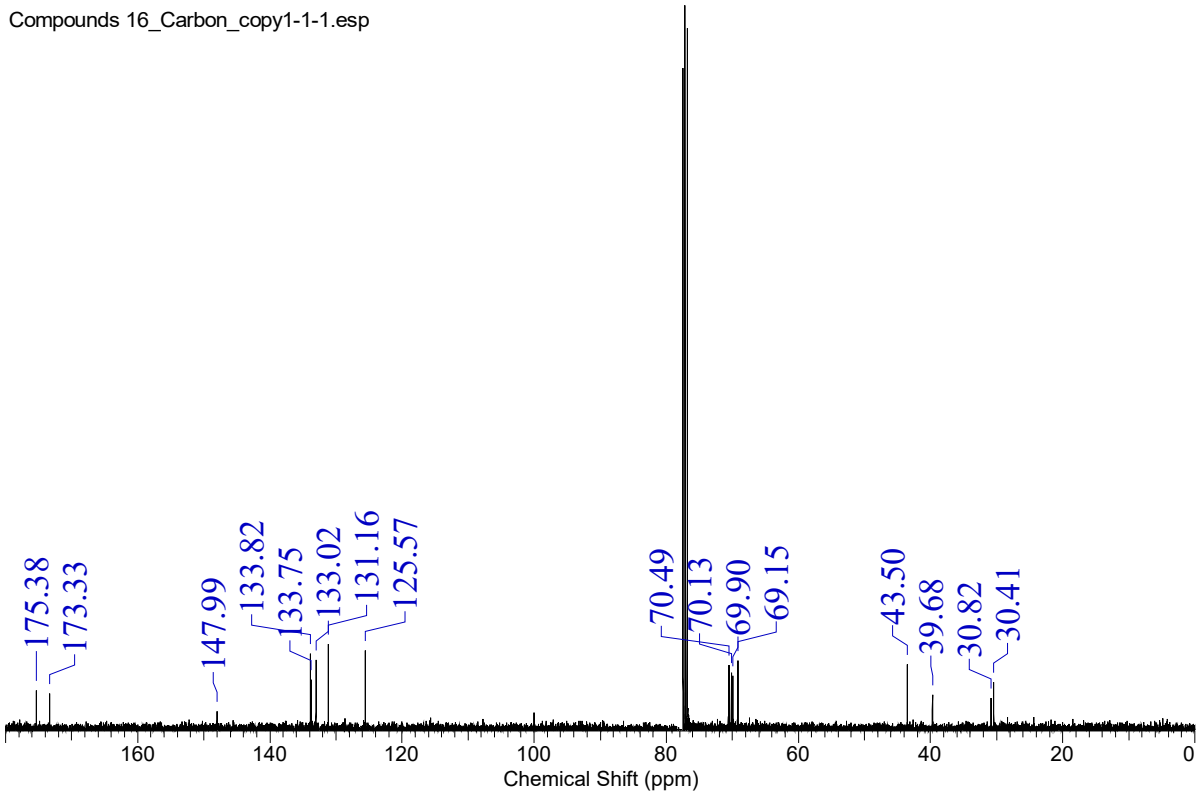

HRMS (ESI)

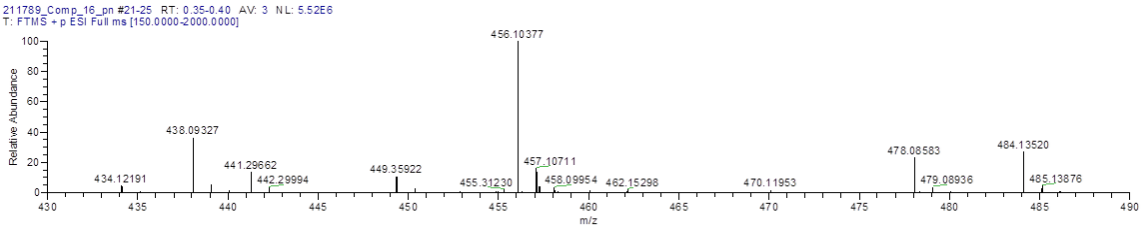

m/z	Theo. Mass	Delta (ppm)	RDB equiv.	Composition
456.10377	456.10376	0.03	14.5	$C_{21}H_{18}O_9N_3$
	456.10445	-1.48	5.0	$C_{15}H_{24}O_{12}N_2S$
	456.10287	1.97	19.5	$C_{28}H_{19}O_2NNaS$
	456.10472	-2.09	6.5	$C_{16}H_{23}O_9N_3NaS$
	456.10269	2.36	11.0	$C_{21}H_{21}O_{10}Na$
	456.10260	2.57	18.0	$C_{27}H_{20}O_5S$
	456.10510	-2.91	14.0	$C_{23}H_{20}O_{10}$
	456.10528	-3.30	22.5	$C_{30}H_{18}O_2NS$
	456.10537	-3.51	15.5	$C_{24}H_{19}O_7NNa$
	456.10204	3.79	2.0	$C_{13}H_{25}O_{12}N_2NaS$
	456.10191	4.09	27.5	$C_{33}H_{14}O_2N$
	456.10177	4.39	0.5	$C_{12}H_{26}O_{15}NS$

Compounds **17** (mixture of 2 diastereomers)

^{1}H-NMR

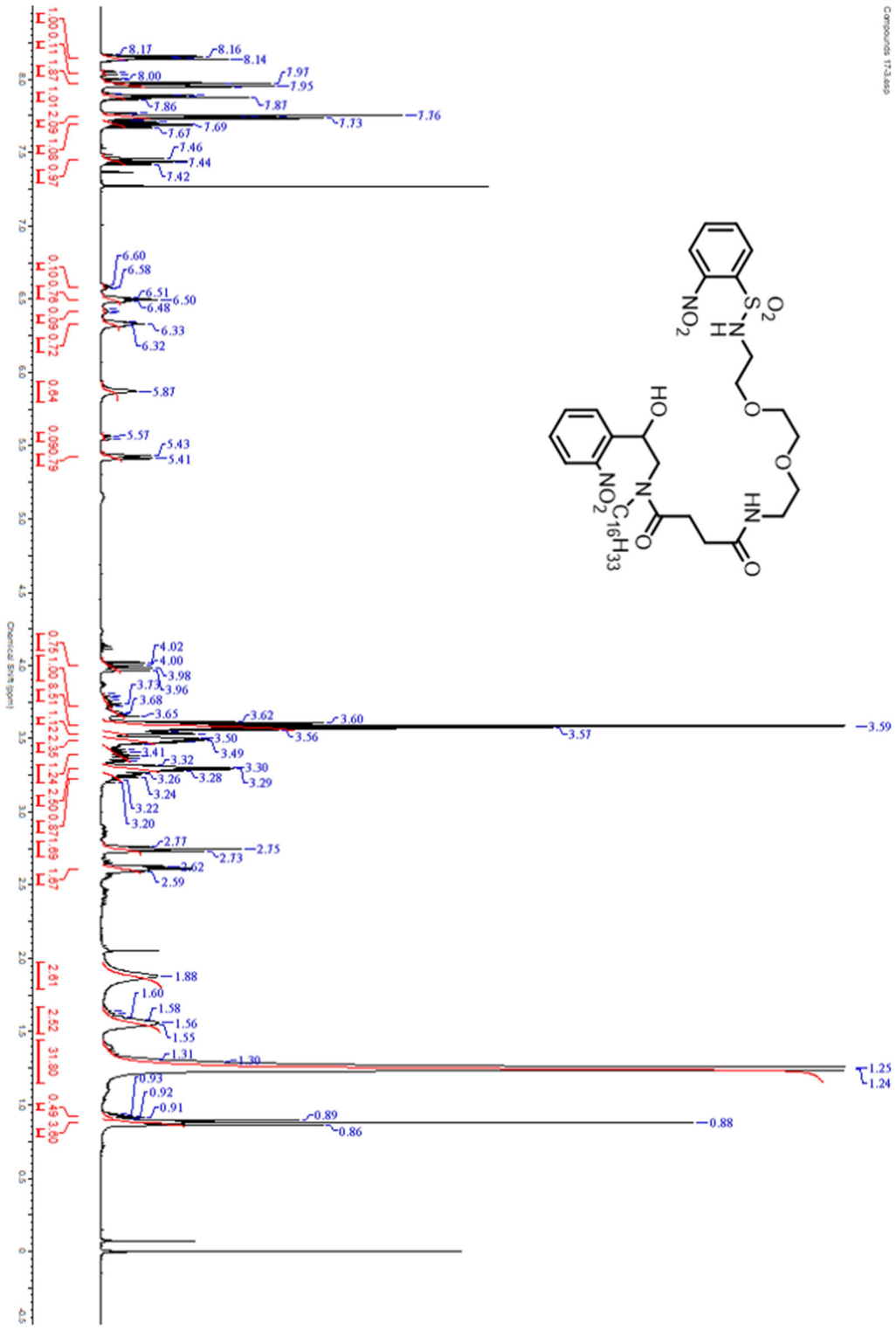

Compounds **18** (mixture of 2 diastereomers)

^{1}H-NMR

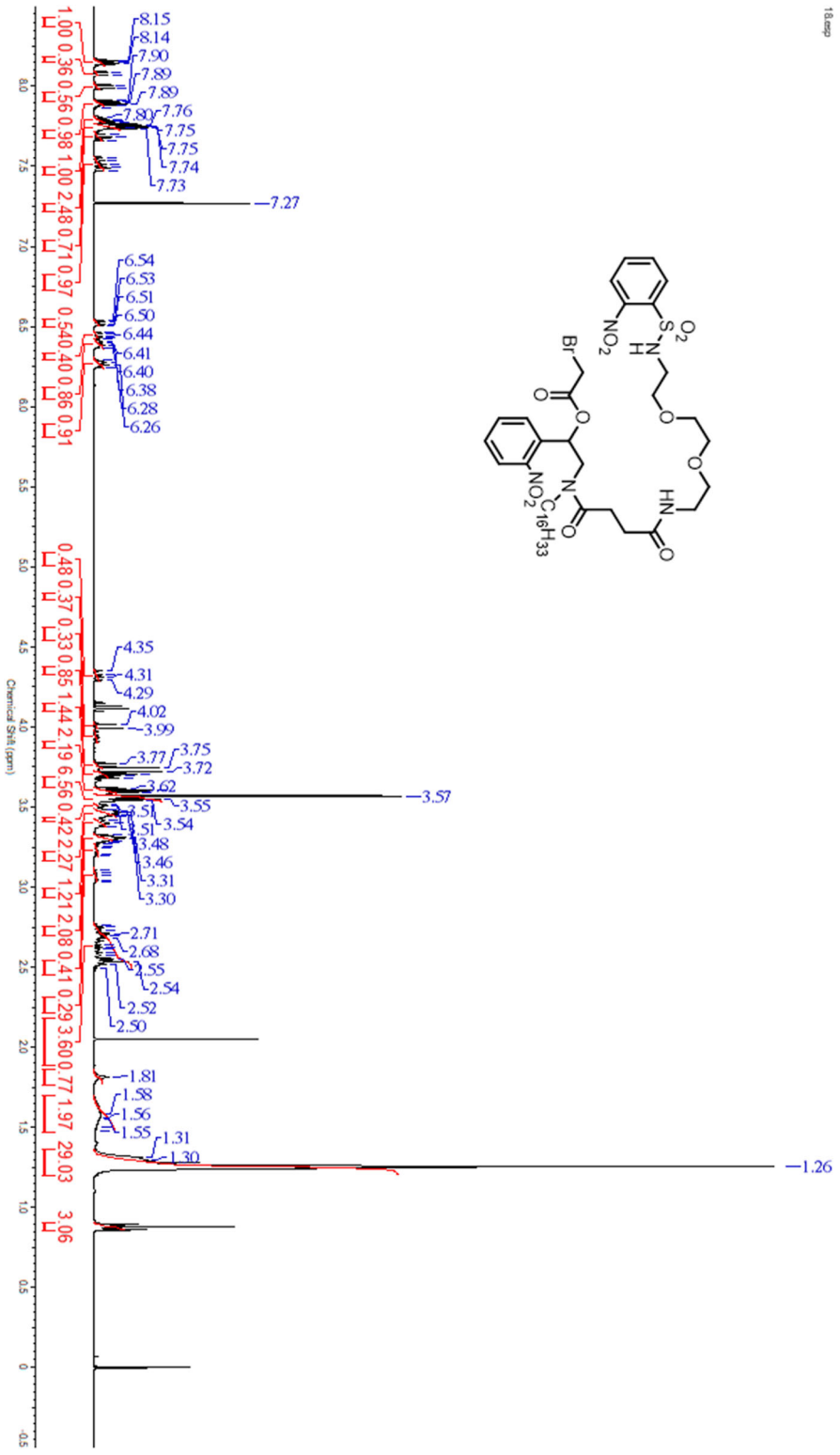

Compounds **19** (mixture of 2 diastereomers)

^{1}H-NMR

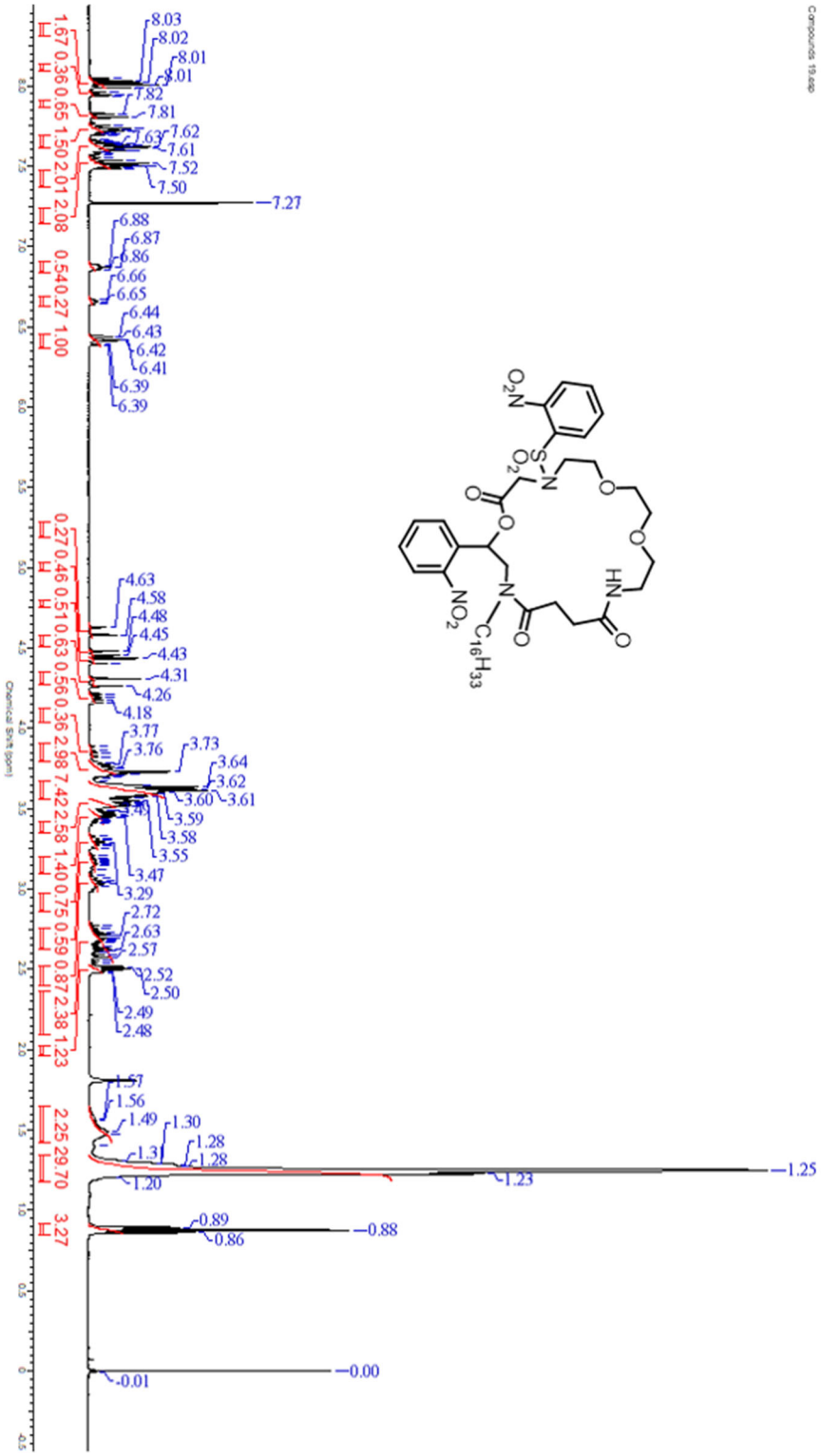

LRMS

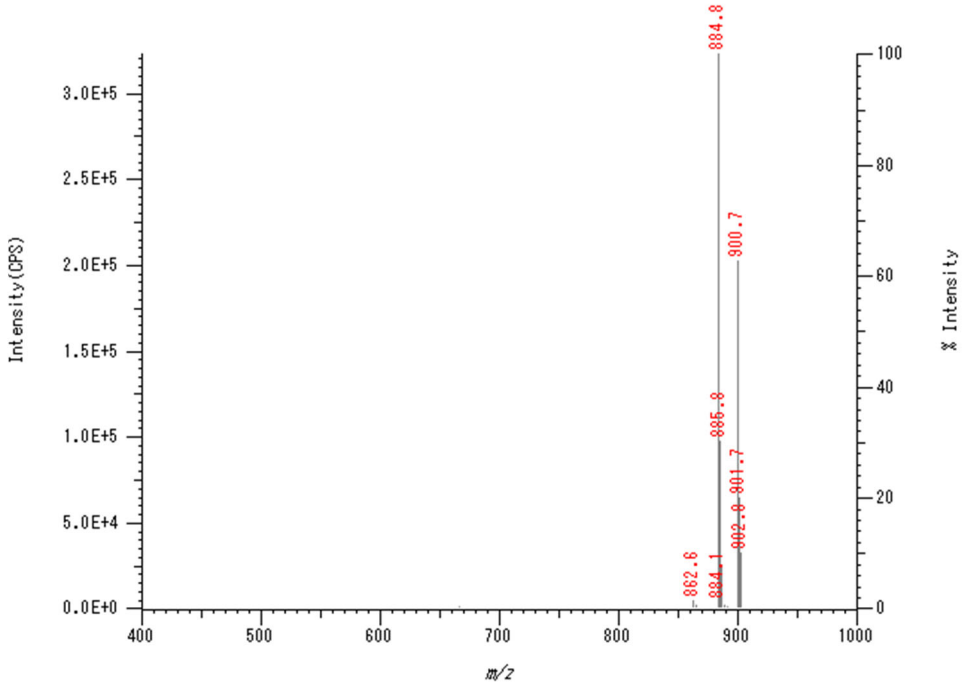

HRMS (ESI)

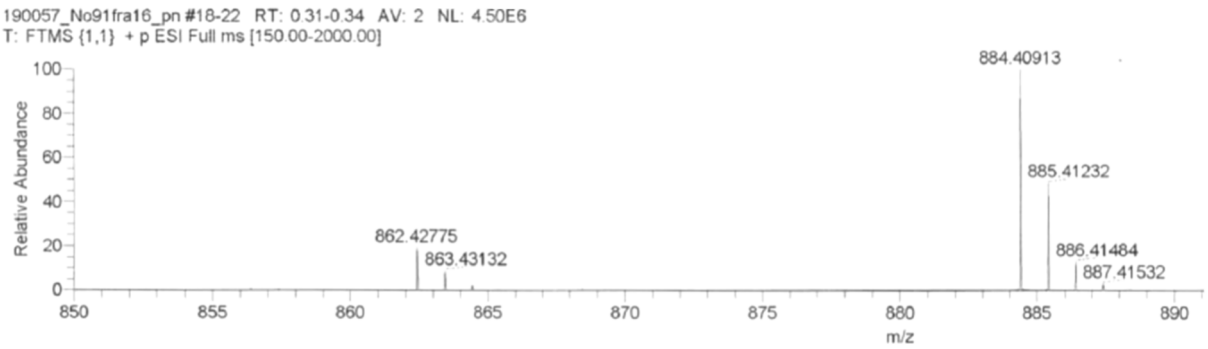

Compounds **20** (mixture of 2 diastereomers)

^{1}H-NMR

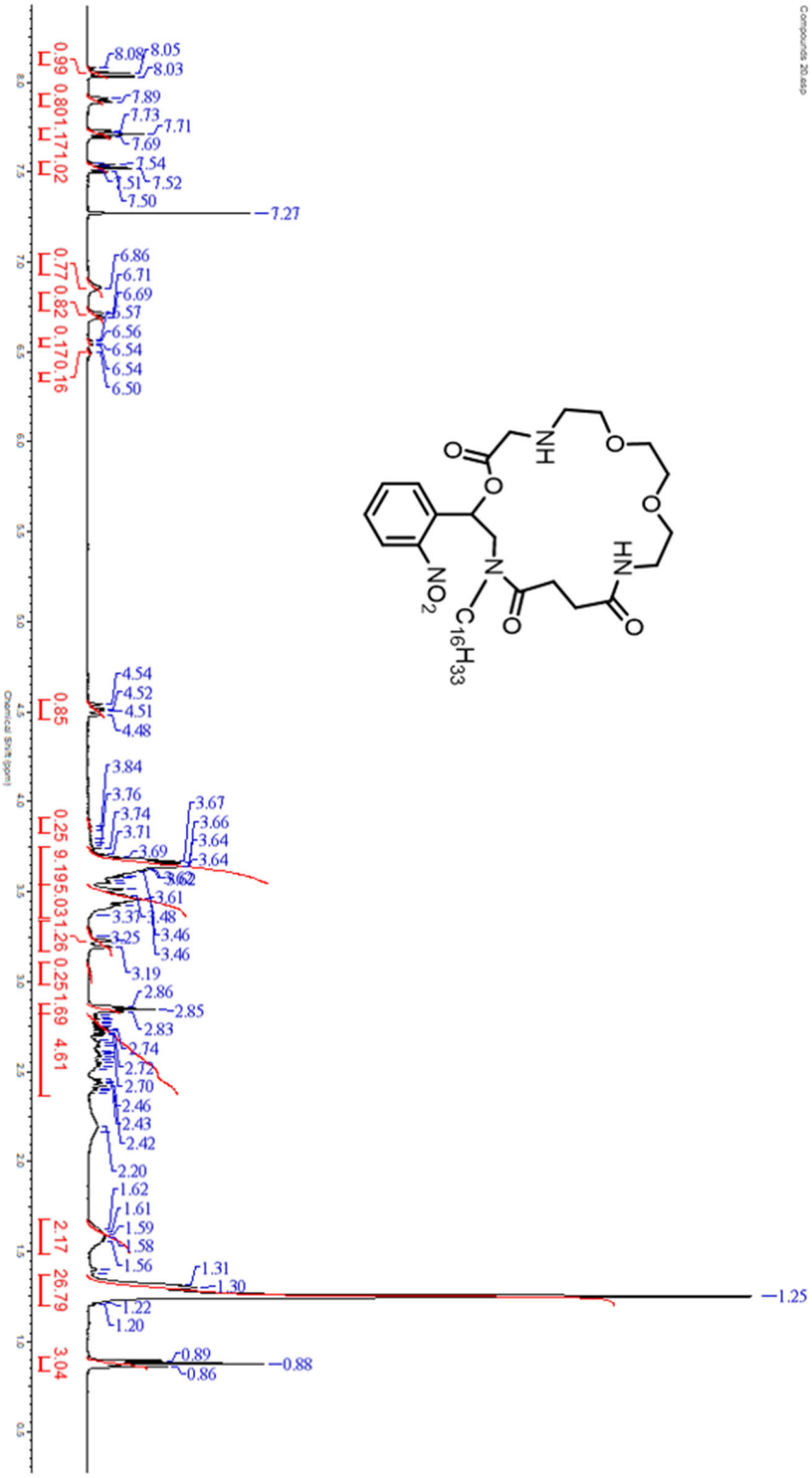

HRMS (ESI)

Elemental composition search on mass 677.44904

m/z= 672.44904-682.44904

Isotope	Min	Max
C-12	0	100
H-1	0	200
N-14	0	6
O-16	0	10
Na-23	0	0

Charge 1
Mass tolerance 5.00 ppm
Nitrogen rule not used
RDB equiv -1.00-100.00
max results 100

m/z	Theo. Mass	Delta (ppm)	RDB equiv.	Composition
677.44904	677.44839	0.96	8.5	$C_{36}H_{61}O_8N_4$
	677.44973	-1.02	8.0	$C_{38}H_{53}O_9N$
	677.45107	-3.00	13.0	$C_{39}H_{59}O_5N_5$
	677.44654	3.69	21.5	$C_{48}H_{57}ON_2$
	677.45241	-4.98	12.5	$C_{41}H_{61}O_6N_2$

Compounds **21**

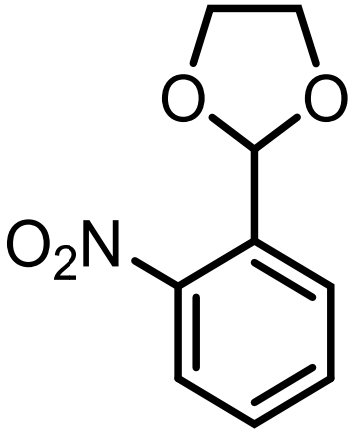

^{1}H-NMR

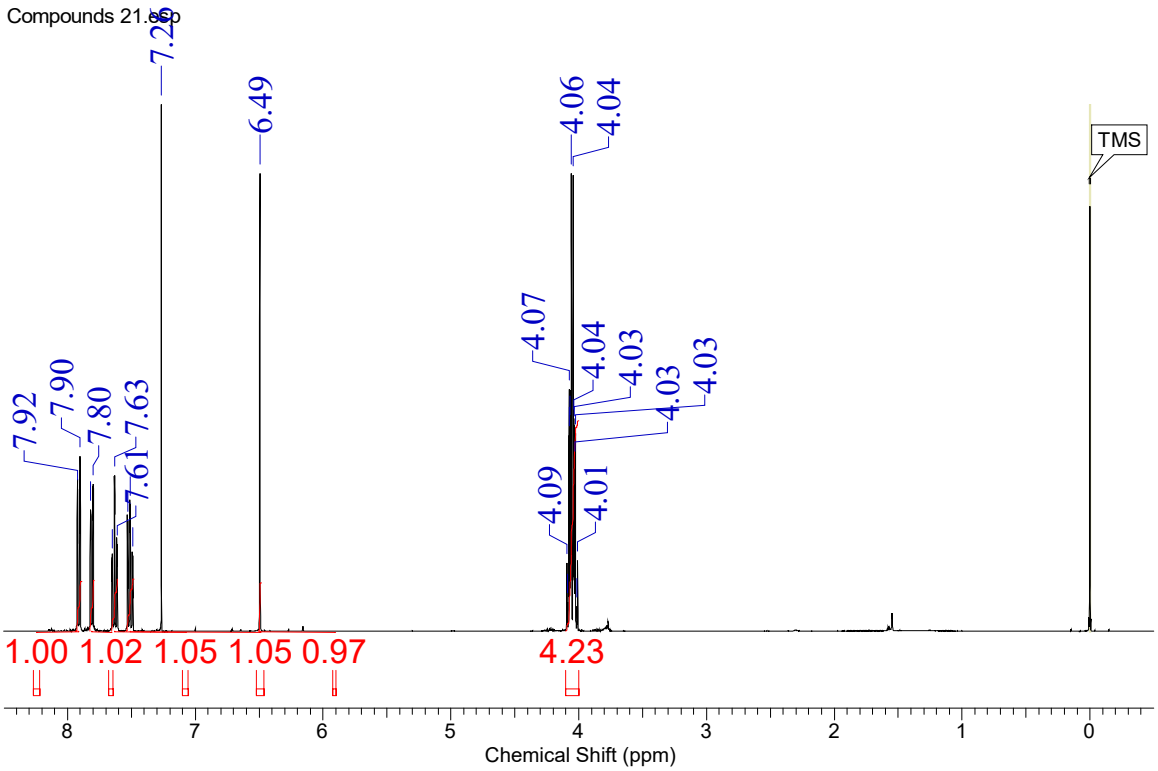

^{13}C-NMR

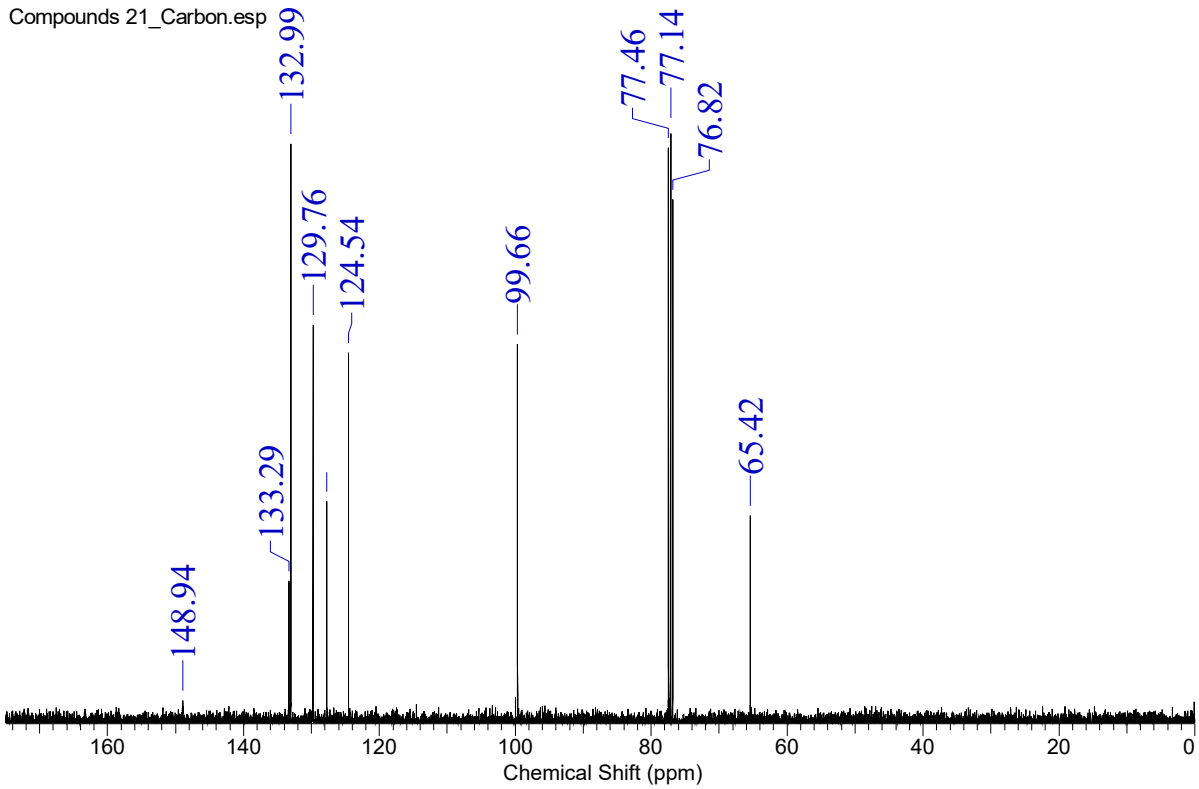
Compounds 21_Carbon.esp
132.99
129.76
124.54
133.29
148.94
99.66
77.46
77.14
76.82
65.42
160
140
120
100
80
60
40
20
0
Chemical Shift (ppm)

Compounds **22**

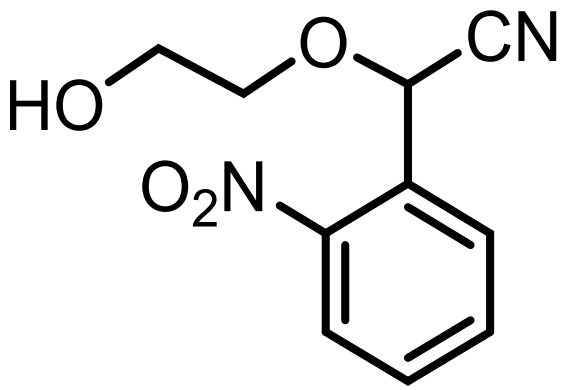

^{1}H-NMR

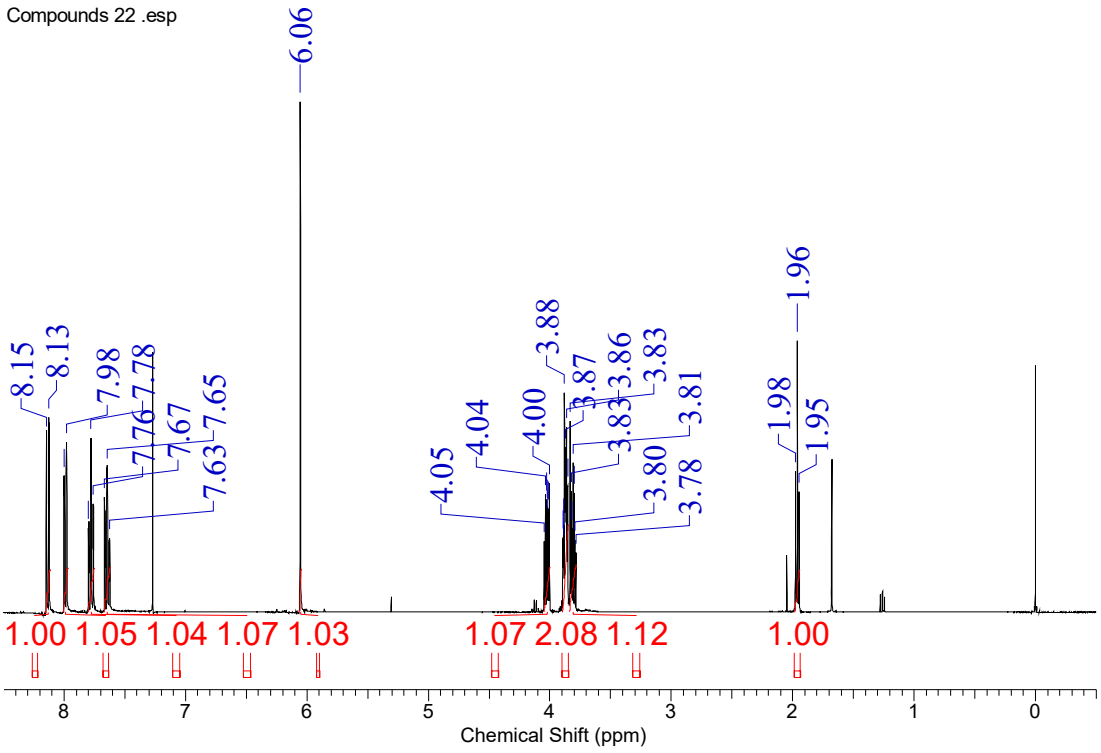

^{13}C-NMR

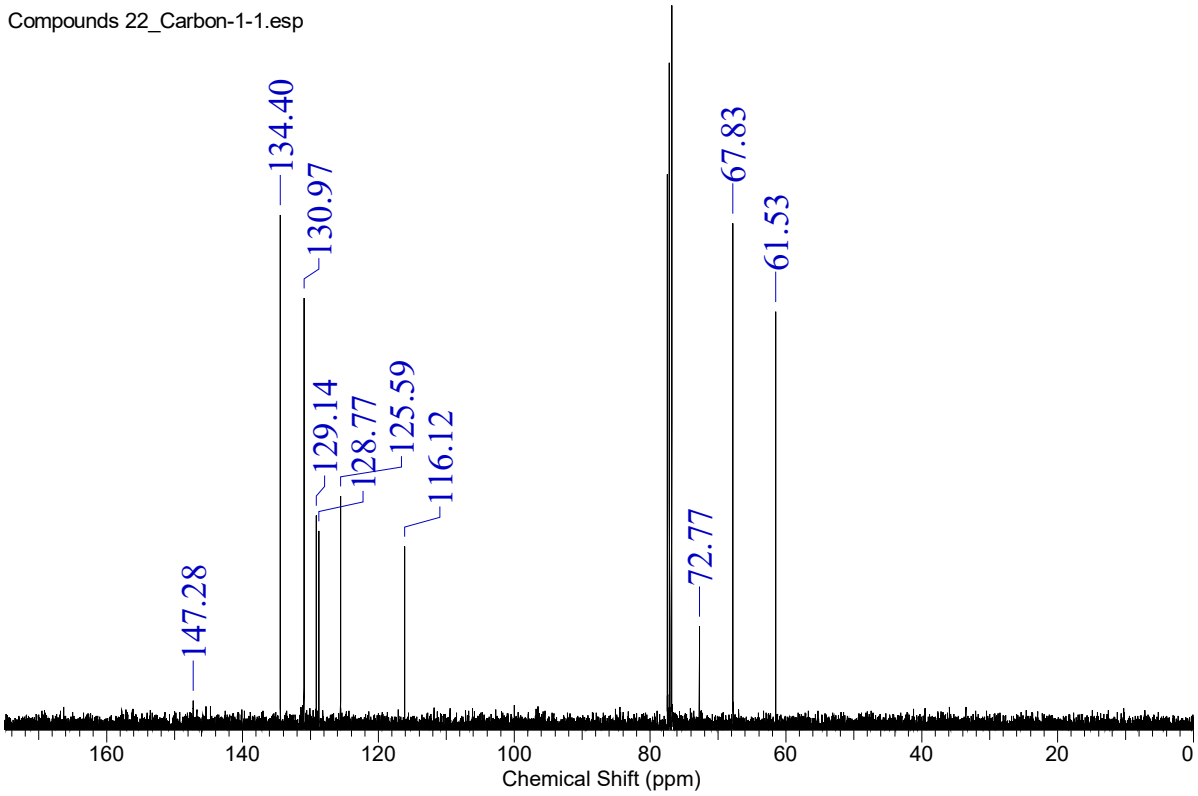

HRMS (ESI)

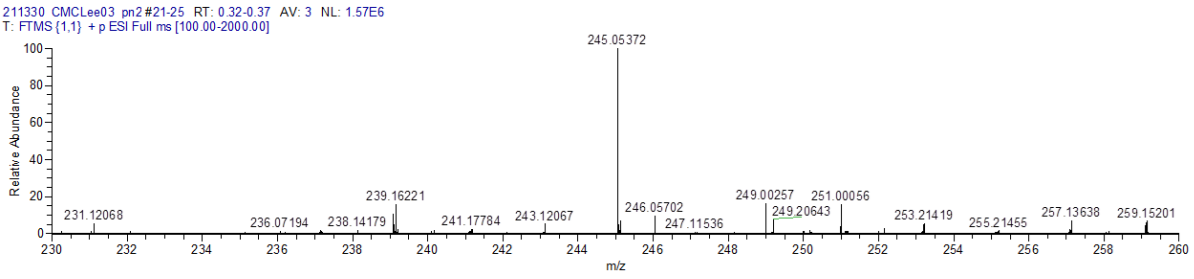

m/z	Theo. Mass	Delta (ppm)	RDB equiv.	Composition
245.05372	245.05328	1.80	6.5	$C_{10}H_{10}O_4N_2Na$
	245.05434	-2.53	10.0	$C_{10}H_7O_3N_5$
	245.05300	2.93	5.0	$C_9H_{11}O_7N$

Compounds **25**

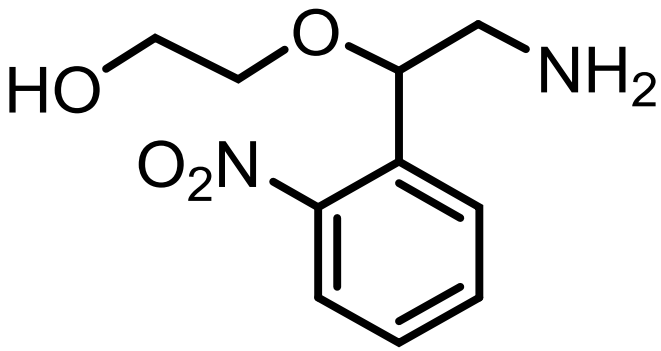

^{1}H-NMR

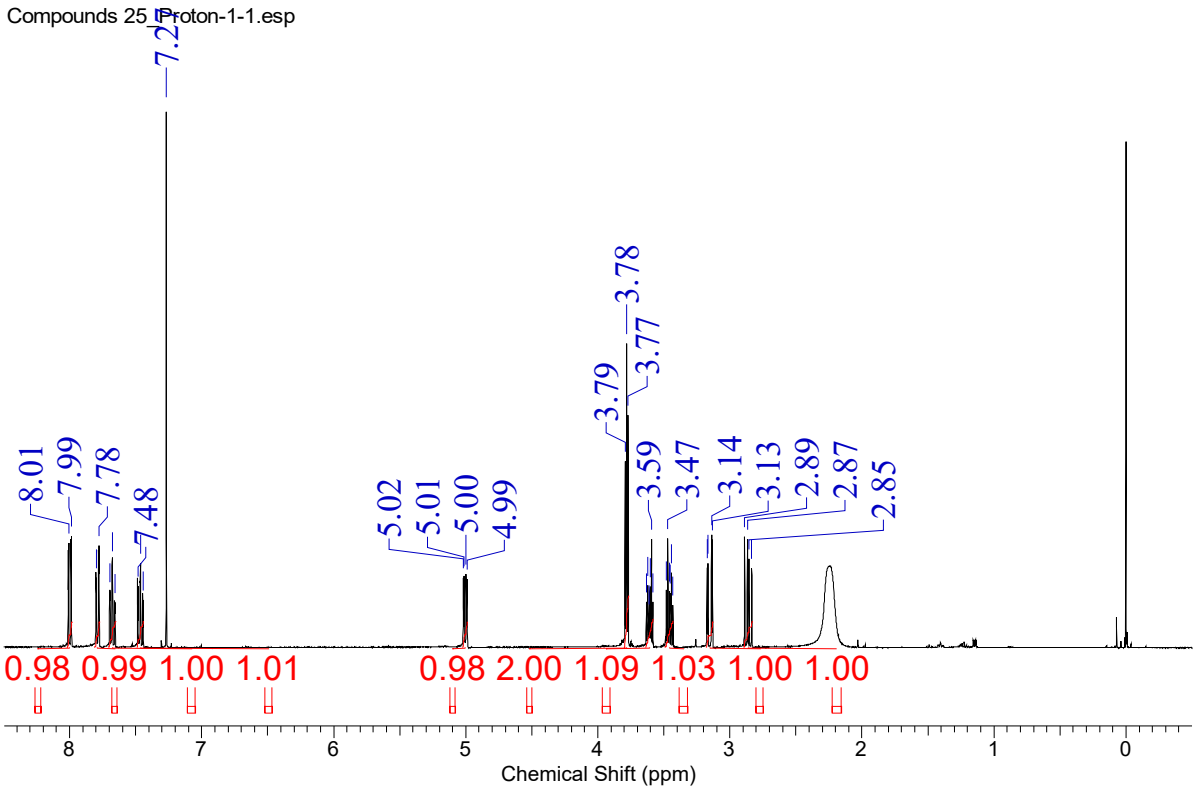

^{13}C-NMR

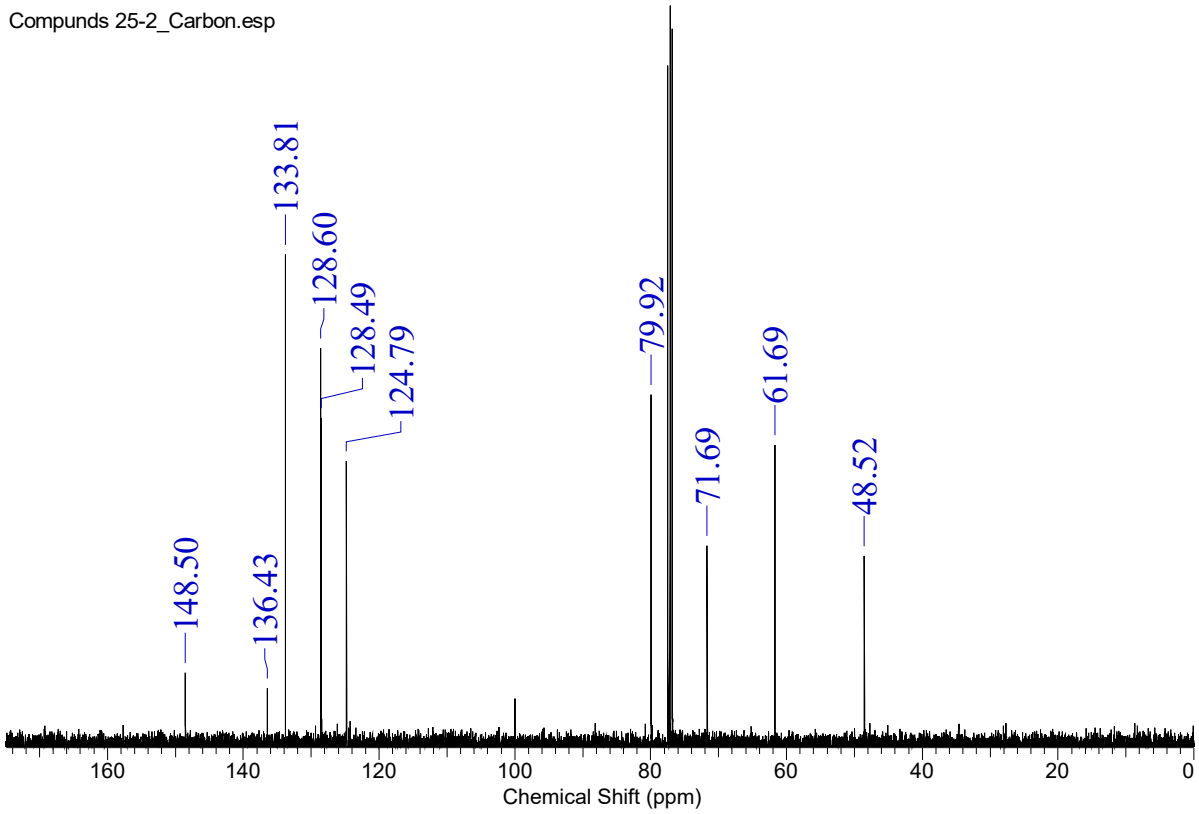

HRMS (ESI)

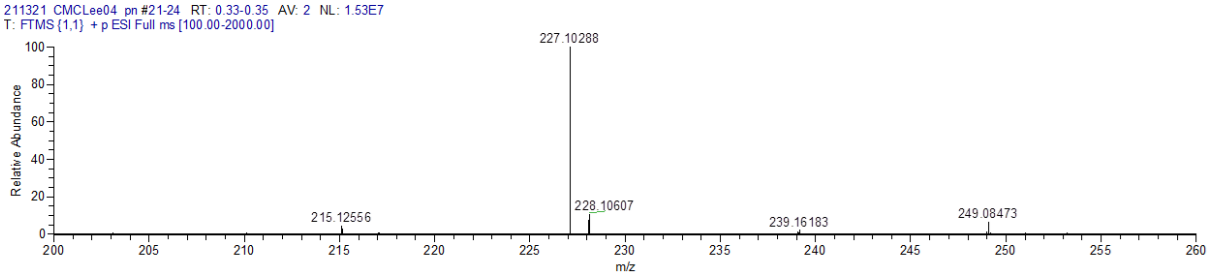

m/z	Theo. Mass	Delta (ppm)	RDB equiv.	Composition
227.10284	227.10291	-0.30	6.0	$C_{11}H_{14}ON_3Na$
	227.10263	0.91	4.5	$C_{10}H_{15}O_4N_2$

Compounds **26**

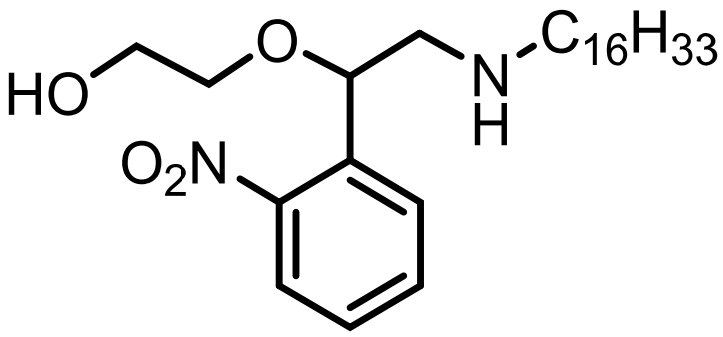

^{1}H-NMR

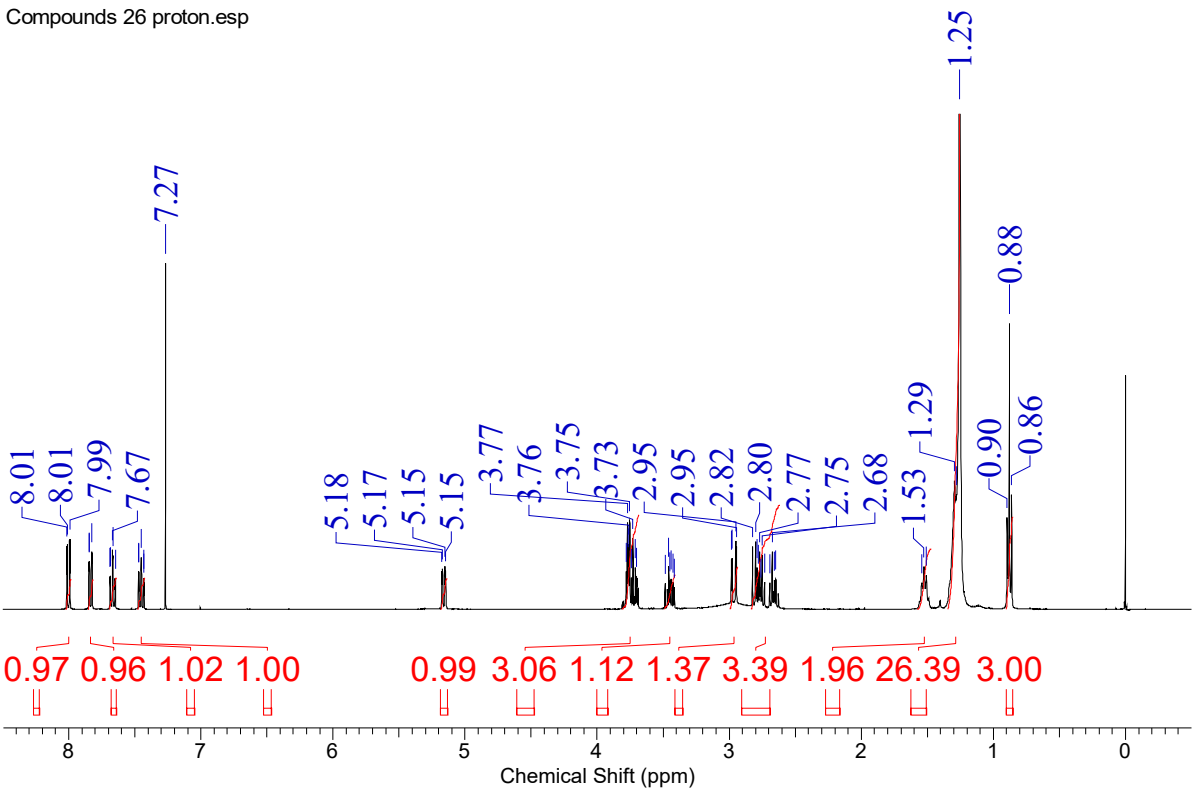

^{13}C-NMR

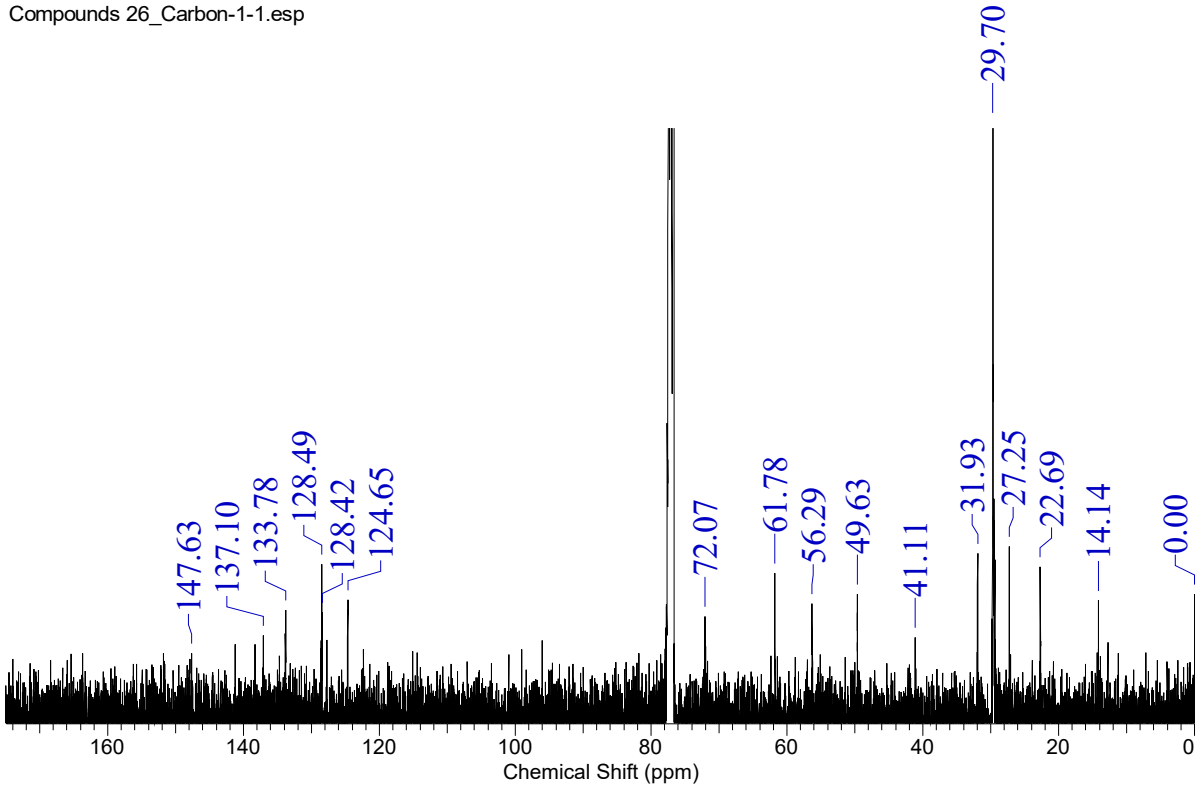

HRMS (ESI)

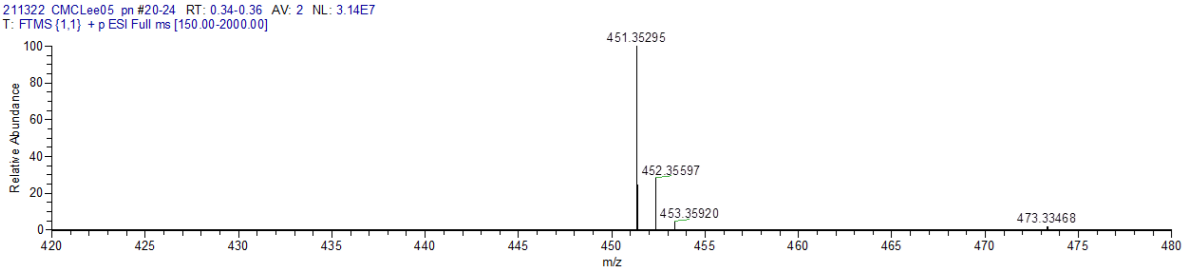

m/z	Theo. Mass	Delta (ppm)	RDB equiv.	Composition
451.35299	451.35303	-0.10	4.5	$C_{26}H_{47}O_4N_2$
	451.35331	-0.71	6.0	$C_{27}H_{46}ON_3Na$
	451.35169	2.88	5.0	$C_{24}H_{45}O_3N_5$
	451.35465	-3.68	5.5	$C_{29}H_{48}O_2Na$

Compounds **27** (mixture of 2 diastereomers)

^{1}H-NMR

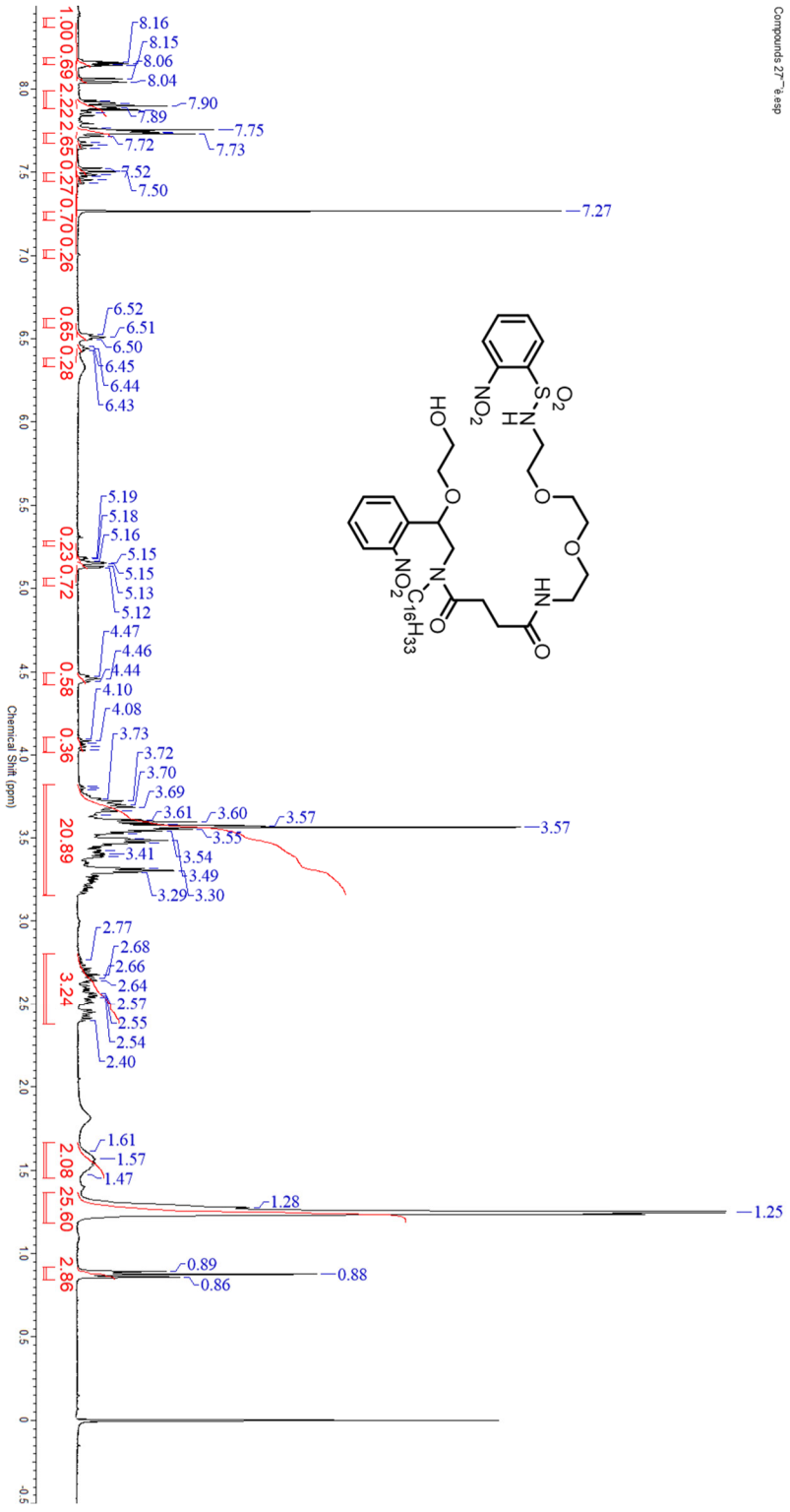

^{13}C-NMR

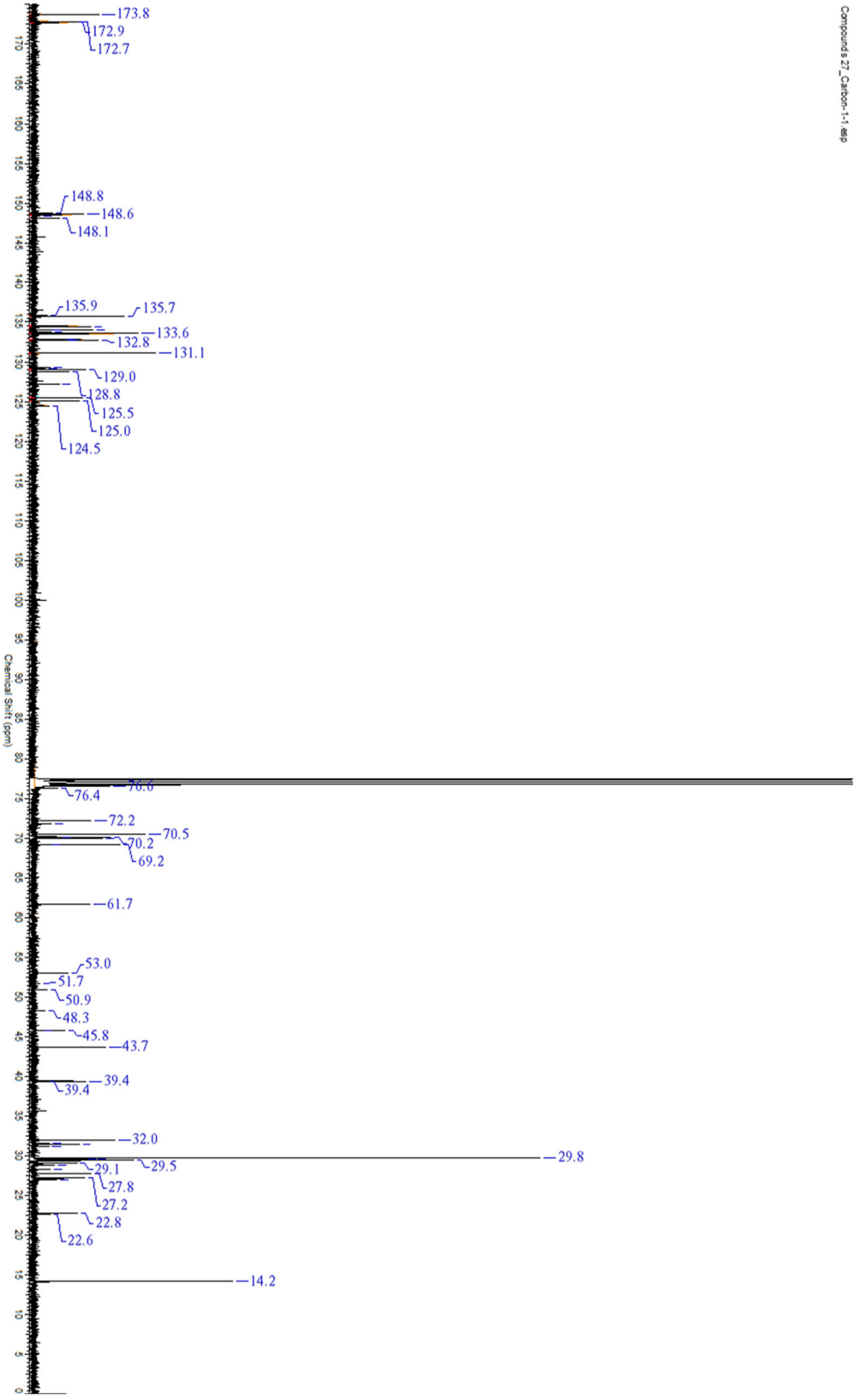
Compounds 27_Carbon- 1-1 esp
Chemical Shift (ppm)
173.8
172.9
172.7
148.8
148.6
148.1
135.9
135.7
133.6
132.8
131.1
129.0
128.8
125.5
125.0
124.5
76.6
76.4
72.2
70.5
70.2
69.2
61.7
53.0
51.7
50.9
48.3
45.8
43.7
39.4
39.4
32.0
29.8
29.5
29.1
27.8
27.2
22.8
22.6
14.2

HRMS (ESI)

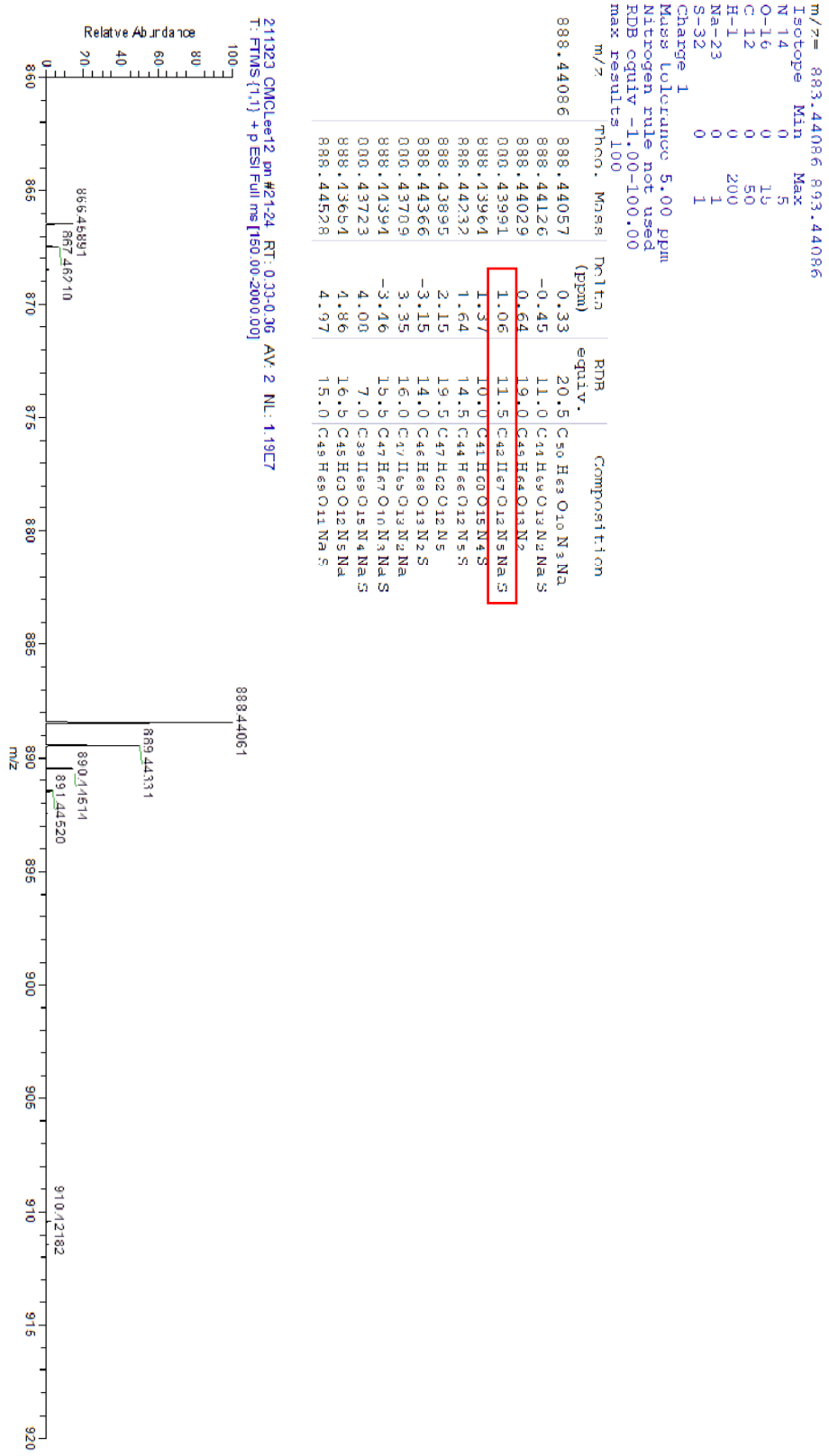
m/z= 883.44086 893.44086
Isotope Min Max
N 14 0 5
O-16 0 15
C 12 0 50
H-1 0 200
Na-23 0 1
S-32 0 1
Charge 1
Mass tolerance 5.00 ppm
Nitrogen rule not used
RDB equiv -1.00-100.00
max results 100
m/z Theo. Mass Delta (ppm) RDB equiv. Composition
888.44086 888.44057 0.33 20.5 C50 H63 O10 N3 Na
888.44126 -0.45 11.0 C41 H59 O13 N2 Na S
888.44029 0.64 19.0 C45 H64 O13 N2
888.43991 1.06 11.5 C42 H67 O12 N5 Na S
888.43964 1.37 10.0 C41 H60 O15 N4 S
888.44232 1.64 14.5 C44 H66 O12 N5 S
888.43895 2.15 19.5 C47 H62 O12 N5
888.44366 -3.15 14.0 C46 H68 O13 N2 S
888.43709 3.35 16.0 C47 H65 O13 N2 Na
888.44394 -3.46 15.5 C47 H67 O10 N3 Na S
888.43723 4.00 7.0 C39 H65 O15 N4 Na S
888.43654 4.86 16.5 C45 H63 O12 N5 Na
888.44528 4.97 15.0 C49 H65 O11 Na S
211323 CMCLee12 on #21-24 RT: 0.33-0.36 AV: 2 NL: 1.19E7
T: FTMS {1,1} + p ESI Full ms [150.00-2000.00]
Relative Abundance
m/z
866.45891
867.46210
888.44061
889.44331
890.44514
891.44520
910.42182

Compounds **28** (mixture of 2 diastereomers)

^{1}H-NMR

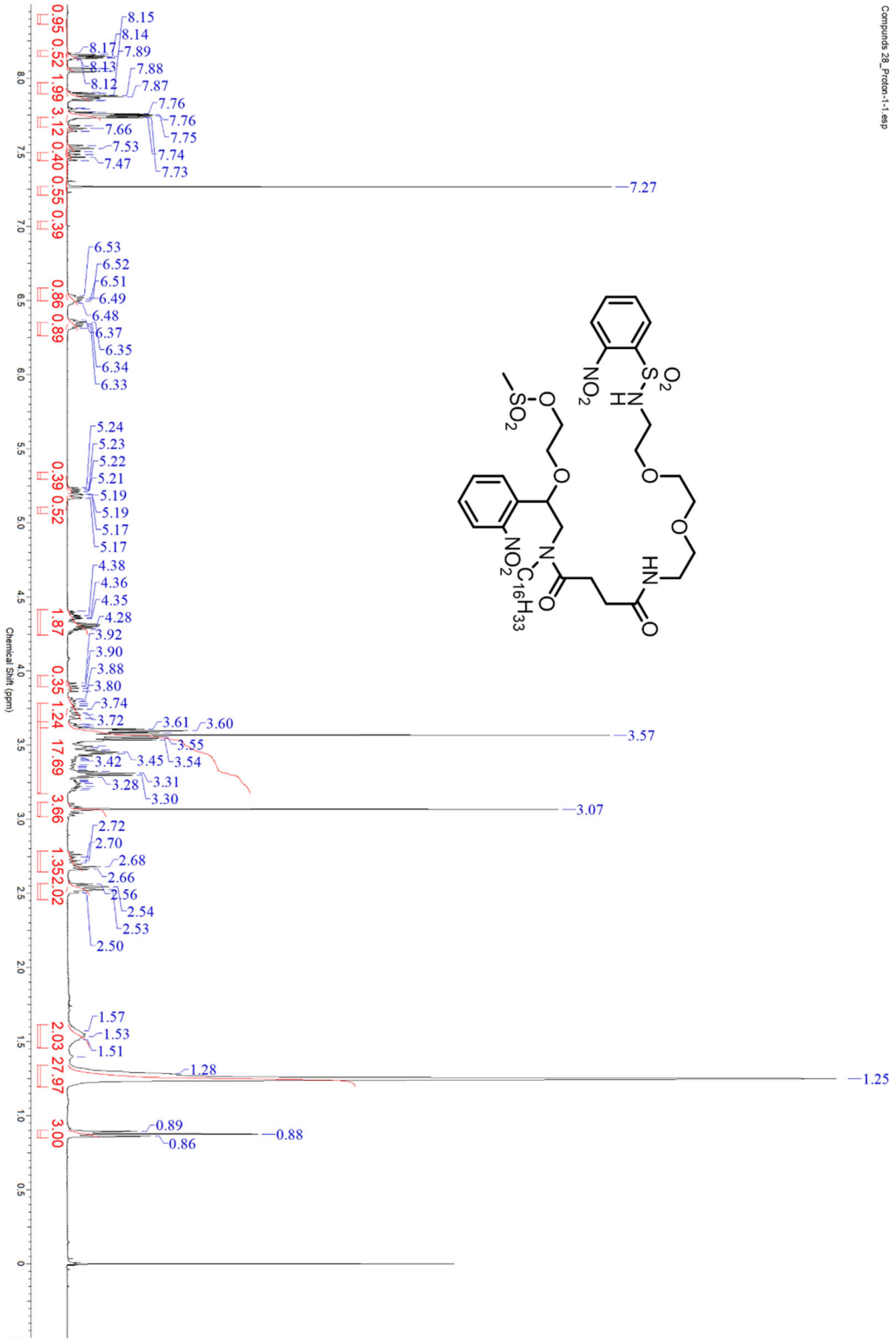

HRMS (ESI)

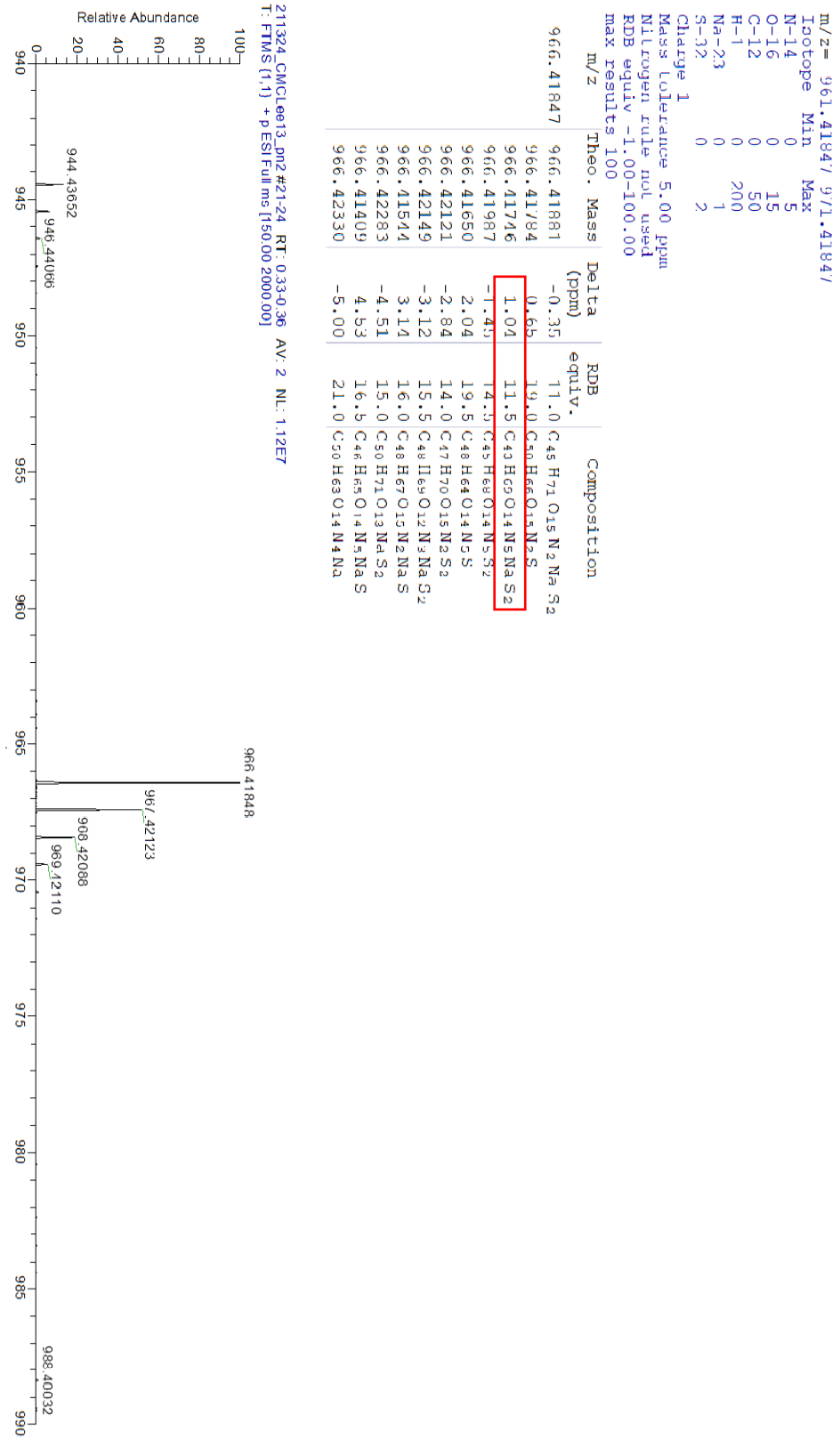
m/z= 961.41847 971.41847
Isotope Min Max
N-14 0 5
O-16 0 15
C-12 0 50
H-1 0 200
Na-23 0 1
S-32 0 2
Charge 1
Mass tolerance 5.00 ppm
Nitrogen rule not used
RDB equiv -1.00-100.00
max results 100
m/z Theo. Mass Delta (ppm) RDB equiv. Composition
966.41847 966.41881 -0.35 11.0 C45 H71 O15 N2 Na S2
966.41784 0.65 19.0 C50 H66 O15 N2 S
966.41746 1.04 11.5 C43 H69 O14 N5 Na S2
966.41987 -1.45 14.5 C45 H68 O14 N5 S2
966.41650 2.04 19.5 C48 H64 O14 N5 S
966.42121 -2.84 14.0 C47 H70 O15 N2 S2
966.42149 -3.12 15.5 C48 H69 O12 N3 Na S2
966.41544 3.14 16.0 C48 H67 O15 N2 Na S
966.42283 -4.51 15.0 C50 H71 O13 Na S2
966.41409 4.53 16.5 C46 H65 O14 N5 Na S
966.42330 -5.00 21.0 C50 H63 O14 N4 Na
211324_CMCLee13_pn2 #21-24 RT: 0.33-0.36 AV: 2 NL: 1.12E7
T: FTMS (1,1) + p ESI Full ms [150.00-2000.00]
Relative Abundance
944.43652
946.44066
966.41848
967.42123
968.42088
969.42110
988.40032

Compounds **29** (mixture of 2 diastereomers)

^{1}H-NMR

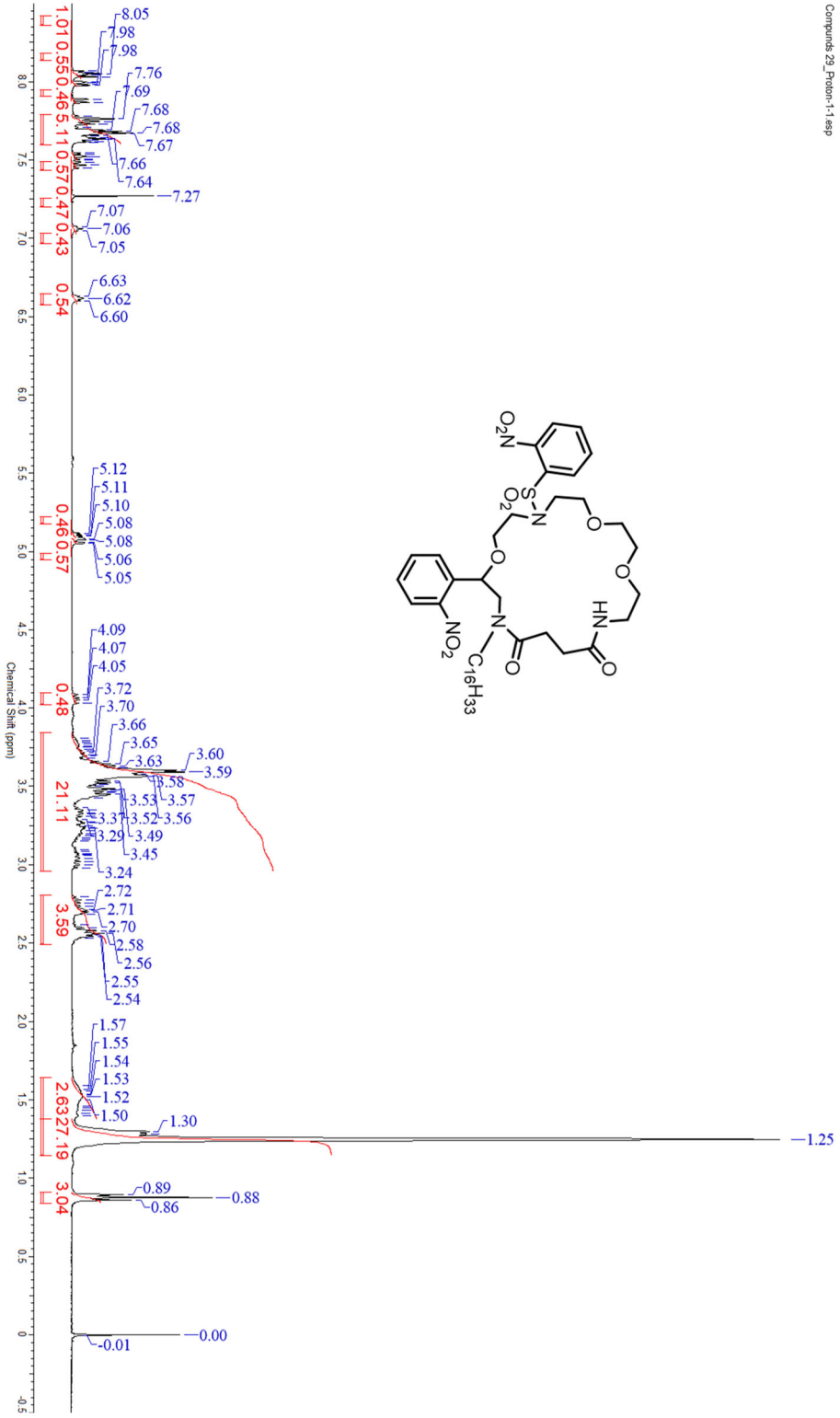

^{13}C-NMR

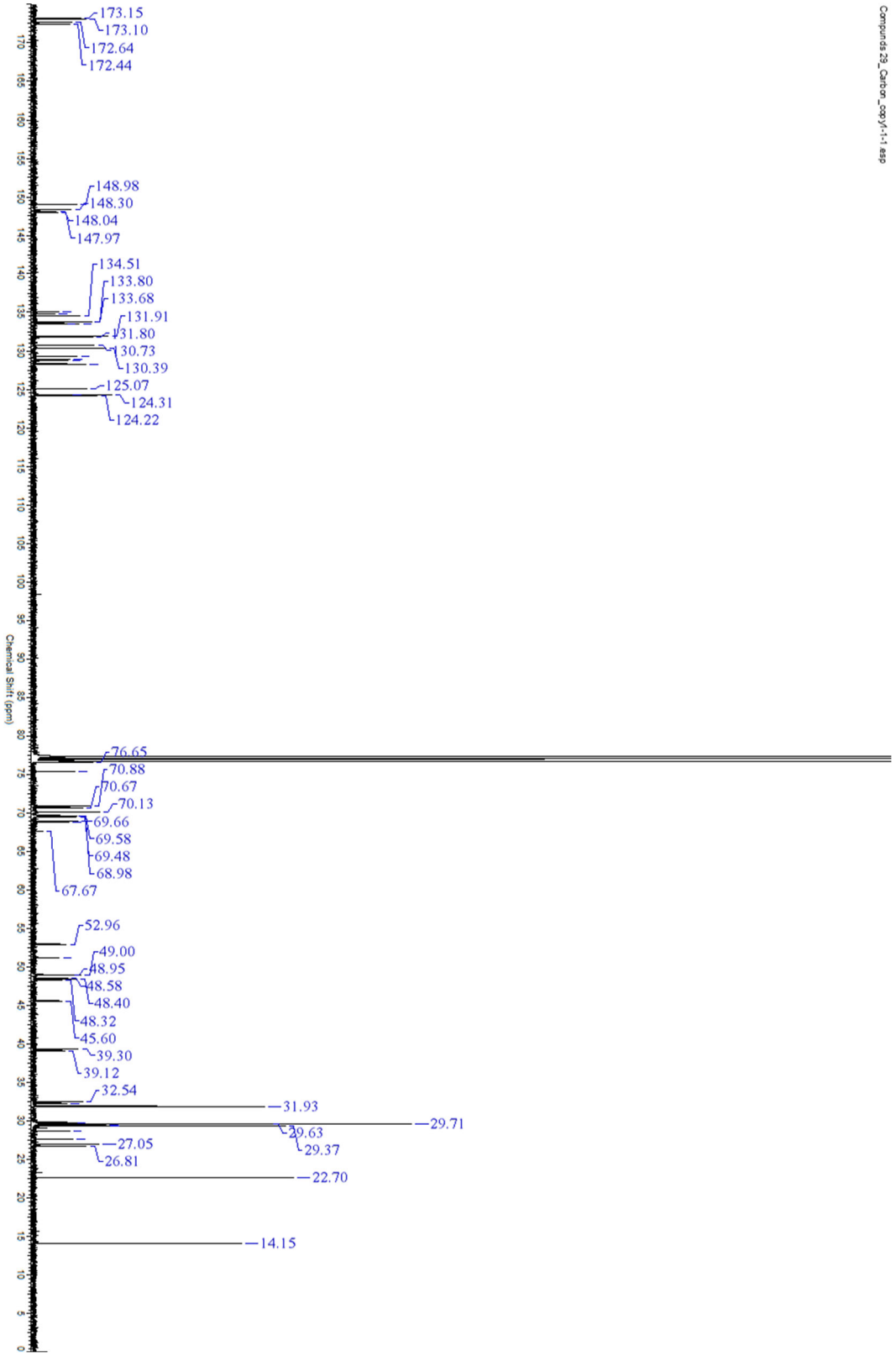
Compound 29_Carbon_copy1-1-1.esp
Chemical Shift (ppm)
173.15
173.10
172.64
172.44
148.98
148.30
148.04
147.97
134.51
133.80
133.68
131.91
131.80
130.73
130.39
125.07
124.31
124.22
76.65
70.88
70.67
70.13
69.66
69.58
69.48
68.98
67.67
52.96
49.00
48.95
48.58
48.40
48.32
45.60
39.30
39.12
32.54
31.93
29.71
29.63
29.37
27.05
26.81
22.70
14.15

HRMS (ESI)

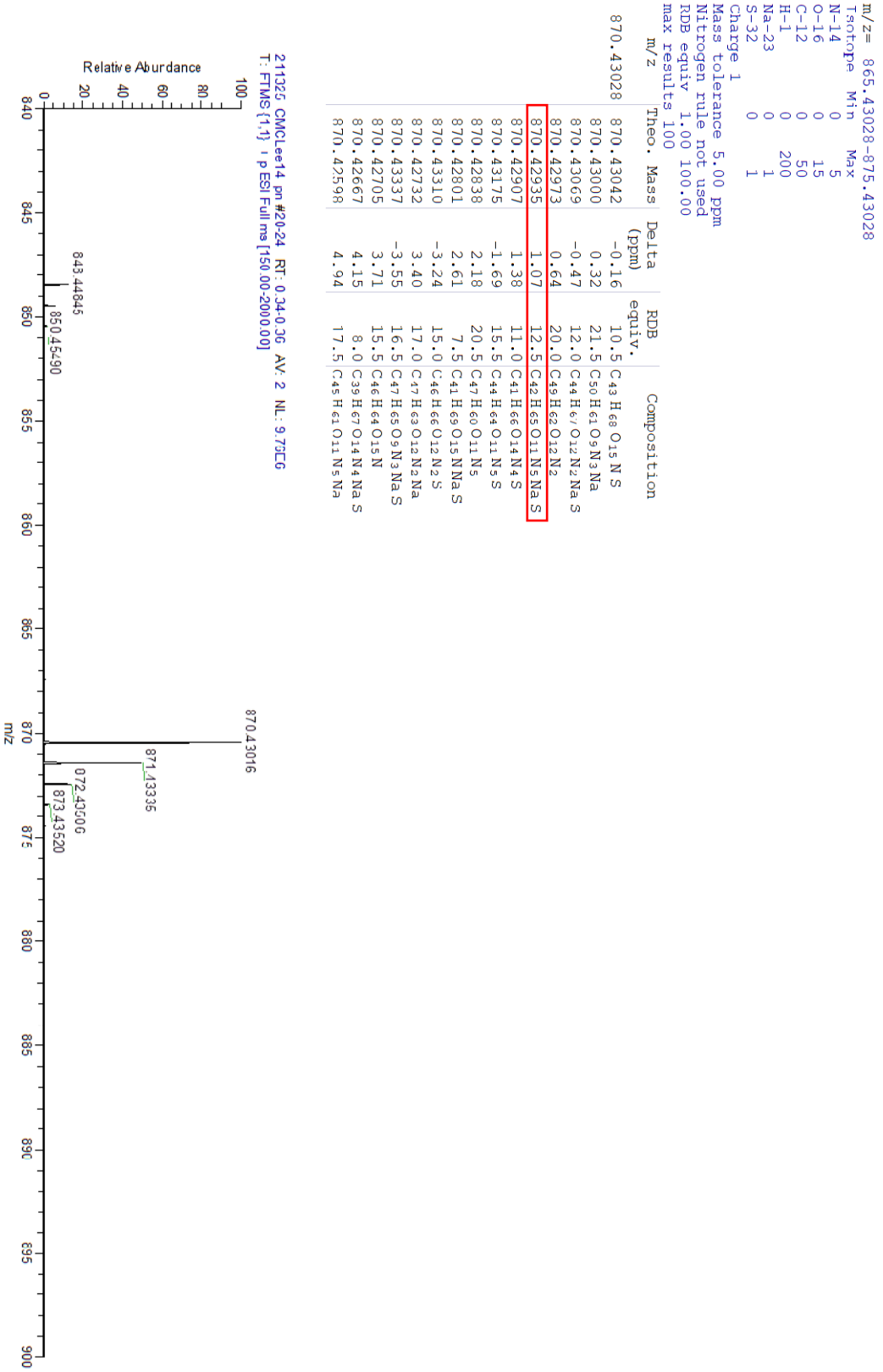

m/z= 865.43028-875.43028
Isotope Min Max
N-14 0 5
O-16 0 15
C-12 0 50
H-1 0 200
Na-23 0 1
S-32 0 1
Charge 1
Mass tolerance 5.00 ppm
Nitrogen rule not used
RDB equiv 1.00 100.00
max results 100

m/z	Theo. Mass	Delta (ppm)	RDB equiv.	Composition
870.43028	870.43042	-0.16	10.5	$C_{43}H_{68}O_{15}NS$
	870.43000	0.32	21.5	$C_{50}H_{61}O_{9}N_{3}Na$
	870.43069	-0.47	12.0	$C_{44}H_{67}O_{12}N_{2}NaS$
	870.42973	0.64	20.0	$C_{49}H_{62}O_{12}N_{2}$
	870.42935	1.07	12.5	$C_{42}H_{65}O_{11}N_{5}NaS$
	870.42907	1.38	11.0	$C_{41}H_{66}O_{14}N_{4}S$
	870.43175	-1.69	15.5	$C_{44}H_{64}O_{11}N_{5}S$
	870.42838	2.18	20.5	$C_{47}H_{60}O_{11}N_{5}$
	870.42801	2.61	7.5	$C_{41}H_{68}O_{15}NNaS$
	870.43310	-3.24	15.0	$C_{46}H_{66}O_{12}N_{2}S$
	870.42732	3.40	17.0	$C_{47}H_{63}O_{12}N_{2}Na$
	870.43337	-3.55	16.5	$C_{47}H_{65}O_{9}N_{3}NaS$
	870.42705	3.71	15.5	$C_{46}H_{64}O_{15}N$
	870.42667	4.15	8.0	$C_{39}H_{67}O_{14}N_{4}NaS$
	870.42598	4.94	17.5	$C_{45}H_{61}O_{11}N_{5}Na$

Compounds **30**

^{1}H-NMR

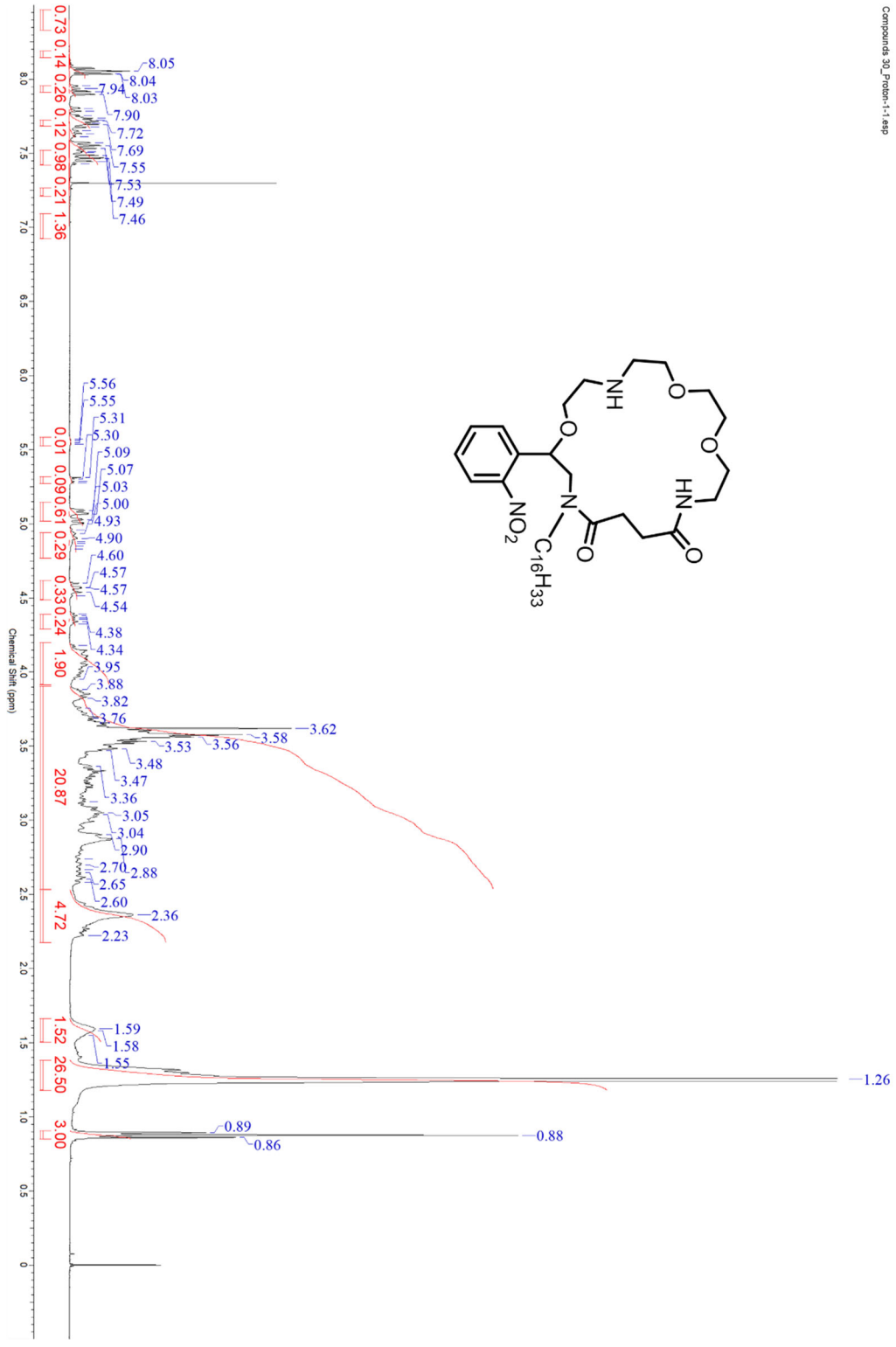

^{13}C-NMR

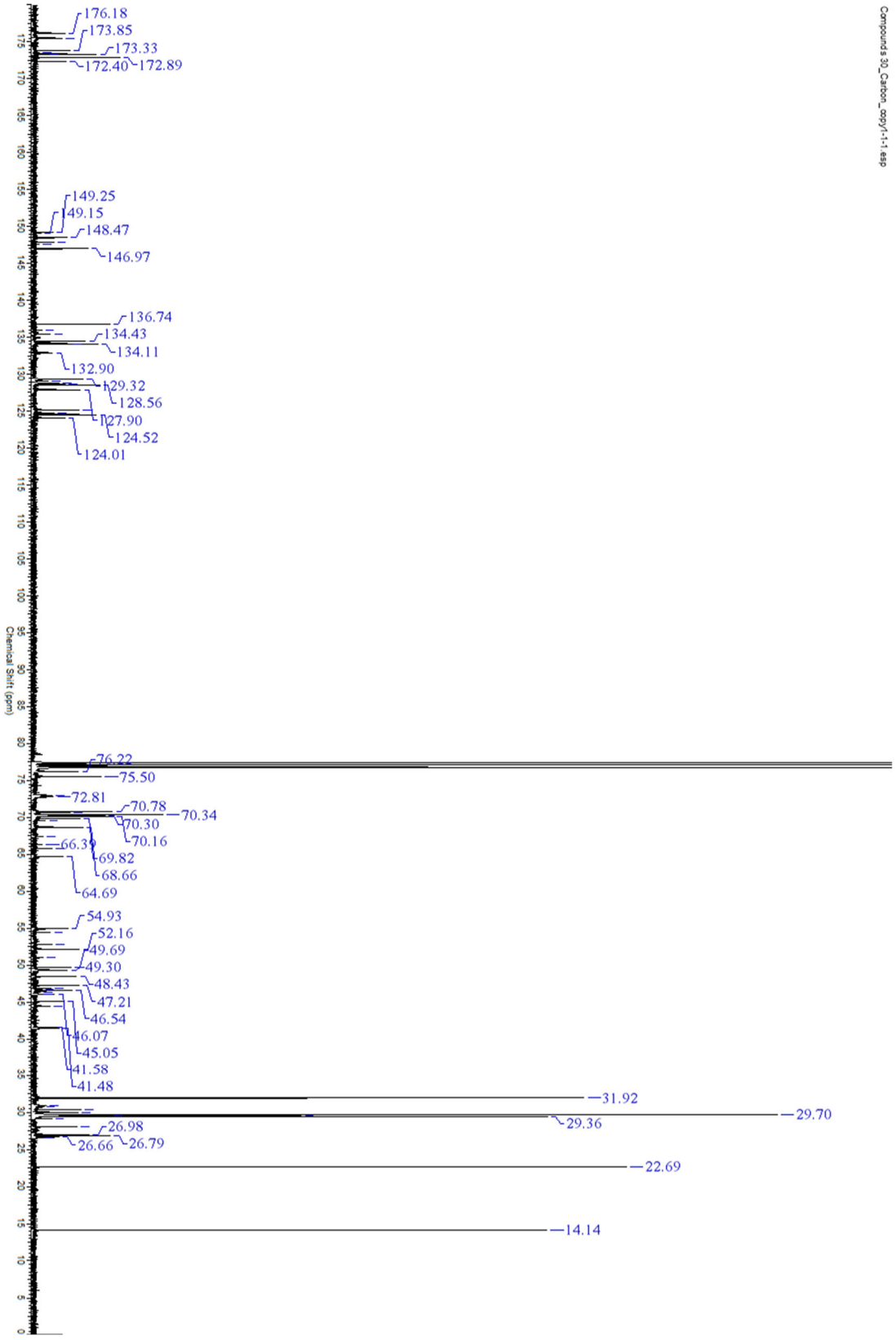
Compound 30_Carbon_copy1-1-1.esp
Chemical Shift (ppm)
176.18
173.85
173.33
172.40
172.89
149.25
149.15
148.47
146.97
136.74
134.43
134.11
132.90
129.32
128.56
127.90
124.52
124.01
76.22
75.50
72.81
70.78
70.34
70.30
70.16
66.39
69.82
68.66
64.69
54.93
52.16
49.69
49.30
48.43
47.21
46.54
46.07
45.05
41.58
41.48
31.92
29.70
29.36
26.98
26.66
26.79
22.69
14.14

HRMS (ESI)

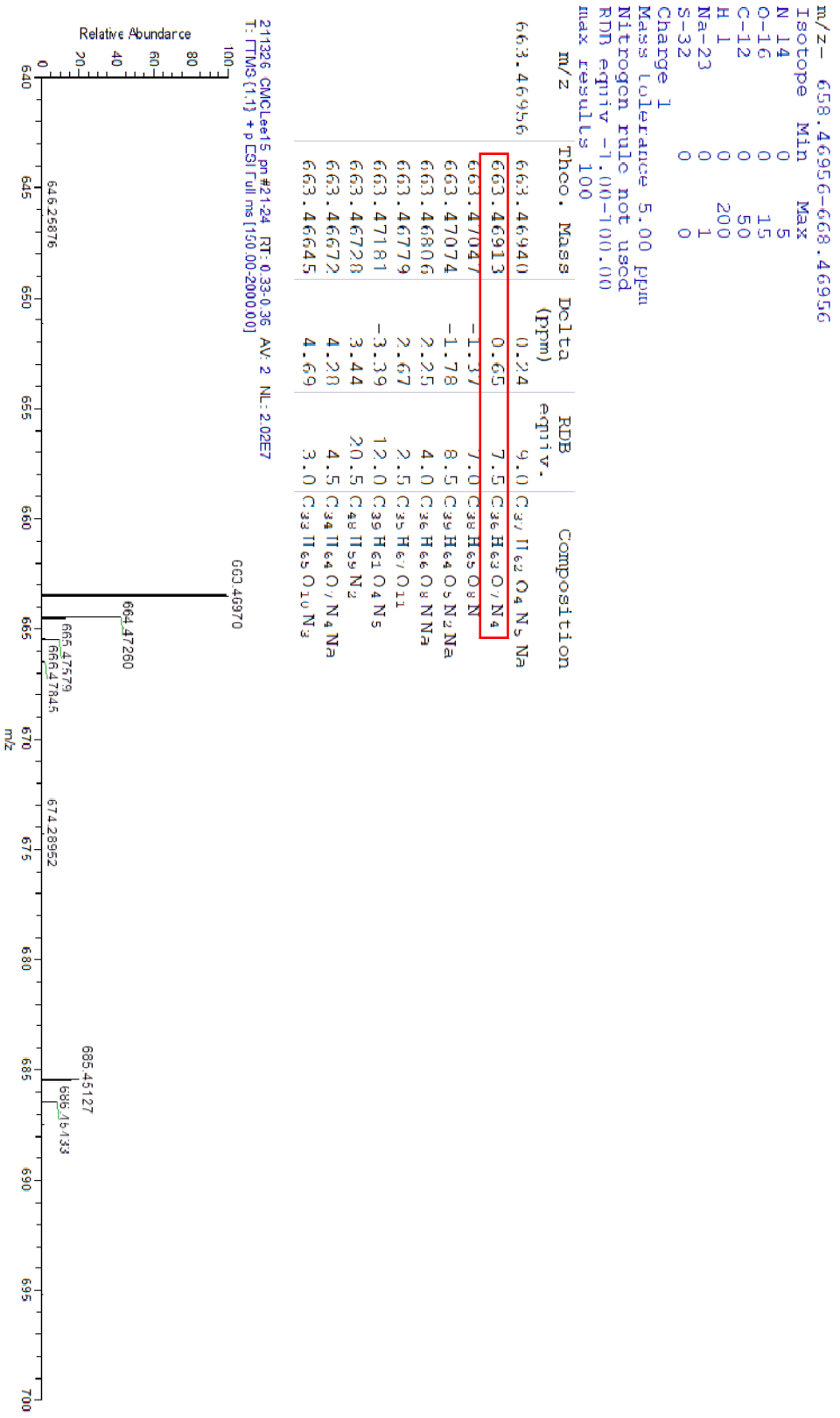

m/z- 658.46956-668.46956
Isotope Min Max
N 14 0 5
O-16 0 15
C-12 0 50
H 1 0 200
Na-23 0 1
S-32 0 0
Charge 1
Mass tolerance 5.00 ppm
Nitrogen rule not used
RDB equiv -1.00-100.00
max results 100

m/z	Theo. Mass	Delta (ppm)	RDB equiv.	Composition
663.46956	663.46940	0.24	9.0	$C_{37}H_{62}O_4N_5Na$
	663.46913	0.65	7.5	$C_{36}H_{63}O_7N_4$
	663.47047	-1.37	7.0	$C_{38}H_{65}O_8N$
	663.47074	-1.78	8.5	$C_{39}H_{64}O_5N_2Na$
	663.46806	2.25	4.0	$C_{36}H_{66}O_8NNa$
	663.46779	2.67	2.5	$C_{35}H_{67}O_{11}$
	663.47181	-3.39	12.0	$C_{39}H_{61}O_4N_5$
	663.46728	3.44	20.5	$C_{48}H_{59}N_2$
	663.46672	4.20	4.5	$C_{34}H_{64}O_7N_4Na$
	663.46645	4.69	3.0	$C_{33}H_{65}O_{10}N_3$

Compounds **33**

^{1}H-NMR

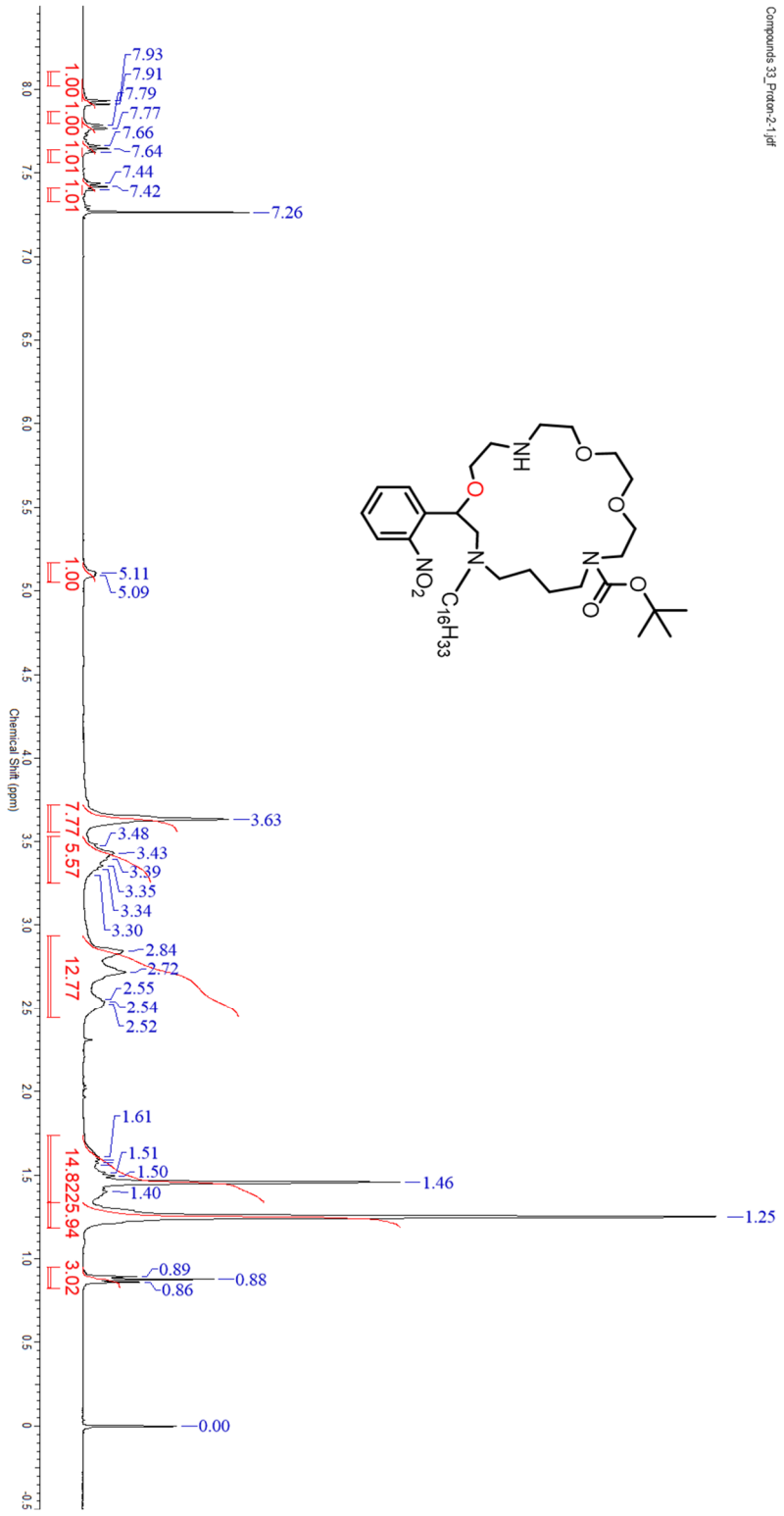

^{13}C-NMR

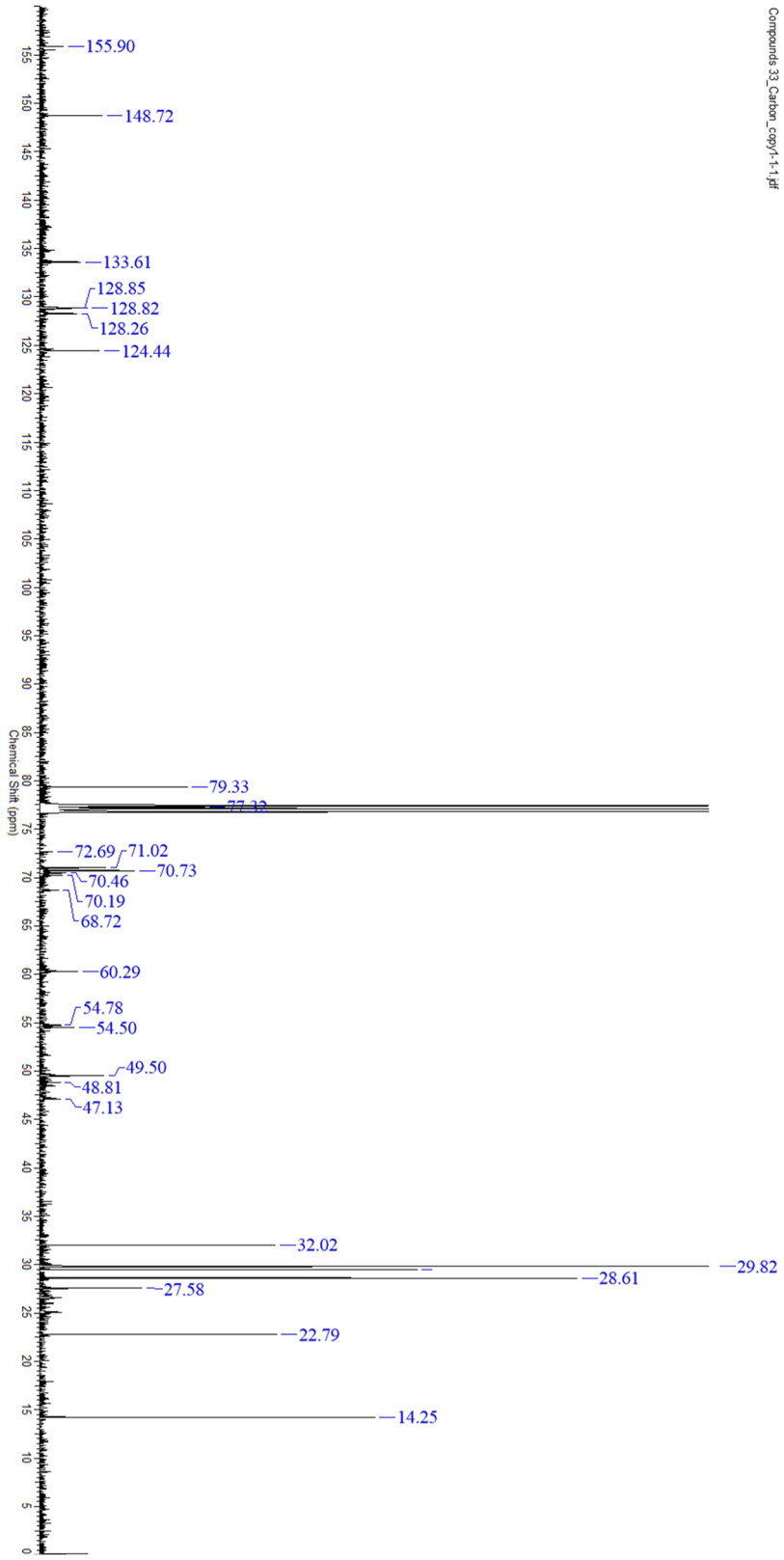
Compounds 33_Carbon_copy1-1-1.jdf
Chemical Shift (ppm)
155.90
148.72
133.61
128.85
128.82
128.26
124.44
79.33
72.69
71.02
70.73
70.46
70.19
68.72
60.29
54.78
54.50
49.50
48.81
47.13
32.02
29.82
28.61
27.58
22.79
14.25

HRMS (ESI)

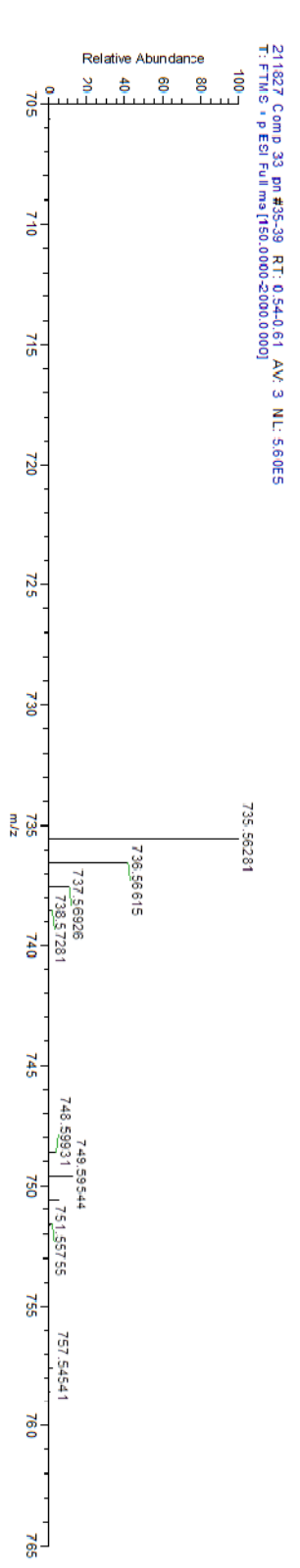

m/z= 730.56 740.56
Isotope Min Max
N-14 0 10
O-16 0 15
C-12 0 100
H-1 0 200
Na-23 0 1
Charge 1
Mass tolerance 5.00 ppm
Nitrogen rule not used
RDB equiv -1.00-100.00
max results 10

m/z	Theo. Mass	Delta (ppm)	RDB equiv.	Composition
735.56295	735.56303	-0.10	6.5	$C_{41}H_{75}O_7N_4$
	735.56330	-0.48	8.0	$C_{42}H_{74}O_4N_5Na$
	735.56196	1.34	3.0	$C_{41}H_{78}O_8NNa$
	735.56196	1.35	0.5	$C_{40}H_{72}O_3N_8Na$
	735.56169	1.71	1.5	$C_{40}H_{79}O_{11}$
	735.56168	1.72	7.0	$C_{39}H_{73}O_6N_7$
	735.56436	-1.92	11.5	$C_{42}H_{71}O_3N_8$
	735.56437	-1.93	6.0	$C_{43}H_{77}O_8N$
	735.56464	-2.30	13.0	$C_{43}H_{70}N_9Na$
	735.56464	-2.30	7.5	$C_{44}H_{76}O_5N_2Na$

Compounds **34**

HRMS (ESI)

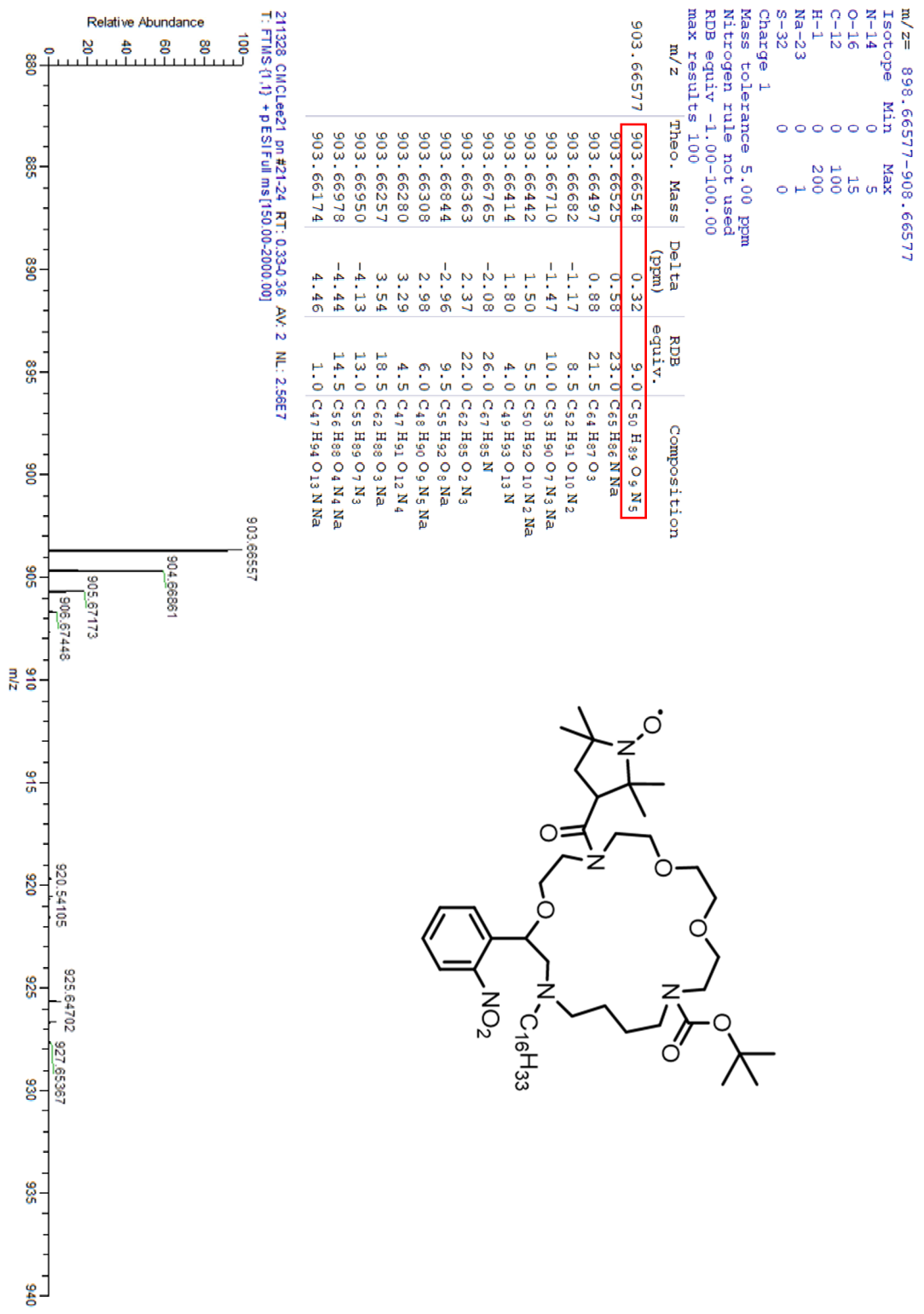

m/z= 898.66577-908.66577
Isotope Min Max
N-14 0 5
O-16 0 15
C-12 0 100
H-1 0 200
Na-23 0 1
S-32 0 0
Charge 1
Mass tolerance 5.00 ppm
Nitrogen rule not used
RDB equiv -1.00-100.00
max results 100

m/z	Theo. Mass	Delta (ppm)	RDB equiv.	Composition
903.66577	903.66548	0.32	9.0	$C_{50}H_{89}O_9N_5$
	903.66525	0.58	23.0	$C_{65}H_{86}NNa$
	903.66497	0.88	21.5	$C_{64}H_{87}O_3$
	903.66682	-1.17	8.5	$C_{52}H_{91}O_{10}N_2$
	903.66710	-1.47	10.0	$C_{53}H_{90}O_7N_3Na$
	903.66442	1.50	5.5	$C_{50}H_{92}O_{10}N_2Na$
	903.66414	1.80	4.0	$C_{49}H_{93}O_{13}N$
	903.66765	-2.08	26.0	$C_{67}H_{85}N$
	903.66363	2.37	22.0	$C_{62}H_{85}O_2N_3$
	903.66844	-2.96	9.5	$C_{55}H_{92}O_8Na$
	903.66308	2.98	6.0	$C_{48}H_{90}O_9N_5Na$
	903.66280	3.29	4.5	$C_{47}H_{91}O_{12}N_4$
	903.66257	3.54	18.5	$C_{62}H_{88}O_3Na$
	903.66950	-4.13	13.0	$C_{55}H_{89}O_7N_3$
	903.66978	-4.44	14.5	$C_{56}H_{88}O_4N_4Na$
	903.66174	4.46	1.0	$C_{47}H_{94}O_{13}NNa$